CHARACTERIZATION of the RATE of WATER INFILTRATION into SOIL

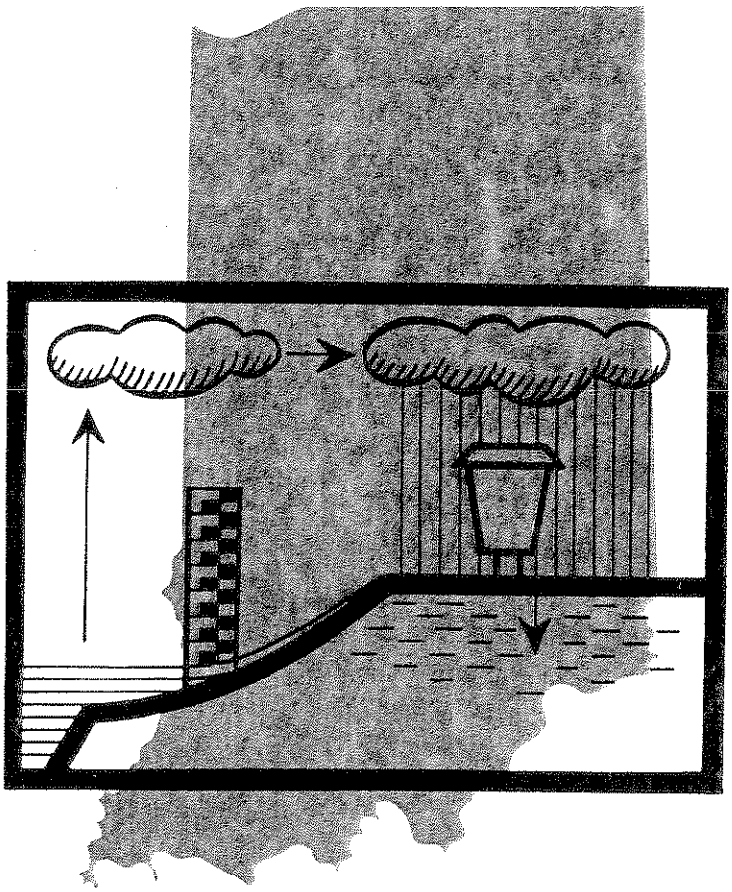

by
D. Swartzendruber
R. W. Skaggs
D. Wiersma

December, 1968

PURDUE UNIVERSITY
WATER RESOURCES RESEARCH CENTER
LAFAYETTE, INDIANA

CHARACTERIZATION OF THE RATE OF WATER INFILTRATION INTO SOIL

A completion report of the likewise entitled OWRR Project No. A-004-IND, Agreement No. 14-01-0001-1082. Period of Project: May, 1965 to June, 1968.

by

D. Swartzendruber

R. W. Skaggs

D. Wiersma

Principal Investigators: E. J. Monke and D. Swartzendruber

Purdue University

Departments of Agricultural Engineering and Agronomy

Lafayette, Indiana

The work upon which this report is based was supported in part by funds provided by the United States Department of the Interior, Office of Water Resources Research, as authorized by the Water Resources Research Act of 1964.

Technical Report No. 5

Purdue University Water Resources Research Center

Lafayette, Indiana

December, 1968

PROJECT PERSONNEL

The following alphabetical-departmental listing includes all persons associated in a meaningful way with the project during its term of activity.

Department of Agricultural Engineering

Dr. Larry F. Huggins, Assistant Professor

Dr. Edwin J. Monke, Professor (Principal Investigator)

Mr. Richard W. Skaggs, Instructor

Department of Agronomy

Dr. Mohamed S. Asseed, Postdoctoral Research Associate

Mr. Paul C. DuChateau, special student assistant

Mr. Royce L. Lambert, Graduate Research Assistant

Mr. David L. Nofziger, Graduate Research Assistant

Dr. Dale Swartzendruber, Professor of Soils
(Principal Investigator)

Mr. Gordon Y. Tsuji, Graduate Assistant

Dr. Daniel Wiersma, Professor

ACKNOWLEDGMENT

The authors express their grateful appreciation for the use of data made available by the Soil and Water Conservation Research Division, Agricultural Research Service, United States Department of Agriculture. The data, in the form of runoff hydrographs from rainfall-simulator field plots, were used to evaluate infiltration equations as described in Chapter 4 of this report.

TABLE OF CONTENTS

TABLE OF CONTENTS (Continued)

LIST OF TABLES

LIST OF FIGURES (Continued)

LIST OF FIGURES (Continued)

LIST OF FIGURES (Continued)

CHAPTER 1. GENERAL INTRODUCTION AND OBJECTIVES

BACKGROUND

Although the hydrologic cycle is itself a set of extremely complex interrelated phenomena, the portion of the cycle having to do with the infiltration of water into soil is hardly any less complex and involved. Particularly at the soil surface and in the upper part of the soil profile does the interaction of atmospheric water take place with the lithosphere. It is here that the complex partitioning between rainfall, infiltration, runoff, evaporation, and deep seepage is initiated and sustained. Obviously also, this is the site of man's own primary location and beginning point for managing and controlling his all-important resource of water.

During the past several decades, significant strides have been made in understanding and mathematically describing many facets of the infiltration process, but it still appears that the overall process retains much of a hard core of seemingly intractable and stubborn inscrutability. Especially is this so with regard to devising a workable, effective, and convenient scheme or methodology for utilizing presently existing infiltration theory and knowledge in characterizations and predictions under field conditions. This simply means that the task is not yet complete, in spite of previous advances.

OBJECTIVES AND DEGREE OF ACHIEVEMENT

The objectives of the present study are listed in the numbered statements below. Each is followed by an identification of the portion of the report that deals with it, along with an assessment of the degree of achievement.

Objective 1. To develop theoretical and experimental means of describing the water-transport properties of soil relevant to the infiltration phenomenon.

The effort on this objective is described in Chapter 2, and was carried out in the Department of Agronomy primarily as mathematical and laboratory studies. This objective was fulfilled quite successfully in principle, inasmuch as mathematical relationships could be developed and reasonably well validated, and in that the experimental procedures developed were adaptable to field-core samples of soil.

Objective 2. To predict the infiltration rate from both the initial water content of the soil profile and the water-transport properties of the soil at various positions in the profile, including the surface.

Realization of the principles of this objective is enabled from the achievement of Objective 1 as described in Chapter 2, in that mathematical predictions are possible for various initial water contents and different soil-stratum characteristics. Determination of such characteristics was carried out to a limited extent as is described in Chapter 3. This work, both in gathering field cores and in making the characterizing water-flow measurements on them in the laboratory, was performed by the Department of Agronomy, is only partially complete, and is in further process currently.

Objective 3. To measure infiltration rates with field-type instrumentation, to analyze and interpret these values, and to compare them with predicted values.

Efforts on this objective involving measurements with a small sprinkling infiltrometer were carried out in the field by the Department of Agronomy, as described in Chapter 3. Analysis and interpretation by the Department of Agricultural Engineering of infiltration data taken with a large rain simulator are presented in Chapter 4. These first two phases of Objective 3 are considered to be well achieved, in that more accurate measurements have been realized and the suitability of several forms of infiltration equation (including one from Objective 1) has been shown. The phase of Objective 3 dealing with comparison of predicted and measured infiltration rates has not been completely realized, however, and is in further process currently, in the related sense as described previously for Objective 2.

CHAPTER 2. INFILTRATION CHARACTERISTICS OF SMALL FLOW COLUMNS IN THE LABORATORY

INTRODUCTORY COMMENTS

Theoretical analyses of infiltration of water into soil have generally been made for physical conditions represented in terms of a vertical column of unsaturated porous material to which water is applied at the top, usually by ponding. In principle, an exact mathematical solution for water inflow into such a column is obtainable for a great variety of conditions, in terms of the diffusivity and conductivity functions of the porous material. Hence, the prediction of infiltration, as well as of other liquid-flow soil-water processes, becomes possible if the diffusivity and conductivity functions can be measured. Efforts of this nature have been summarized recently (Swartzendruber, 1966; Childs, 1967).

Utilization of this so-called exact approach, however, as done by Green, Hanks, and Larson (1964), is greatly complicated by the experimental difficulties attendant to the measurement of the diffusivity and conductivity functions. Steady-state flow methods for determining the conductivity function are time consuming. Furthermore, the pressure-plate outflow (or inflow) method for measuring both the diffusivity and conductivity functions is not only lengthy, but the results are subject to 7- to 10-fold variations in precision (Jackson, van Bavel, and Reginato, 1963; Bazargani, 1964).

In view of these difficulties, a somewhat different approach would appear to be justified. Specifically, it would seem worthwhile to investigate the validity and utility of infiltration equations of simpler mathematical form, involving parameters of characterization that are easier to measure experimentally. Admittedly, such an attack would be less capable of rigorous physical interpretation, and the soil-characterizing parameters therefrom might be of little if any utility for describing other types of soil-water transfer. But, if a workable and self-consistent approximate theory and method could be put together successfully just for the infiltration process alone, the result would still be of considerable merit and utility.

THEORETICAL CONSIDERATIONS

Uniform Systems

One-dimensional downward infiltration is diagrammed in Figure 1A. To the infinitely deep uniform porous material of initial constant volumetric water content θ_o, the constant depth H of ponded water is applied at time $t = 0$. If θ_o is on the order of air dryness, a distinct visual wet front will be present, the depth of which is designated z, and which increases with time $t > 0$. The first analysis of this flow problem was given by Green and Ampt (1911), considering the soil to behave in an idealized fashion which implied complete water saturation behind the wet front, so that the mean volumetric water content $\bar{\theta}$ behind the wet front (for all z) would equal the total porosity. This assumption was first shown to be untenable by Kirkham and Feng (1949). Philip (1954) in effect relaxed the requirement of total saturation. He assumed for all z that $\bar{\theta}$ was constant, but left open the possibility of it being less than the total porosity. But the infiltration equation he derived was still in essence the same functional relation as that of Green and Ampt. We shall develop this equation in brief fashion here, but the basic limitations and approximations will remain as in the result of Philip (1954).

The Darcy equation can be written as

$$v = dy/dt = Ki \qquad (1)$$

where v is the flux of water transmitted, y is the volume of water transmitted per unit cross sectional area of soil column, t is the time, K is the hydraulic conductivity, and i is the total hydraulic gradient. It is granted that certain questions about the ultimate validity of the Darcy equation are as yet unresolved (Swartzendruber, 1968). But, since equation (1) will here be used in a development which from the outset is admitted to be approximate, the existence of some possible approximate character in the basic equation is not considered forbiddingly serious, especially since the final results are to be assessed experimentally.

To obtain an expression for i of equation (1) for the column in Figure 1A, we envision a fictitious tensiometer to be inserted at or just slightly behind the wet front and to be capable of moving along with it. The water level in this fictitious moving tensiometer is considered to stand at the

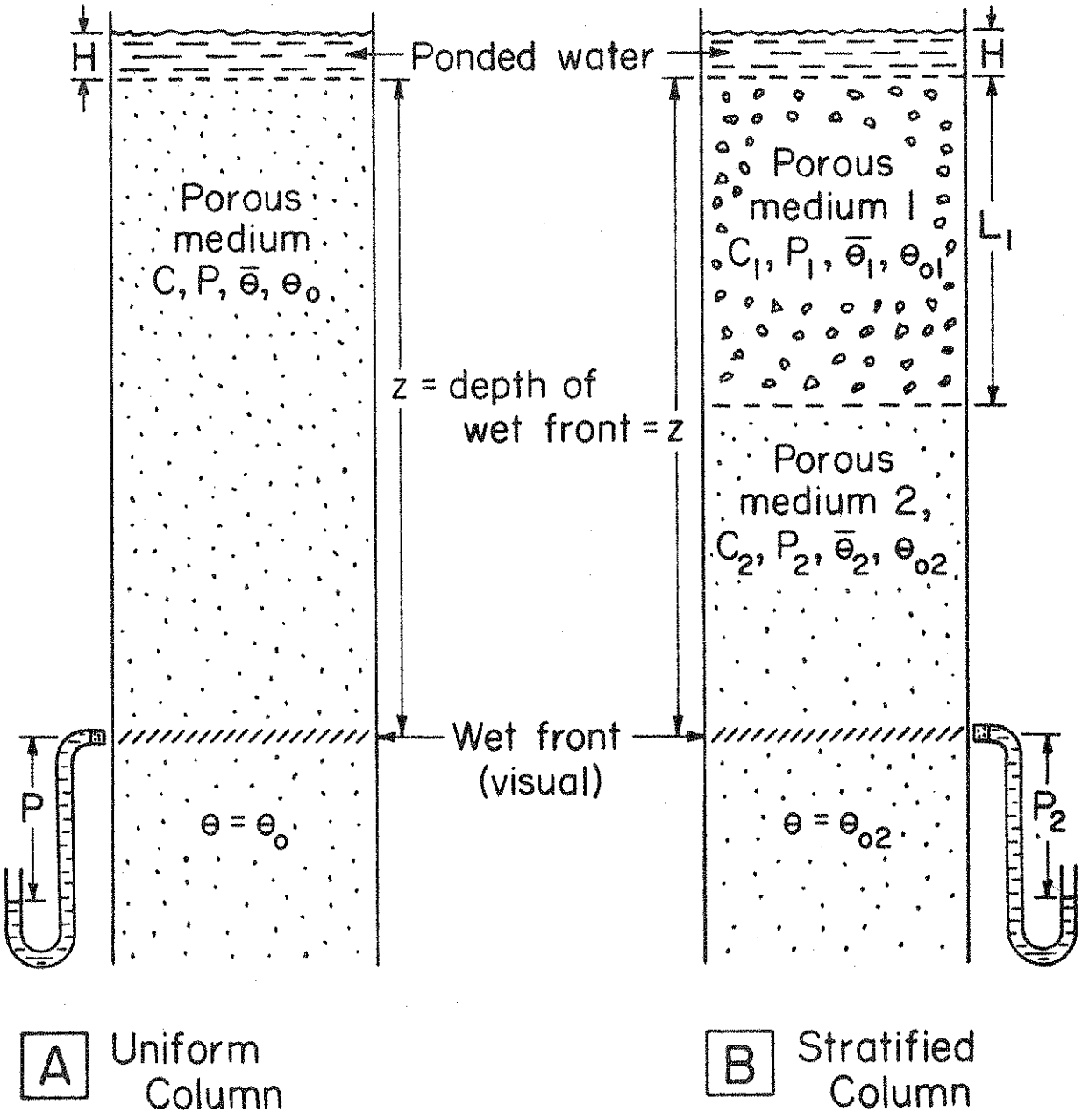

Figure 1--Diagrams of water infiltration into columns of porous media, (A) a uniform column, and (B) a stratified column.

constant distance P below the wet front. Philip (1954) terms -P as "the capillary potential of the wetting front." Taking the top of the column as an arbitrary datum plane for hydraulic head, the total hydraulic head h_{wf} at the wetting front becomes $h_{wf} = -(P + z)$ while that at the inlet end (top) of the column becomes $h_{inlet} = H$. Forming the total hydraulic head difference yields $h_{inlet} - h_{wf} = H + P + z$. We express gradient i as $(h_{inlet} - h_{wf})/z = (H + P + z)/z$. We now put this result into equation (1), but at the same time replace K by another constant C, to allow for any distinction from the Darcian K which might be needed later; the result becomes

$$dy/dt = C(P + H + z)/z \qquad (2)$$

Since C plays an analogous role to K and has the same units, it may at this stage be of some interest to speculate whether C might ultimately be interpretable as the value of K corresponding to the water content $\overline{\theta}$. This is somewhat akin to van Duin's (1955) suggestion that throughout the transmission zone the hydraulic conductivity is nearly constant and is associated with a water content of about 80% pore-space saturation.

Making use of Philip's (1954) assumption of a constant $\overline{\theta}$ behind the wet front, we can write

$$(\overline{\theta} - \theta_o)z = y = Mz \qquad (3)$$

where $\overline{\theta} - \theta_o = M$ is introduced merely as an economy of symbols. Solving equation (3) for z and putting the result into equation (2), separating variables, integrating, and using the condition $y = 0$ at $t = 0$, yields

$$(y/a) - \ln (1 + y/a) = Ct/a \qquad (4)$$

as the form of the Green-Ampt equation, where

$$a = M(H + P) = (\overline{\theta} - \theta_o)(H + P) \qquad (5)$$

Although the derivation just given does not impart rigor to equation (4), Philip (1957a) has considered an alternative derivation based upon diffusivity-conductivity approaches, and reports that the form of equation (4) will result from assuming that the diffusivity is given by the Dirac delta function. Physically, however, this implies a porous medium of coarse texture and low initial water content, and, if these special

conditions are not met, the validity of equation (4) is still left in doubt. In spite of this, Philip (1957a, 1957b, 1958) has reported fairly good success in comparing equation (4) with the general results of his more exact analysis, although Childs (1967) has criticized some of the comparisons as not being particularly meaningful. Nevertheless, both W. R. Gardner (1967) and Childs (1967) have encouraged a greater use of the Green-Ampt equation to characterize infiltration properties.

If characterizing infiltration were the only goal, then it would not particularly matter whether C and P were precisely interpretable in terms of the commonly accepted basic soil-physics concepts of unsaturated conductivity and soil-water suction, as long as both C and P were dependable and self-consistent characterizers of the infiltration process. It would be particularly convenient if both parameters were determined only by the soil material and $\overline{\theta}$. This would seem a reasonable possibility if, in accord with van Duin's (1955) suggestion, C were closely associated with the hydraulic conductivity of the transmission zone, and if P were essentially the hydraulic head loss through this zone. It can also be argued, however, that P should be related in some inverse fashion to the mean radius of curvature of the air-water interface in the soil, and this implies P to decrease as the initial water content θ_o increases. Resort to experiment would seem to be the most meaningful way of resolving the matter.

It might well be asked why the Green-Ampt equation should deserve detailed examination and scrutiny any more than the somewhat simpler appearing equation of Philip (1957a), which is

$$y = St^{1/2} + Gt \qquad (6)$$

where S and G are constants for flooding applications of water and a given initial water content. In considering this general question, it is granted that equation (6) is not theoretically rigorous for long periods of time (Philip, 1957a). But this limitation may well be no more serious than the approximations made in deriving the Green-Ampt equation, particularly if the intended use is just for characterizing infiltration as set forth at the beginning of the previous paragraph. In actuality, the relationship specified between y and t by both equations

is remarkably similar. To show this, equation (6) is rearranged into the form

$$yG/S^2 = (Gt^{1/2}/S)(1 + Gt^{1/2}/S) \qquad (7)$$

from which corresponding values of yG/S^2 and $Gt^{1/2}/S$ can be computed and plotted on log-log scales. Doing the same for y/a and Ct/a of equation (4), the match between the two log-log curves is determined by horizontal and vertical translation of the graphs, without rotation. The result of such matching of the extremities of the two curves is shown in Figure 2. Analytically, these matching conditions turn out to be $C = G$ and $a = S^2/2G$. The maximum amount by which the yG/S^2 of equation (7) exceeds the y/a of equation (4) at a given abscissa value in Figure 2 is 15%. If an error of this magnitude could be tolerated, the matching conditions could then be used to calculate the Green-Ampt parameters from those of equation (6), and vice versa. For restricted portions of the range in y (or t), matching conditions could be found graphically for which the maximum discrepancy would be even less than 15%.

In spite of the close similarity between equations (4) and (6) as just described, the Green-Ampt approach and equation would seem to possess some inherent advantages. Parameter a, for example, depends on θ_o in a much less complicated fashion than does S. Furthermore, the considerations which produce equation (6) are not simply extendable to stratified porous media, whereas the approximate reasoning used to derive equation (4) can also be applied straightforwardly to stratified media, a matter to which we now turn.

Stratified Systems

Consider the system of Figure 1B, where a stratum of infiltration properties C_1, P_1, $\overline{\theta}_1$, and θ_{o1}, and of length L_1, is underlain by an infinitely deep stratum of infiltration properties C_2, P_2, $\overline{\theta}_2$, and θ_{o2}. For $z < L_1$, that is, before the wet front reaches the junction between the two strata, the infiltration behavior is simply that of the Green-Ampt expression [equation (4)], namely

$$(y/a_1) - \ln (1 + y/a_1) = C_1 t/a_1 \qquad (8)$$

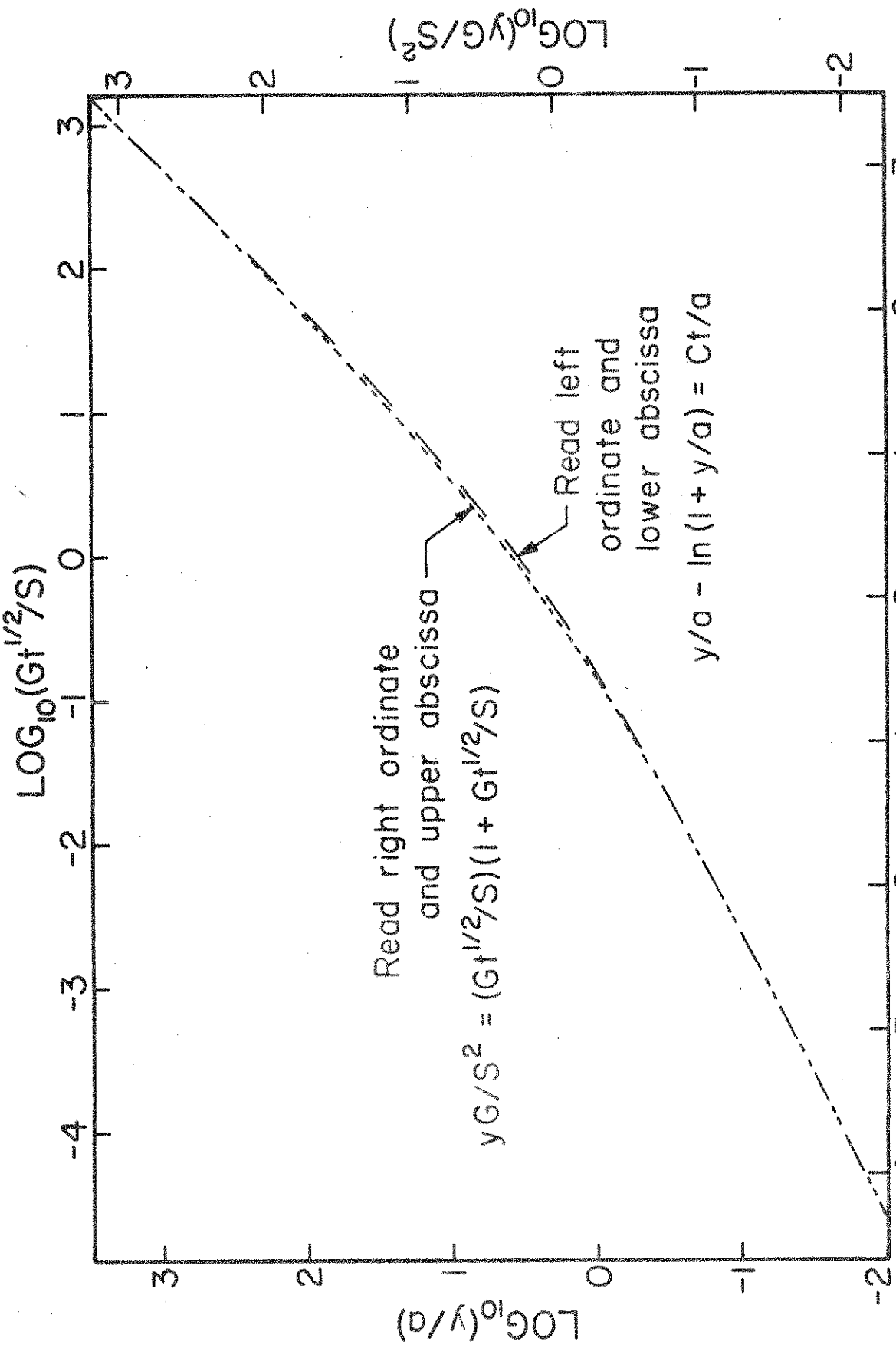

Figure 2--Matching of log-log plots of the curves specified by infiltration equations (4) and (7). Maximum discrepancy between yG/S2 and y/a is 15% at log (Ct/a) = 0.6, or Ct/a = 4.

where $a_1 = M_1(H + P_1) = (\bar{\theta}_1 - \theta_{o1})(H + P_1)$. When the wet front penetrates into the lower stratum, for $z > L_1$ as actually depicted in Figure 1B, a somewhat different expression eventually will emerge. The equivalent of equation (2) becomes

$$dy/dt = C_e(H + P_2 + z)/z \tag{9}$$

where C_e is analogous to the equivalent conductivity of the two regions of C_1 and C_2 spanned by the wet-front depth z. C_e is thus expressed (Swartzendruber, 1960) as $C_e = z/[L_1/C_1 + (z - L_1)/C_2]$. Combining this with equation (9) and rearranging yields

$$dy/dt = C_1C_2(H + P_2 + z)/[L_1(C_2 - C_1) + C_1z] \tag{10}$$

For later simplification, it is convenient to reckon y and t of equation (10) from the point at which the wet front strikes the junction of the two strata ($z = L_1$), using y_2 and t_2 for this purpose but remembering that they are still variables. The counterpart of equation (3) is then written

$$y_2 = M_2(z - L_1) \tag{11}$$

Setting $y = y_2$ and $t = t_2$ in equation (10) and combining with equation (11) tc eliminate z will result in a differential equation in which the variables can be separated and the differentials integrated. Using $y_2 = 0$ at $t_2 = 0$ in the integrated result enables the final result to be written

$$y_2/b - (1 - c/b) \ln (1 + y_2/b) = C_2t_2/b \tag{12}$$

where

$$b = M_2(H + P_2 + L_1) = a_2 + M_2L_1 \tag{13}$$

and

$$c = L_1M_2C_2/C_1 \tag{14}$$

Note the similarity of equation (12) with equation (4). In particular, if $L_1 = 0$ then Figure 1B becomes a uniform system for the subscript 2 material, whereupon $c = 0$, $b = M_2(H + P_2) = a_2$, and, as it should, equation (12) reduces to the Green-Ampt equation for the subscript 2 material. Equation (12) was first presented by van Duin (1955), but without details of derivation.

To construct a complete curve of water infiltrated versus time for a column of $L_1 > 0$, equation (8) is used until the wet front reaches the stratum junction. Hereupon, let y and t from equation (8) be designated as y_o and t_o, respectively. As the wet front penetrates into the lower stratum, equation (12) becomes applicable, and the overall accumulative curve, reckoned from the origin of equation (8), becomes $y_o + y_2$ versus $t_o + t_2$.

The foregoing general approach can readily be extended to as many strata as desired, and the basic form of the resulting equation remains that of equation (12). Consider, for example, that the L_1 stratum of Figure 1B be underlain by a stratum of properties C_2, P_2, and M_2, and of length L_2, and that this in turn be underlain by an infinitely deep stratum of properties C_3, P_3, and M_3. Then, for the wet front in the subscript 3 layer, the resulting equation will take the form of equation (12), but with the b of it and equation (13) replaced by $M_3(H + P_3 + L_1 + L_2)$, and the c of equations (12) and (14) replaced by $M_3(L_1 + L_2)C_3/C_{el2}$, where $C_{el2} = (L_1 + L_2)/(L_1/C_1 + L_2/C_2)$ is the equivalent C for the two top strata.

EXPERIMENTAL EVALUATION

Theoretical Aspects to be Tested

To keep the experimental phase of this study within bounds, certain key aspects of the foregoing infiltration theory were selected for testing. For uniform porous media initially air dry, and thus exhibiting distinct wet-front behavior, the validity of equations (3) and (4) can be determined directly, and, if valid, parameters M, a, and C can be calculated, along with P of equation (5). If such parameters are determined for two different media, the predicted behavior for air-dry stratified systems as in Figure 1B can be obtained from equations (8), (11), (12), (13), and (14) for various stratum characteristics and values of L_1. This predicted behavior can then be compared with direct measurements on stratified columns prepared for these same stratum characteristics and lengths. Furthermore, equations (3) and (11) can be directly tested for a given material, and M can be compared with M_2 if equational validity is obtained.

As mentioned earlier, the behavior of P with respect to θ_o for a given material is another important test of equations (4) and (5), to determine if P decreases as θ_o increases, or whether P is unaffected by θ_o and hence to be considered as governed largely by $\overline{\theta}$. These evaluations are somewhat less direct than desired, since a visual wet front is almost always absent for θ_o in excess of the air-dry value. Thus, instead of determining $M = \overline{\theta} - \theta_o$ by observing y versus z in equation (3), an estimate of M will need to be taken as the quotient of the total column length divided into the value of y at which free water just begins to drip from the bottom end of the column.

Determination of parameters a and C from experimental data would preferably be based on equation (4), since y and t are cumulative quantities quite suitable for relatively easy measurement. Mathematical adaptation for fitting purposes, however, is somewhat complicated by the presence of the parameter a in the logarithmic term. If the rate aspect of equation (4) is considered, differentiation and rearrangement provides the form

$$ydy/dt = aC + Cy \qquad (15)$$

If dy/dt can be evaluated from the data of y versus t, by such as the curve-slope method of Swartzendruber and Olson (1963), a plot of ydy/dt versus y should thus yield a straight line of slope C and intercept aC [equation (15)], from which C and a are thus determined. A few data have been reported (Swartzendruber, 1968), however, in which ydy/dt initially decreased with increasing y, reached a minimum value, and then eventually did increase approximately linearly with increasing y. Such behavior was tentatively accounted for as a manifestation of greater-than-proportional non-Darcian breakdown in equation (1) (Swartzendruber, 1968), but a possible alternative explanation could be developed by postulating that fine particles of the porous medium were being translocated out of the near-surface region by the high velocity of infiltrating water that occurs when the free water of depth H (Figure 1) is initially applied to the column. Any such translocated particles should be redeposited somewhere deeper in the column when the velocity of water movement has substantially decreased. The translocation process should be detectable as a change in porous-medium bulk density when considered as a function of distance below the top surface

of the column. Experimental assessment of the existence and extent of such behavior is possible through the technique of gamma-ray attenuation (W. H. Gardner, 1965).

Experimental Techniques

Application of Water

The attainment at time zero of essentially instantaneous application of a depth H of ponded water as in Figure 1 can prove troublesome. Simply pouring a quantity of water on the top surface of the column will often cause serious disturbance to the column surface. More elaborate apparatus involving porous plates (Davidson, Nielsen, and Biggar, 1963), while not too difficult to construct, is subject to some lingering question as to whether the normally very high initial water infiltration rate is reduced by some unknown amount by the flow resistance of the porous plate. Figure 3 illustrates the apparatus here developed, the central feature of the water applicator being a plexiglas plate perforated by 2.26-mm diameter holes (No. 43 drill). As viewed from the bottom of the applicator, these holes were drilled on an equilateral triangular pattern in which each hole was equally spaced from its six nearest neighbors by a distance of 4 mm. For column diameters of 3.8 and 6.2 cm, the thickness of the perforated applicator plate was 1.6 and 6.2 mm, respectively.

The water applicator and burettes were fixed in rigid position, the manometer, applicator, and burettes all being filled with water as indicated in the figure. An H of about 1 cm would cause slight protrusion of a meniscus of water at the bottom of each hole in the perforated plate. At time zero, the column of porous medium was quickly lifted to bring its top surface in contact with the bottom of the perforated applicator plate and the slightly protruding water menisci. The supporting bolts (three altogether) parallel to the column were then securely tightened for the remainder of the experiment. The bottom end of the porous column, supported by several sheets of glass wool on a perforated plexiglas disc, was open to the atmosphere at all times. Lapsed time t was recorded with a stopwatch. Wet-front progress, if the porous medium was initially air dry, was recorded by means of circumferential scribe marks placed every 2 cm on the exterior of the porous-medium-confining plexiglas tube. The volume of water absorbed

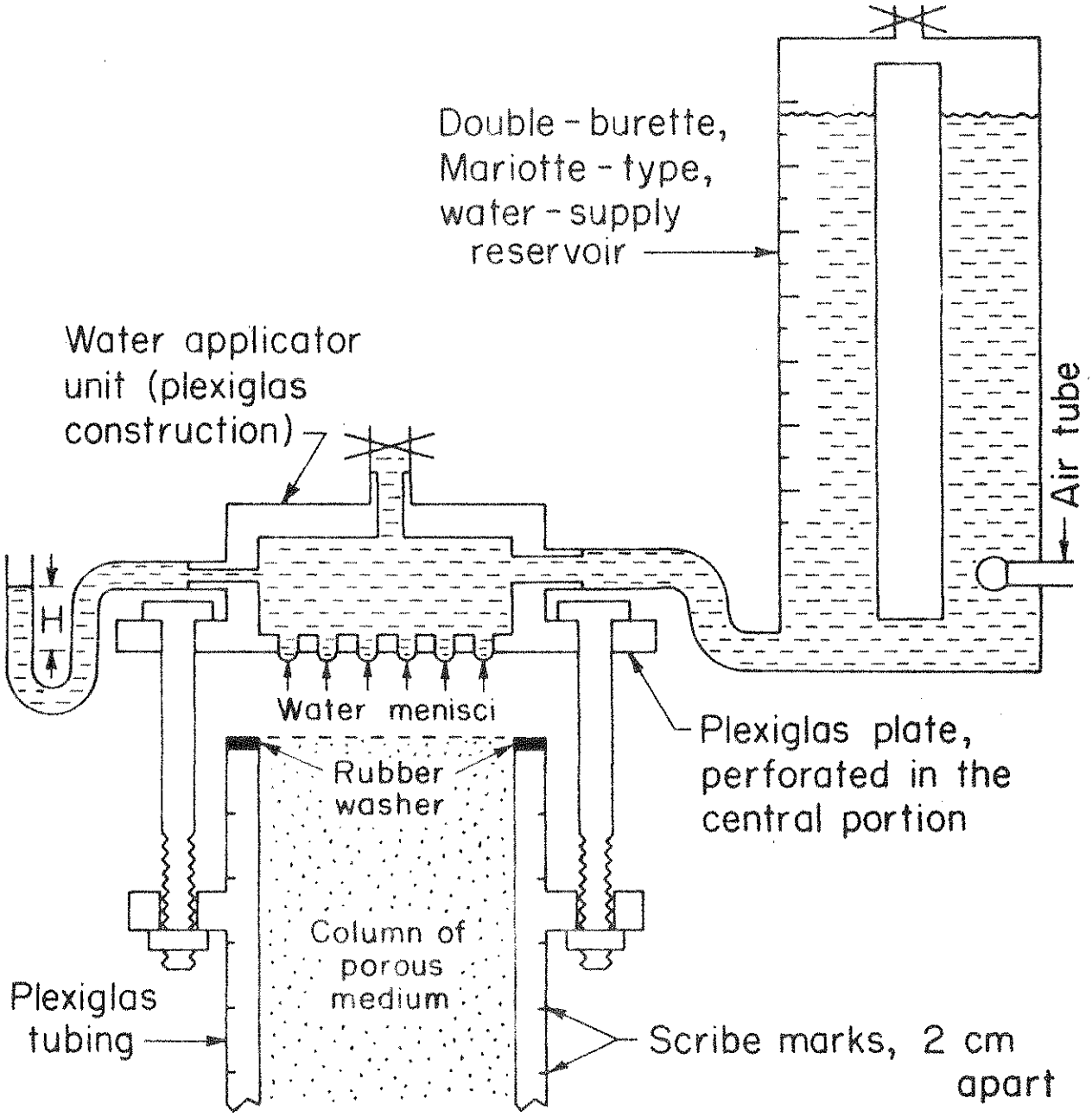

Figure 3--Diagram of experimental apparatus for applying depth H of ponded water essentially instantaneously to the upper-end surface of a column of porous medium.

was determined periodically from the burette readings. These volumes were divided by the cross sectional area of the porous-medium column to obtain the experimental values of y. Air temperature was observed in the vicinity of the flow column, and remained within $\pm$ 0.5 C for any given experiment.

Preparation of Columns

Porous Materials Used

Two porous mixtures were employed, hereinafter referred to as "coarse" and "fine", the coarse one being a weight-basis mixture of 93.75% banding sand[1/] and 6.25% of ground silica (No. 290)[1/], while the fine one was 75% banding sand and 25% ground silica. Both of these materials are essentially composed of quartz, and the air-dry water content of both the coarse and fine mixtures was zero.

Method of Packing

Uniformity of packing is usually somewhat of a problem in column studies, and absolute uniformity is extremely difficult to obtain. It is unrealistic to argue, however, that natural soils will always be perfectly uniform. Hence, the degree of control attempted here was to obtain a reasonable rather than perfect uniformity, and, particularly, to avoid distinct trends in bulk density change from one end to the other of a packed column. To achieve this, the empty confining columns, consisting of plexiglas tubing of 6-mm wall, were circumferentially scribed at 2-cm intervals of column length. Equal masses of porous material were then packed into each of 2-cm section, the amount depending on the bulk density desired. Each individual section was tamped with a large rubber stopper fastened to the end of a long rod. An indication of the uniformity obtained by this method will be given later in this report.

Different Initial Water Contents

For most of the experiments performed, the initial water content was simply the $\theta_o = 0$ of the air-dry mixtures of the coarse and fine materials. However, several series of experiments with $\theta_o > 0$ were carried out, the

---

[1/] Supplied by Ottawa Silica Company, Ottawa, Illinois.

different water contents being obtained as follows:

Mixing porous materials with pulverized ice. A quantity of both the coarse and fine mixtures was placed in a below-freezing cold room to reach temperature equilibrium, and portions were then thoroughly mixed with various amounts of finely pulverized ice. The mixtures were then put in sealed containers and brought again to equilibrium at room temperature, whereupon they were packed in the plexiglas columns as previously. The mixtures with the highest water contents, however, could not be packed as tightly as the corresponding air-dry mixtures. Hence, these experiments at different θ_o had to be carried out at a lower bulk density (dry-weight basis) than those experiments involving only air-dry mixtures. In the case of the coarse mixture, this caused a slight difficulty with the infiltration experiment for the air-dry case ($\theta_o = 0$), in that the total length of column over the course of the experiment contracted by about 0.5 cm, from an initial value of 56.2 cm. However, this affects the overall bulk density by less than 1%, and thus should have negligible direct effects on C and P. Furthermore, indirect effects on C and P, arising from contraction-induced errors in y, can be shown to be inappreciable under the rather reasonable assumption that the instantaneous contraction is proportional to the wet-front depth z.

Water removal by porous pressure plates. To avoid the drawback of working at low bulk densities as just described, shorter flow columns (20.2 cm length) were packed with the fine air-dry ($\theta_o = 0$) material to the usual high (1.90 g/cc) bulk density. Free water was then introduced to the bottoms of the columns as positioned vertically, until free water appeared at the tops of the columns also. The columns, still in vertical position, were then transferred to porous-plate pressure extractors[2/] as slightly modified to accommodate the 20.2-cm columns. Different constant air pressures were then applied in regular sequence to desaturate the columns to different equilibrium water contents, which then became the differing θ_o values for infiltration measurements conducted as before with the apparatus of Figure 3. The disadvantage of this procedure is the long time required for column lengths even as short as 20.2 cm to come to water-

2/ Soilmoisture Equipment Company, 3005 De LaVina Street, Santa Barbara, California.

content equilibrium when positioned on the pressurized porous plates.

Gamma-Ray Apparatus and Measurements

The bulk density and water content of a porous column can be determined by the attenuation of a beam of gamma rays passed through the column perpendicularly to its longitudinal axis. The principles and techniques have been presented in detail by W. H. Gardner (1965), and will not be considered here except as needed to describe the apparatus generally or to indicate special aspects of procedure.

Attenuation Equation Calculations

The basic attenuation equation is

$$I = I_o \exp\left(-X\mu_s\rho_s - X\mu_w\rho_w\theta - X_c\mu_c\rho_c\right) \tag{16}$$

where I_o is the incident flux (counts per unit time) from the gamma-ray source. I is the flux having passed through a distance X of porous medium of bulk density ρ_s, water content θ, and water density ρ_w, as well as a distance X_c of container wall of density ρ_c. Mass attenuation coefficients for the porous-medium particles, the water, and the container walls are denoted by μ_s, μ_w, and μ_c, respectively. For a beam of appreciable width relative to the diameter of a column of circular cross section, the X of equation (1) is some average value less than the diameter of the column, and X_c is also some average value arising from the annular shape of the container-wall cross section. Hence, we set $U_s = X\mu_s$, $U_w = X\mu_w\rho_w$, and $U_c = X_c\mu_c$, so that equation (16) becomes

$$I = I_o \exp\left(-U_s\rho_s - U_w\theta - U_c\rho_c\right) \tag{17}$$

where U_s, U_w, U_c, and $U_c\rho_c$ are simply lumped constants.

If I_d is the flux for a dry soil ($\theta = 0$), the attenuation equation becomes

$$I_d = I_o \exp\left(-U_s\rho_s - U_c\rho_c\right) \tag{18}$$

If I_a is the flux for the empty container tube ($\theta = 0$ and $\rho_s = 0$), the equation is

$$I_a = I_o \exp\left(-U_c\rho_c\right) \tag{19}$$

If I_b is the flux for the tube filled only with water ($\rho_s = 0$ and $\theta = 1$), the equation is

$$I_b = I_o \exp(-U_w - U_c\rho_c) \tag{20}$$

Combining equation (17) with (18), equation (18) with (19), and equation (19) with (20), and solving these combinations for θ, ρ_s, and U_w, respectively, yields

$$\theta = [\ln (I_d/I)]/U_w \tag{21}$$

$$\rho_s = [\ln (I_a/I_d)]/U_s \tag{22}$$

$$U_w = \ln (I_a/I_b) \tag{23}$$

It is seen that U_w in equation (21) is a calibration constant that can be evaluated by equation (23). Determining the calibration constant in equation (22), however, is not so direct when dealing with long columns as in the present study, in which only an average $\bar{\rho}_s$ is known accurately for the column as a whole. Nevertheless, I_a and I_d can be obtained at a number of positions along the column, and equation (22) should apply at each position. Hence, an average ρ_s can be calculated from repeated applications of equation (22), and should be the same as $\bar{\rho}_s$ above; hence

$$U_s = [\overline{\ln (I_a/I_d)}]/\bar{\rho}_s \tag{24}$$

where $\overline{\ln (I_a/I_d)}$ is the average value of all $\ln (I_a/I_d)$ at each position, and $\bar{\rho}_s$ is the average bulk density as determined from the total dry mass of porous medium in the column divided by the total volume of the column, or as known from packing a given mass of dry porous medium into the column volume specified by each 2-cm increment of column length. A similar evaluation applied to U_w of equation (21) yields

$$U_w = [\overline{\ln (I_d/I)}]/\bar{\theta} \tag{25}$$

where $\overline{\ln (I_d/I)}$ again is the average of all $\ln (I_d/I)$ at each position, and $\bar{\theta}$ is the average water content of the porous-medium column as determined by such as direct gravimetric methods.

The brief developments just given for equations (24) and (25) tacitly require U_s and U_w to be the same at all positions along the column, whereas

in actuality both would change somewhat with slight changes in column diameter, as was noted in the development of equation (17). Errors arising from this should be relatively slight, however. Also, although the details will not be presented here, it can be shown that if the variations in U_s are within 2% of its mean $\overline{U}_s$, and those in ρ_s within 25% of its mean $\overline{\rho}_s$, then $\overline{U}_s$ itself is given quite accurately by the right-hand side of equation (24). The same property can be shown for equation (25). Hence, U_s and U_w of these equations can validly be interpreted as means even if they are not strict constants.

In actual practice, progressive decay of source strength and all types of gradual instability in the electronic components of the counting equipment can cause sustained change in the observed value of I_o. This problem is easily circumvented by obtaining occasional gamma-ray fluxes through a constant-length standard such as a rectangular bar of brass. The resulting corrections are obtained by applying the attenuation equation to the brass standard, in a manner similar to the procedures used in obtaining equations (18), (19), and (20), and appear ultimately as standard intensity ratios appropriately multiplying the intensity ratios of equations (21) to (25). If I_o does not change appreciably over the experimentation period involved, the standard intensity ratios will be unity.

Apparatus and Instrumentation

A gamma-ray beam from a 250-mc lead-encapsulated source of Cesium 137 is collimated through a slit in a lead cylinder, with a slit height of 1.9 cm, a horizontal width of 1.0 mm, and a length (in the direction of the beam) of 6.0 cm. The beam is received through a second collimating lead-cylinder slit placed in front of a 5.1-cm diameter sodium iodide crystal of a scintillation probe, the vertical height of this receiving slit being 4.0 cm, the width 1.0 mm, and the beam-direction length 5.2 cm. The distance between the two collimators is 20.0 cm, the central axis of the beam being horizontal. The source and the receiving crystal (also lead shielded) are mounted on the moving carriage of a 3-m metal lathe. The porous-medium column is placed between the collimators horizontally parallel to the lathe-bed ways, so that the longitudinal axis of the

column is perpendicular both to the center axis and vertical plane of the gamma beam. Since the horizontal thickness of the gamma-ray beam is only 1.0 mm, the longitudinal increment of the column "sampled" by the beam is also 1.0 mm.

Pulses from the scintillation crystal are led to an amplifier-analyzer, and thence to an electronic scaler operated by an electronic timer. Simultaneously, the output from the amplifier-analyzer can also go to a ratemeter that drives a strip-chart recorder, an essential feature for transient measurements but not needed for determining bulk densities or steady water contents.

Figure 4 is a photograph of the complete gamma-ray apparatus. 3/

Verification of Attenuation Equation

An experimental test of the attenuation equation was deemed desirable as a check on the overall operational validity of the gamma-ray setup. A short cylindrical plexiglas container 6.34 cm in diameter and 2.0 cm long was used to confine the porous medium consisting of ground silica and banding sand, singly and in mixture, to obtain various values of bulk density $\overline{\rho}_s$. Beginning at 1.5 mm from each end of the 2.0-cm column, gamma-ray readings were taken at 18 positions spaced 1.0 mm apart along the column. Since the sampling thickness of the gamma-ray beam was also 1.0 mm, this means that essentially all of the 2.0-cm column length was eventually subjected to the beam, with the exception of 1 mm at each end. A complete set of 18 readings was taken for the empty plexiglas container, and again for each filling of dry porous medium, to enable the calculation of $\overline{\ln (I_a/I_d)}$ of equation (24) corresponding to the $\overline{\rho}_s$ determined gravimetrically for each filling. Figure 5 shows the results as a plot of $\overline{\ln (I_a/I_d)}$ against $\overline{\rho}_s$, which is in excellent conformity with the linearity of equation (24) rewritten as $\ln (I_a/I_d) = U_s\overline{\rho}_s$. The straight line in the figure is the least squares fit not forced through the origin. However, the small positive intercept of 0.006 fails to be statistically different

3/ The gamma-ray source and all associated electronic components were supplied by the Nuclear-Chicago Corporation, Box 367, Des Plaines, Illinois, except for the strip-chart recorder, which was a Speedomax H of the Leeds and Northrup Company, 4901 Stenton Ave., Philadelphia, Pennsylvania.

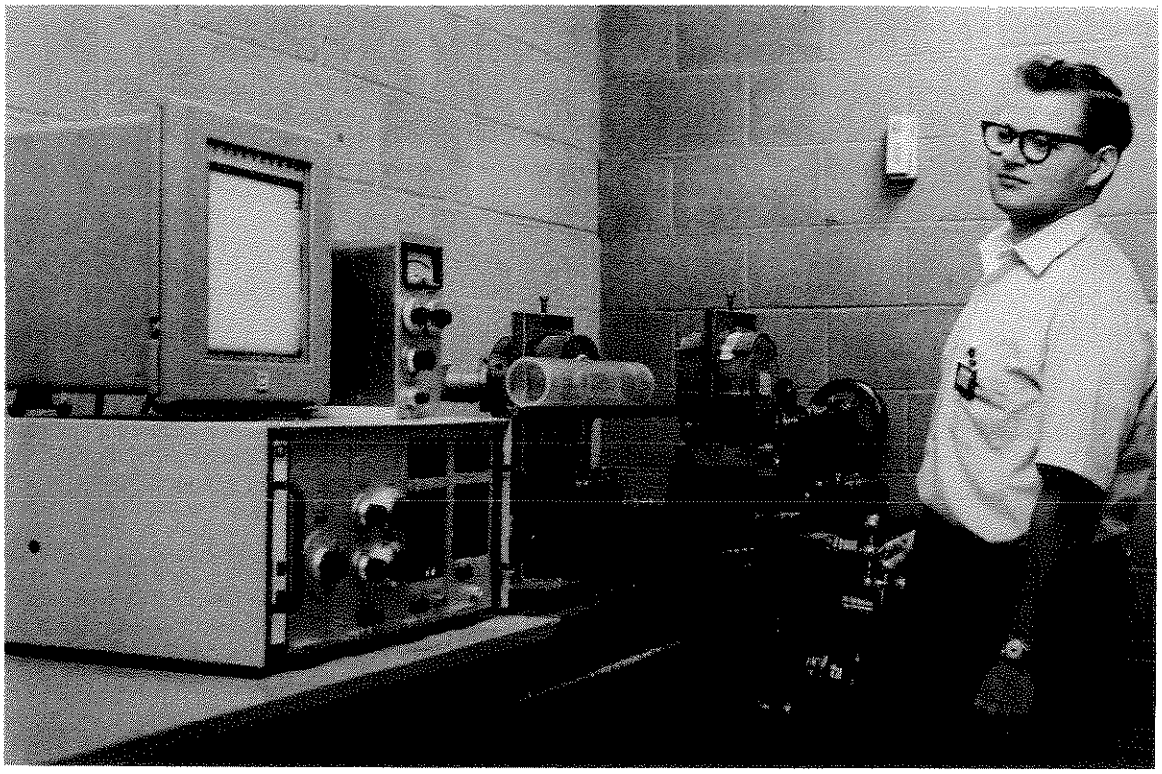

Figure 4--Apparatus for measuring water content and bulk density of a porous medium by gamma-ray attenuation. Horizontal plexiglas tube for confining the porous medium is positioned between the gamma-ray source and the scintillation probe.

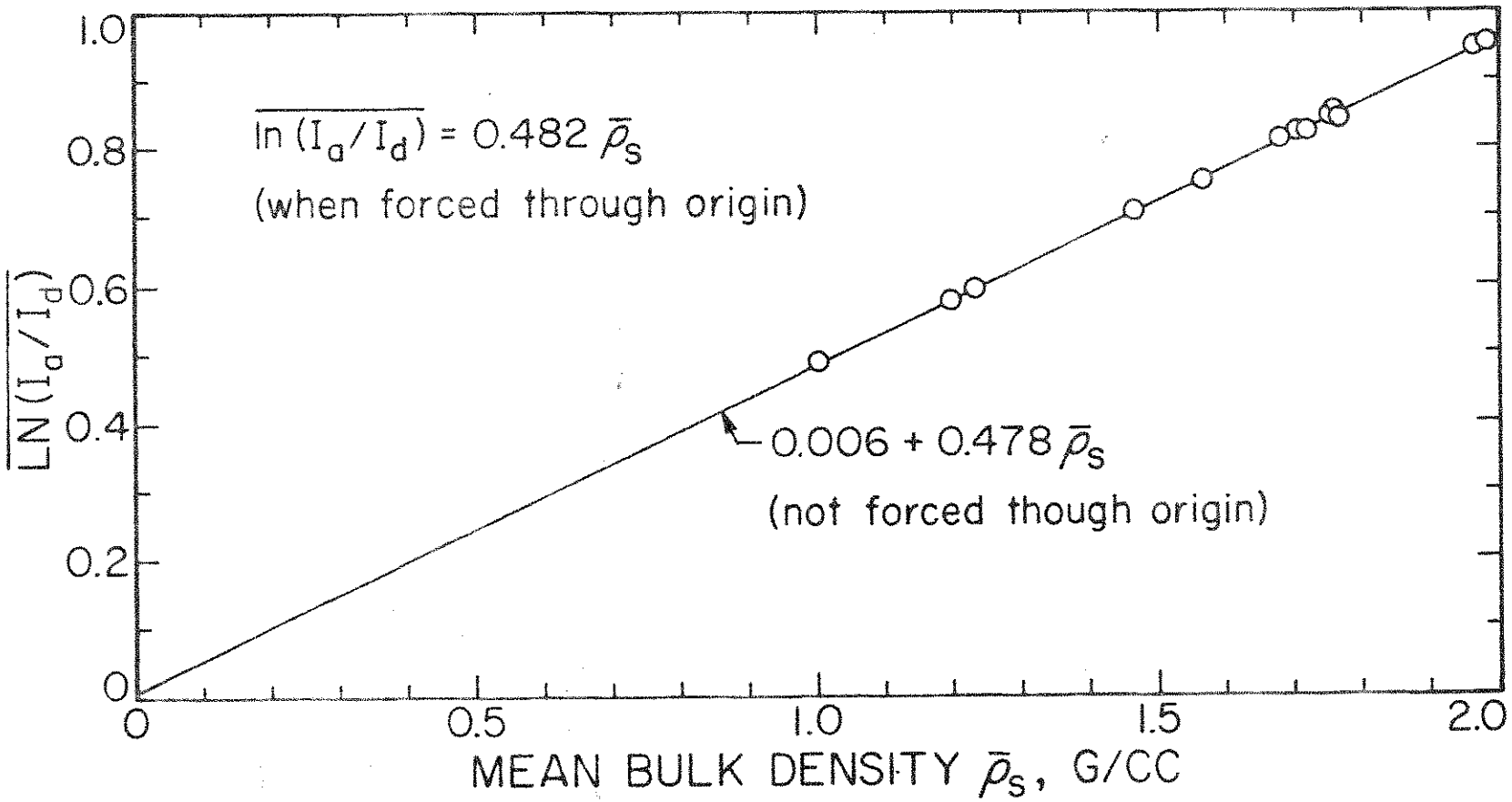

Figure 5--Experimental verification of the gamma-ray attenuation equation, with mean bulk density $\bar{\rho}_s$ as the independent variable.

from zero when the standard t-test is applied, even if the criterion of statistical significance is relaxed to the 25% level instead of the more demanding 5 or 1% levels as commonly used. Hence, the least-squares line can be forced through the origin, to yield $U_s = 0.482$ cc/g.

For seven $\overline{\rho}_s$ values above 1.65 g/cc, and after the I_d readings had been obtained, the porous column was evacuated to less than 1 mm of mercury pressure, and then wetted with water under vacuum. At the 18 positions along the column, gamma-ray readings for wet conditions were taken to enable calculation of $\overline{\ln (I_d/I)}$ of equation (25), whereupon the wet sand was removed and oven dried to determine $\overline{\theta}$. In one instance ($\overline{\rho}_s = 1.718$ g/cc), the column was wetted at atmospheric pressure instead of under vacuum, and was then subjected to water removal by passing dry air through it. This cycle of wetting and drying was repeated several times to obtain different $\overline{\theta}$ as assessed by change in weight of the wet column. At each chosen $\overline{\theta}$, the series of 18 measurements of I for equation (25) was obtained. All of the results are shown in Figure 6 as a plot of $\overline{\ln (I_d/I)}$ against $\overline{\theta}$, which again is in good general conformity with the linearity of equation (25) rewritten as $\overline{\ln (I_d/I)} = U_w\overline{\theta}$. Again the straight line in the figure is the least-squares fit not forced through the origin, and the small intercept of +0.0008 fails to be statistically different from zero at a significance level relaxed to 50% instead of the more demanding 5 or 1% levels commonly used. Hence, the least-squares line can be forced through the origin, to yield $U_w = 0.5291$.

Finally, 18 readings along the cylindrical container were taken with it filled with water only, thus enabling 18 measurements of I_b, and hence U_w, of equation (23). The average U_w from these 18 determinations was 0.5316, and all 18 values were within $\pm$ 1% of this average U_w. Clearly, this value of 0.5316 is very close to the 0.5291 inferred from the origin-forced least-squares straight line fitted to the data of Figure 6, the difference being less than 0.5%. Hence, it was concluded that the gamma-ray setup was operating quite satisfactorily, in the sense that attenuation theory as represented by equations (24) and (25) was well validated. In particular, the close agreement between the determinations of U_w from equations (23) and (25) is taken as good verification of the averaging technique represented by both equations (24) and (25). It should be

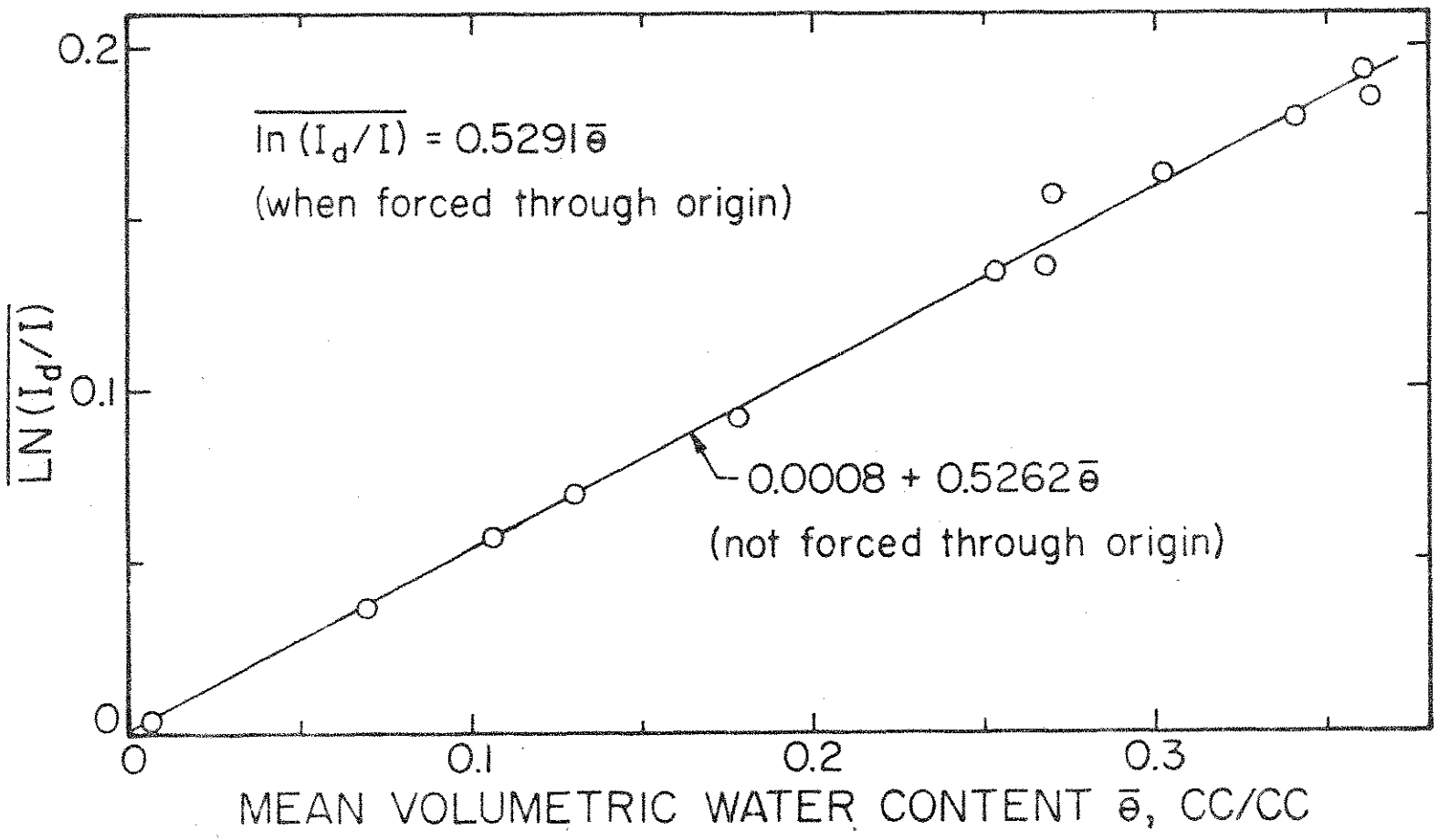

Figure 6--Experimental verification of the gamma-ray attenuation equation, with mean water content $\bar{\theta}$ as the independent variable.

emphasized, however, that the evaluation of U_w normally proceeds most accurately and simply from equation (23) rather than equation (25), whereas for U_s the only approach in most instances will be that of equation (24).

Fine-Particle Translocation

To investigate whether initially high infiltration velocities would measurably translocate the finer particles in a particulate porous medium, two plexiglas tubes 40.0 cm long, 6.2 cm inside diameter, and of 0.6-cm wall thickness were used as confining columns. The empty tubes were first placed in the gamma-ray apparatus to obtain I_a readings [equation (22)] at 0.5-cm increments of tube length. Using the 2-cm increment filling method described earlier, both tubes were filled with the fine mixture, one to a bulk density of 1.80 g/cc and the other to 1.90 g/cc. Gamma-ray measurements at each 0.5-cm position were repeated to obtain the I_d values of equation (22). Equation (24) was used to obtain U_s, in turn used to calculate ρ_s from equation (22) at each 0.5-cm position. Each tube was then positioned vertically and subjected to downward infiltration as described in connection with Figure 3. Thereupon, dried and slightly warmed air was forced through each column at a slow rate until all water had been removed, as determined by precise weighings of each column compared with its initial dry weight prior to infiltration. Each dried column was then placed horizontally into the gamma-ray apparatus to obtain a second set of I_d readings at each 0.5-cm position, with ρ_s again calculated from equation (22). Thus, it was possible to obtain precise and nondestructive measurements of bulk density versus position, both before and after the occurrence of water infiltration. If fine particles were translocated out of the water-inlet region of the column and redeposited at some deeper position, a corresponding shift in the bulk-density distribution should be detectable. From the infiltration data, a test of equation (15) was possible, to determine whether flow deviations, if any, could be meaningfully related to any shift in the bulk-density distribution.

Analysis of Data

The fitting of equation (4) to data of cumulative infiltration y versus time t is complicated by the presence of the constant a in the

logarithmic term. Experimental data, however, can be plotted on translucent log-log graph paper used as an overlay, which is then matched by horizontal and vertical translation to an underlay plot of equation (4) prepared on the same kind of log-log graph paper. This method, similar to the matching of the theoretical curves of Figure 2, is workable only if the experimental data follow the theoretical curve very precisely; otherwise subjective fitting errors are inevitable. Because of this weakness, the log-log overlay-underlay graphical technique was eventually discarded, even though a number of attempts had been made to use it.

To fit equation (4) by least squares, the sum of squares of the t deviations is minimized, since t is given as an explicit function of y rather than vice versa. The sum of squares thus formulated is

$$\sum_{j=1}^{p} (t_j - \hat{t}_j)^2 = \sum_{j=1}^{p} [t_j - (y_j/C) + (a/C) \ln (1 + y_j/a)]^2 \qquad (26)$$

where $\hat{t}_j$ is simply the t of equation (4) with a subscript j, and p is the total number of experimental pairs of y_j and t_j. The sum in equation (26) is minimized in the conventional way by taking partial derivatives with respect to C and a and setting equal to zero. Doing this for C and solving for C yields

$$C = \frac{\sum_{j=1}^{p} a[(y_j/a) - \ln (1 + y_j/a)]^2}{\sum_{j=1}^{p} t_j[(y_j/a) - \ln (1 + y_j/a)]} \qquad (27)$$

Taking the partial derivative with respect to a and setting equal to zero yields

$$\sum_{j=1}^{p} [Ct_j - y_j + a \ln (1 + y_j/a)][\ln (1 + y_j/a) - y_j/(y_j + a)] = T = 0 \qquad (28)$$

where T simply denotes the summation expression.

Equation (28) with T = 0 cannot be solved explicitly for a, since a is in the logarithmic term. Note, however, that for a given set of p pairs of y_j and t_j, C of equations (27) and (28) becomes a function only

of a, so that T defined by the first equality of equations (28) also becomes a function only of a. Hence, in equation (27) and the first of equations (28), trial values of a can be used until one is found that makes T = 0. This is the least-squares value of a, and its substitution into equation (27) yields the least-squares value of C. The computations just described are much too lengthy for a desk calculator, but can be handled with ease by electronic computer. Using Newton's method of iterative approximation, the calculational process was programmed and carried out on Purdue University's CDC 6500 Computer.

A computer approach to the fitting of equation (15) was also developed, primarily as a more objective and rapid method of determining dy/dt for experimental data. The technique may be viewed as a sliding least squares. For a given group of six consecutive experimental pairs of y and t (designated as points 1, 2, 3, 4, 5, and 6), the second-degree polynomial

$$t = \alpha + \beta y + \gamma y^2 \tag{29}$$

is fitted by a special least-squares scheme in which the two central points (3 and 4) are weighted most heavily, the next two outlying points (2 and 5) less heavily, and the two outermost points (1 and 6) are weighted least. Specifically, the weights chosen were 5.0, 3.0, and 1.0 for points 3 and 4, 2 and 5, and 1 and 6, respectively. From equation (29), $dt/dy = \beta + 2\gamma y$, which by taking the reciprocal gives

$$dy/dt = 1/(\beta + 2\gamma y) \tag{30}$$

Using the β and γ fitted by the special least-squares technique, dy/dt was calculated from equation (30) at the midpoint of the center interval (delimited by points 3 and 4), the midpoint being specified on the basis of the y variable as $(y_3 + y_4)/2$. The foregoing six-point analysis is then repeated by including the next point beyond point 6 and excluding the former point 1, continuing until all data points have been thus analyzed in sliding groups of six.

If derivatives are to be calculated for the first two and last two intervals of a complete set of (y,t) data, the foregoing procedure must be somewhat modified when dealing with the first six and last six points. Using the first six points to illustrate, and considering the first interval (delimited by points 1 and 2), the weighting scheme of the

least-squares fit of equation (29) is changed to 5.0 for point 1, 4.0 for point 2, 3.0 for point 3, 2.0 for point 4, and 1.0 for points 5 and 6. The dy/dt of equation (30) is then calculated for the midpoint $(y_1 + y_2)/2$ of the first interval. For the second interval (delimited by points 2 and 3), the weighting scheme is changed to 5.0 for points 2 and 3, 3.0 for points 1 and 4, and 1.0 for points 5 and 6; the dy/dt of equation (30) is then calculated for the midpoint $(y_2 + y_3)/2$ of the second interval. For the third interval, the procedure becomes the primary one described in the previous paragraph. When the last six points are reached, the weightings and procedures become simply the reverse of those just described for the first six points.

Computations of bulk density and water content on the basis of equations (21) through (25), while capable of being handled without an electronic computer, were nevertheless programmed for and performed by Purdue's CDC 6500. A primary reason for this was to avoid the lengthy task of looking up logarithms in a table.

Summarization of Flow Experiments Performed

The various flow experiments as conducted are gathered in Table 1, to express in a concise, orderly, and uniform manner the flow studies that were carried out.

Table 1. Summary of flow experiments.

Experiment No.	Type[1] and material	No. of determinations	θ_o	$\bar{\rho}_s$	Overall column		L_1
					Length	Diameter[2]	
			cc/cc	g/cc	cm	cm	cm
1	Uniform, coarse	2	0	1.75	56.2	3.8	--
2	Uniform, fine	2	0	1.90	56.2	3.8	--
3	Stratified, coarse/fine	1	0	1.75/ 1.90	56.2	3.8	10.2
4	"	1	0	"	"	"	20.2
5	"	1	0	"	"	"	30.2
6	"	1	0	"	"	"	40.2
7	Stratified, fine/coarse	1	0	1.90/ 1.75	56.2	3.8	10.2
8	"	1	0	"	"	"	20.2
9	"	1	0	"	"	"	30.2
10	"	1	0	"	"	"	40.2
11	Uniform, coarse	1	0	1.54	56.2	3.8	--
12	"	1	0.046	"	"	"	--
13	"	1	0.082	"	"	"	--
14	"	1	0.129	"	"	"	--
15	Uniform, fine	1	0	1.64	56.2	3.8	--
16	"	1	0.066	"	"	"	--
17	"	1	0.116	"	"	"	--
18	"	1	0.152	"	"	"	--
19	Uniform, fine	1	0	1.90	20.2	3.8	--
20	"	1	0.078	"	"	"	--
21	"	1	0.116	"	"	"	--
22	"	1	0.126	"	"	"	--
23	"	1	0.128	"	"	"	--
24	"	1	0.144	"	"	"	--
25	Uniform, fine[3]	1	0	1.80	40.2	6.2	--
26	Uniform, fine[3]	1	0	1.90	40.2	6.2	--

[1] Refers to whether column is uniform or stratified.

[2] Nominal value of diameter.

[3] These columns particularly included to study fine-particle translocation.

RESULTS AND DISCUSSION

Infiltration into Initially Dry Media

Uniform Columns

The results here considered are for the four uniform columns of experiments 1 and 2 of Table 1, labelled in Table 2 as 1A and 1B for the two replicates on coarse material, and 2A and 2B for the two replicates on fine material. In each case, data were taken until the wet-front depth z approached the bottom end of the 56.2-cm columns. Thus, the least squares fits [from equations (27) and (28)] for these complete sets of data are identified in Table 2 as having a maximum wet-front depth of 56.2 cm. However, it was deemed instructive also to calculate the fit for certain sub-ranges of the data, to determine the effect on the fitted C and a. These subranges were chosen as y-versus-t data for z intervals of 0 to 10.2, 0 to 20.2, 0 to 30.2, and 0 to 40.2 cm, to match with the values of L_1 of the stratified systems of Table 1.

The mean-square deviations shown for each full range and sub-range of data in Table 2 give an indication of goodness of fit of equation (4), and would be zero if the data points fell perfectly on the theoretical curve. For any given column, it is seen that the mean-square deviation increases progressively as the sub-range changes from a maximum z of 10.2 cm up to the full-range value of 56.2 cm. The largest mean-square deviation (18.31 min^2) in Table 2, occurring in experiment 2B for the full range (56.2 cm) of data, should represent the poorest fit of any set of data in the table. Therefore, these data are plotted in Figure 7, along with equation (4) using the least-squares values a = 9.52 cm and C = 0.00559 cm/min. It is apparent that even for this so-called poorest fit, the curve passes through the points in quite an acceptable manner.

Experiment 1B for a maximum z of 10.2 cm, however, represents a difficulty worthy of special description. The computer solution of equations (27) and (28) yielded a = 7677 cm and C = 8.23×10^{-5} cm/min, both values being quite out of line with all other values of a and C for experiments 1A and 1B. Nevertheless, the product aC = 0.632 cm^2/min did compare very reasonably with its counterpart values in these two experiments. To account for such behavior, it is noted that for small y/a equation (4) becomes

$$y^2 = 2aCt \qquad (31)$$

Table 2. Fitted infiltration parameters for duplicate columns of coarse and fine material, θ_o = 0 (air-dry).

Description	Max. z	M.S. deviation [1]	C	a	aC	M	P	C_{20}
		10^{-2}	10^{-3}		10^{-2}		cm	10^{-3}
	cm	min^2	cm/min	cm	cm^2/min	cc/cc	H_2O	cm/min
Exp. No.1A	10.2	0.20	84.1	6.47	54.4	0.246	25.2	76.7
coarse, ρ_s=	20.2	0.40	52.2	11.07	57.8	0.246	43.9	47.6
1.75 g/cc,	30.2	2.38	71.7	7.41	53.1	0.248	28.8	65.4
23.9 °C	40.2	4.33	79.9	6.33	50.6	0.249	24.3	72.9
	56.2	11.06	90.4	5.14	46.5	0.252	19.3	82.4
						Means:	28.3	69.0
Exp. No.1B	10.2	--	73.4 [2]	8.61 [3]	63.2	0.249	33.5	66.1
coarse, ρ_s=	20.2	1.99	67.8	8.40	57.0	0.249	32.6	61.0
1.75 g/cc,	30.2	4.44	58.2	10.06	58.5	0.249	39.3	52.4
24.4 °C	40.2	34.71	88.8	5.55	49.3	0.255	20.6	80.0
	56.2	57.62	78.8	6.66	52.5	0.255	25.0	71.0
						Means:	30.2	66.1
Exp. No.2A,	10.2	6.5	7.36	7.23	5.32	0.197	35.6	6.89
fine, ρ_s =	20.2	28.8	5.21	10.65	5.55	0.206	50.5	4.88
1.90 g/cc,	30.2	41.3	5.42	10.18	5.52	0.212	46.8	5.07
22.8 °C	40.2	411.1	4.15	14.26	5.92	0.212	66.0	3.88
	56.2	637.6	4.77	11.94	5.70	0.212	55.1	4.46
						Means:	50.8	5.04
Exp. No.2B	10.2	1	6.39	9.38	5.99	0.192	47.7	5.90
fine, ρ_s =	20.2	32	3.60	17.02	6.13	0.202	82.9	3.33
1.90 g/cc,	30.2	70	3.66	16.66	6.10	0.204	80.4	3.38
23.3 °C	40.2	112	3.91	15.42	6.03	0.203	74.9	3.61
	56.2	1831	5.59	9.52	5.32	0.215	43.2	5.17
						Means:	65.8	4.28

[1] Mean-square deviation = $\sum_{j=1}^{p}(t_j - \hat{t}_j)^2/p$, from equation (26).

[2] Mean of four C's immediately following.

[3] Calculated as aC/(mean C) = (0.632)/(0.0734).

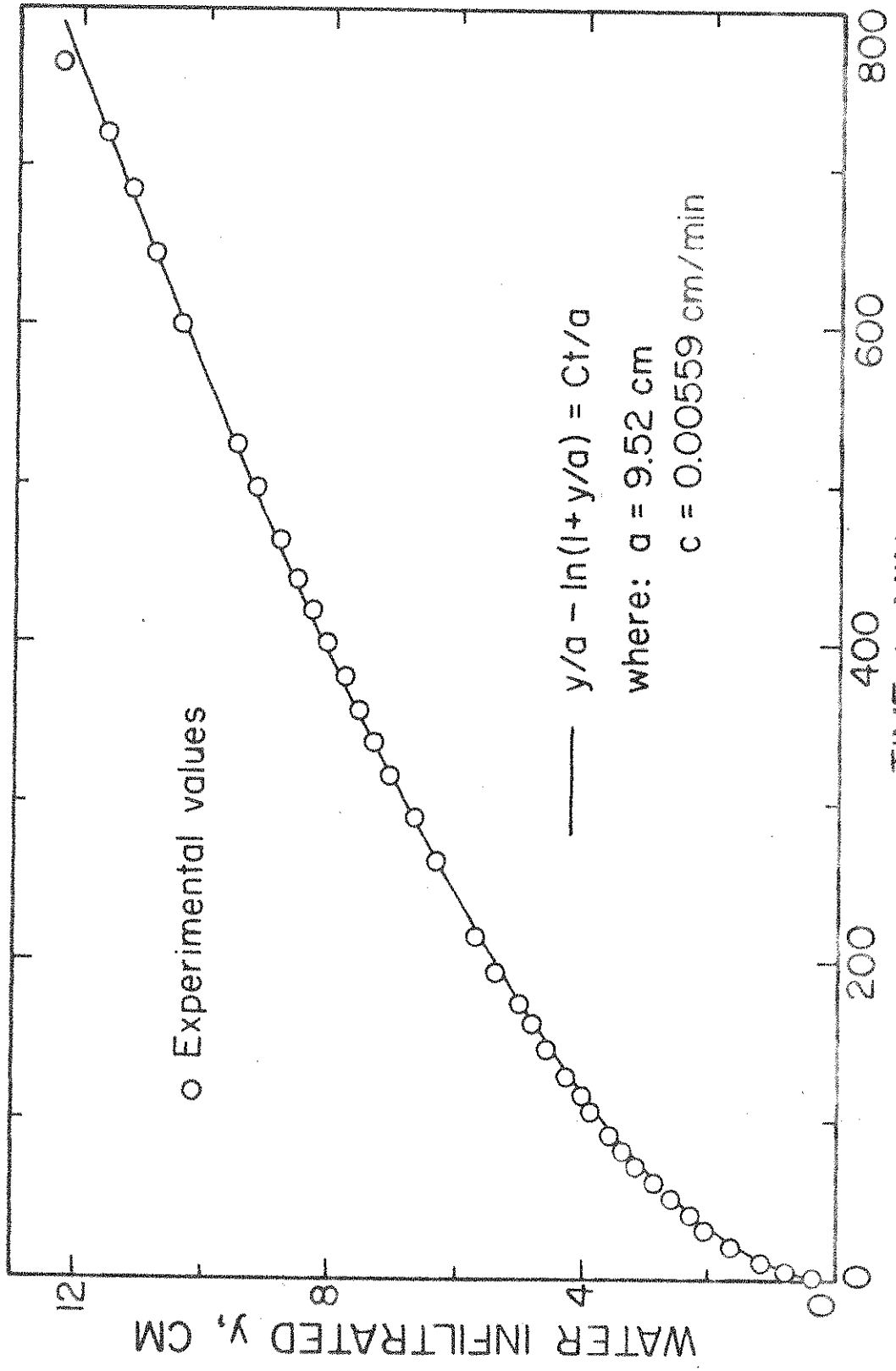

Figure 7--Illustration of the least-squares fit of equation (4), using data of experiment 2B of Table 2 for a maximum z of 56.2 cm, and for which the mean-square deviation is the largest in Table 2.

which, if solved for y, expresses the familiar square-root-of-time relationship for horizontal water absorption, which can also be readily derived for a horizontal porous-medium column by the approach embodied in equations (1) through (4). Hence, the mathematical solution for horizontal flow, as given by equation (31), may be viewed as a first-stage solution for vertical infiltration at sufficiently small times. In Figure 2, this is the region where the log-log plot has a slope of 1/2, and it is impossible to evaluate a and C separately. Instead, only the produce aC can be evaluated from data of y versus t or vice versa. Thus, for a given set of (y,t) data which appears to be parabolic in the sense of equation (31), whether because of small times or experimental error, the least-squares fitting process represented by equations (28) as solved by Newton's method can only make T approach zero by letting a become large. This, then, makes y/a small, as required to make equation (4) degenerate into equation (31). So, even though the large a and small C are meaningless individually, their product should still be meaningful in the sense of equation (31). If the foregoing arguments are correct, then an alternative and more direct least-squares fitting method could be devised on the basis of equation (31), by choosing $\hat{t}_j = y_j^2/2aC$ for use in equation (26). When this was done and the calculations carried out, the resulting aC agreed perfectly with the 0.632 cm^2/min as found earlier. In view of all of the foregoing, more realistic individual estimates of a and C for this particular 10.2-cm sub-range (experiment 1B) were sought as follows: C was taken as the mean of the four C's determined for the full range and the three remaining sub-ranges of experiment 1B. This mean C (0.0734 cm/min) was then divided into the least-squares aC (of 0.632 cm^2/min) to obtain a = 8.61 cm.

The values of M in Table 2 were calculated on the basis of equation (3) from experimental plots of y against z. In general, the proportionality of these plots was quite good, and straight lines through the origin were drawn through the points by eye. Lines of different slope were drawn for the different sub-ranges if required, but it is clear from the table that these differences are very slight within a given material. From a, M, and H (=1.1 cm in most cases), P was calculated by equation (5). Corrections of C for temperature effects on water viscosity were made by assuming C to be inversely proportional to viscosity η at the temperature of the experi-

ment. If C_{20} and η_{20} are the respective values of C and η at 20 degrees centigrade, the correction takes the form

$$C_{20} = C\eta/\eta_{20} \qquad (32)$$

which is the basis on which the C_{20} values in Table 2 were calculated.

Perusal of Table 2 shows that M varies but slightly within sub-ranges or duplications, whereas between coarse and fine materials there is a small difference that is correctly related to the difference in bulk density. With regard to P and a, however, it is somewhat disappointing to encounter 2-fold variations within sub-ranges, since effort was made to achieve uniform packing. Nevertheless, for P the means within duplications are reasonably close, and the means for coarse and fine materials are distinctly separated in the proper sense; that is, the coarse would be expected to have a smaller P than the fine, and this is what is actually found. Considering C_{20}, the variation within sub-ranges is also disappointingly high even though it is somewhat less than 2 fold, but within duplications the means are satisfactorily close. Furthermore, C_{20} distinguishes between coarse and fine in drastic fashion, with at least a 13-fold difference in values and in the correct sense of designating the coarse material to be more permeable than the fine.

Finally, it is pertinent to consider the behavior of aC, since this quantity from equation (31) could be made the basis for characterizing water absorption by a horizontal column. Clearly, aC is nicely stable within sub-ranges and duplications, and still distinguishes properly and quite markedly between coarse and fine materials. Hence, the use of aC in establishing a and C would appear to have merit, but for fullest utilization would require an independent and more precise means of determining either C alone or a alone, so that the remaining undetermined parameter could in turn be calculated more precisely from aC.

Stratified Columns

The results considered here are for experiments 3 through 10 of Table 1, involving stratified columns as diagrammed in Figure 1. First to be assessed is whether the mean water content behind the wet front, expressed as $\overline{\theta} - \theta_o = M$ [equation (3)], is the same for a given material whether in uniform or stratified conditions. Graphical illustrations of

how M_1 and M_2 for stratified columns were obtained are shown in Figure 8 for experiments 5 and 9, for an upper layer of L_1 = 30.2 cm for both coarse above fine and fine above coarse. For coarse above fine, the shift from M_1 to M_2 is just a very simple break in the slope of the two straight lines at $z = L_1$ = 30.2 cm. But for fine above coarse, the transition from one major straight line to the other is somewhat more complex. On the whole, the data in the figure indicate a reasonably good initial proportionality of slope M_1, followed eventually by a linearity of different slope M_2.

When the wet front is in the upper (subscript 1) stratum of a stratified column, there is little reason to expect that the resulting M_1 should be different from the M of the same material in a completely uniform column. This is well verified in Table 3, where in every case M_1 agrees very well with the corresponding M. The same is true when M_2 [equation (11)] is compared with M for all of the stratifications in which the coarse material is above the fine (experiments 3 through 6). But when the fine material is above the coarse, M_2 for the underlying coarser material is distinctly less than M, and tends to become progressively smaller as the length L_1 of the upper (fine) stratum increases (experiments 7 through 10). This implies that if a finer textured material is interposed between a given porous material and the free-water depth H on the surface, the given (coarser) material will not wet to as great a $\bar{\theta}$ as it would if it were itself extended all the way to the free water, or as it would if the interposed stratum were even more coarse than the given material. Hence, this suggests that equation (12) might be less applicable for fine-over-coarse than for coarse-over-fine stratifications, particularly if M_2 in equation (13) were taken as the M determined from uniform-column experiments.

We next consider the use of equations (8) and (12) to predict the actual stratified-column behavior as observed in experiments 3 through 10. Two schemes were employed for arriving at the constants to be used in the equations. In the first scheme, the duplicate determinations for the coarse and fine materials of uniform experiments 1 and 2 were averaged to obtain the necessary values of M_1 and P_1 to calculate a_1, of M_2 and P_2 for calculating b and c, and of C_1 and C_2 to be used directly and in calculating c. C_1 and C_2 were also corrected to the temperature of the stratified experiments by a calculation similar to equation (32). It should be noted that the foregoing scheme is the one

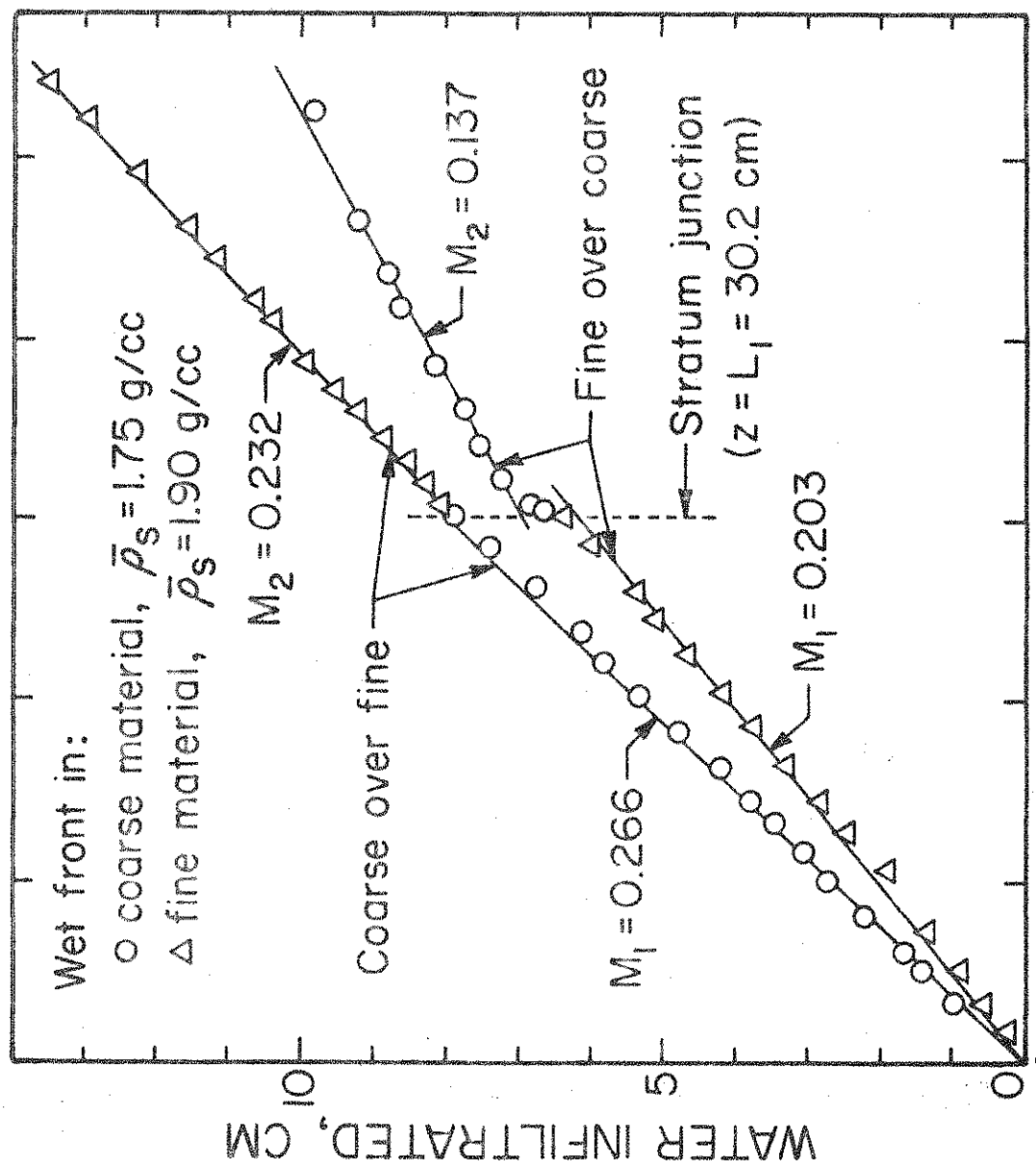

Figure 8.--Water infiltrated versus wet-front advance, for stratified porous-medium columns of coarse over fine and fine over coarse, with depth of upper stratum L_1 = 30.2 cm in both instances.

Table 3. Comparison of M_1 and M_2 of stratified systems with corresponding values of M for uniform systems.

Stratified Columns						Uniform Columns		
Exp. No.[1]	Stratum Subscript[2]	Length	Material	M_1	M_2	M[3]	Max. z	Exp. No.[1]
		cm		cc/cc	cc/cc	cc/cc	cm	
3	1	10.2	coarse	0.249	--	0.248	10.2	1
	2	46.0	fine	--	0.216	0.214	56.2	2
4	1	20.2	coarse	0.267	--	0.248	20.2	1
	2	36.0	fine	--	0.230	0.208	40.2	2
5	1	30.2	coarse	0.266	--	0.248	30.2	1
	2	26.0	fine	--	0.232	0.208	30.2	2
6	1	40.2	coarse	0.255	--	0.252	40.2	1
	2	16.0	fine	--	0.230	0.204	20.2	2
7	1	10.2	fine	0.182	--	0.194	10.2	2
	2	46.2	coarse	--	0.185	0.253	56.2	1
8	1	20.2	fine	0.204	--	0.204	20.2	2
	2	36.0	coarse	--	0.155	0.252	40.2	1
9	1	30.2	fine	0.203	--	0.208	30.2	2
	2	26.0	coarse	--	0.137	0.248	30.2	1
10	1	40.2	fine	0.204	--	0.208	40.2	2
	2	16.0	coarse	--	0.138	0.248	20.2	1

[1] From Table 1.

[2] Subscript 1 denotes upper stratum and subscript 2 denotes lower stratum in Figure 1B.

[3] Mean of two determinations.

which would have to be employed in any practical utilization of equations (8) and (12) for predicting infiltration into stratified systems.

Nevertheless, the foregoing scheme is subject to any discrepancies involved in predicting the behavior of even a single uniform column from the mean characterization of two uniform columns, and the variations of C and P within sub-ranges in Table 2 suggest that such discrepancies might be appreciable. To attempt to remove such error, a second scheme was devised in which as many as possible of the constants in equations (8), (12), (13), and (14) were obtained from experimental observations on the stratified column itself. Hence, M_1, P_1, and C_1 were determined for the stratified column while the wet front was within the upper (subscript 1) stratum, C_1 and a_1 being the constants of the least-squares fit of equation (8). When the wet front was in the lower (subscript 2) stratum, M_2 was determined by plotting y_2 against z in accord with equation (11) (the M_2 values of Table 3). Effort also was made to determine b, c, and C_2 while the wet front was in the lower stratum, but without success. Hence, to enable a calculation of b and c from equations (13) and (14), the values of C_2 and a_2 [second of equations (13)] as computed in the first scheme were retained for use in the second scheme also. The parameters as used in both schemes are summarized in Table 4.

The results of the two foregoing prediction schemes, along with the experimentally observed infiltration data for the stratified columns of experiments 3 through 10, are shown in Figures 9 through 12. Results for both coarse-over-fine and fine-over-coarse for a given L_1 are shown on the same graph, with the solid-line curve representing the first-scheme prediction, and the broken-line curve the second scheme. The origin of coordinates is that of equation (8), the ordinate and abscissa becoming $y_o + y_2$ and $t_o + t_2$, respectively, when the wet front moves into the lower stratum, as discussed previously following equation (12). Where no broken-line curve is shown, it is essentially the same as the solid-line curve. The theoretical points at which the wet front strikes the stratum junction are indicated by arrows on the curves.

For all coarse-over-fine cases, the agreement between experiment and theoretical prediction is reasonably good, and in two cases is some-

Table 4. Parameters used in equations (8) and (12) for predicting infiltration into stratified columns.

For Exp.No.	L_1	Scheme[1]	y_o[2]	a_1	C_1	b	C_2	c
	cm		cm	cm	10^{-3} cm/min	cm	10^{-3} cm/min	cm
3	10.2	first	2.515	7.54	80.3	12.91	5.42	0.1465
		second	2.530	5.51	73.3	12.93	5.42	0.1619
4	20.2	first	4.990	9.74	61.0	19.06	4.22	0.2899
		second	5.383	10.25	46.0	19.51	4.22	0.4257
5	30.2	first	7.495	8.73	66.2	19.78	4.75	0.4512
		second	8.022	5.22	87.1	20.49	4.75	0.3817
6	40.2	first	10.132	5.94	86.0	22.07	4.61	0.4401
		second	10.241	5.38	86.8	23.10	4.61	0.4906
7	10.2	first	1.976	8.31	6.84	8.46	82.0	30.84
		second	1.849	9.05	5.84	7.77	82.0	26.40
8	20.2	first	4.123	13.86	4.44	11.03	82.7	94.77
		second	4.113	13.02	4.60	9.06	82.7	56.10
9	30.2	first	6.288	13.49	4.52	16.22	63.0	104.41
		second	6.132	7.54	6.84	12.85	63.0	37.95
10	40.2	first	8.345	14.87	4.00	19.68	58.0	144.14
		second	8.205	6.96	7.10	15.27	58.0	45.17

1/ In the first scheme, tabular values are derived from averages determined from uniform columns; in the second scheme, values are derived from the stratified column itself, inasmuch as possible.

2/ Calculated as $L_1 M_1$, where M_1 is an average for the first scheme, and a single value for the second scheme.

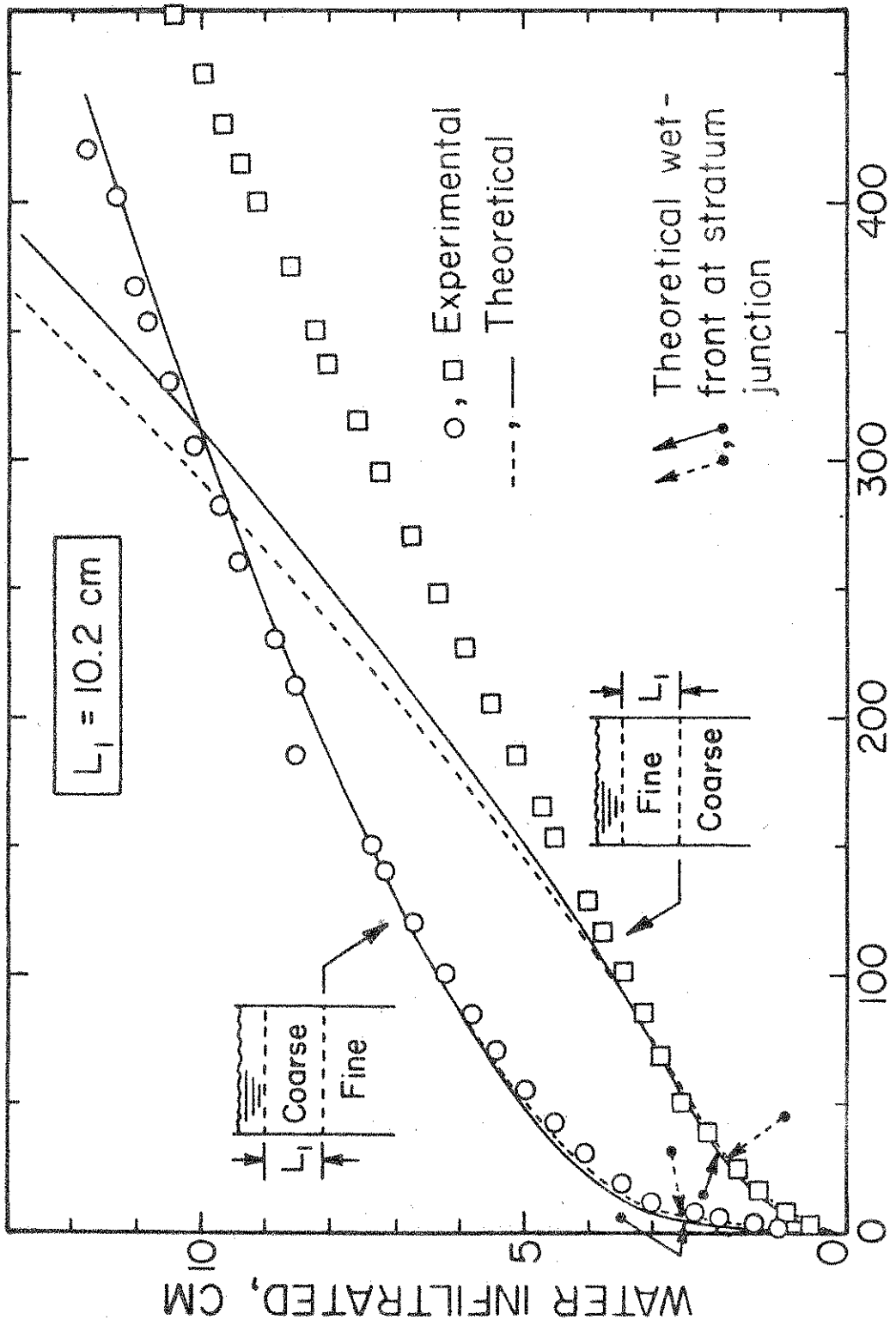

Figure 9--Water infiltrated versus time, experimental and predicted [equations (8) and (12)] for coarse-over-fine and fine-over-coarse stratifications, upper stratum L_1 = 10.2 cm. See text for explanation of theoretical curves.

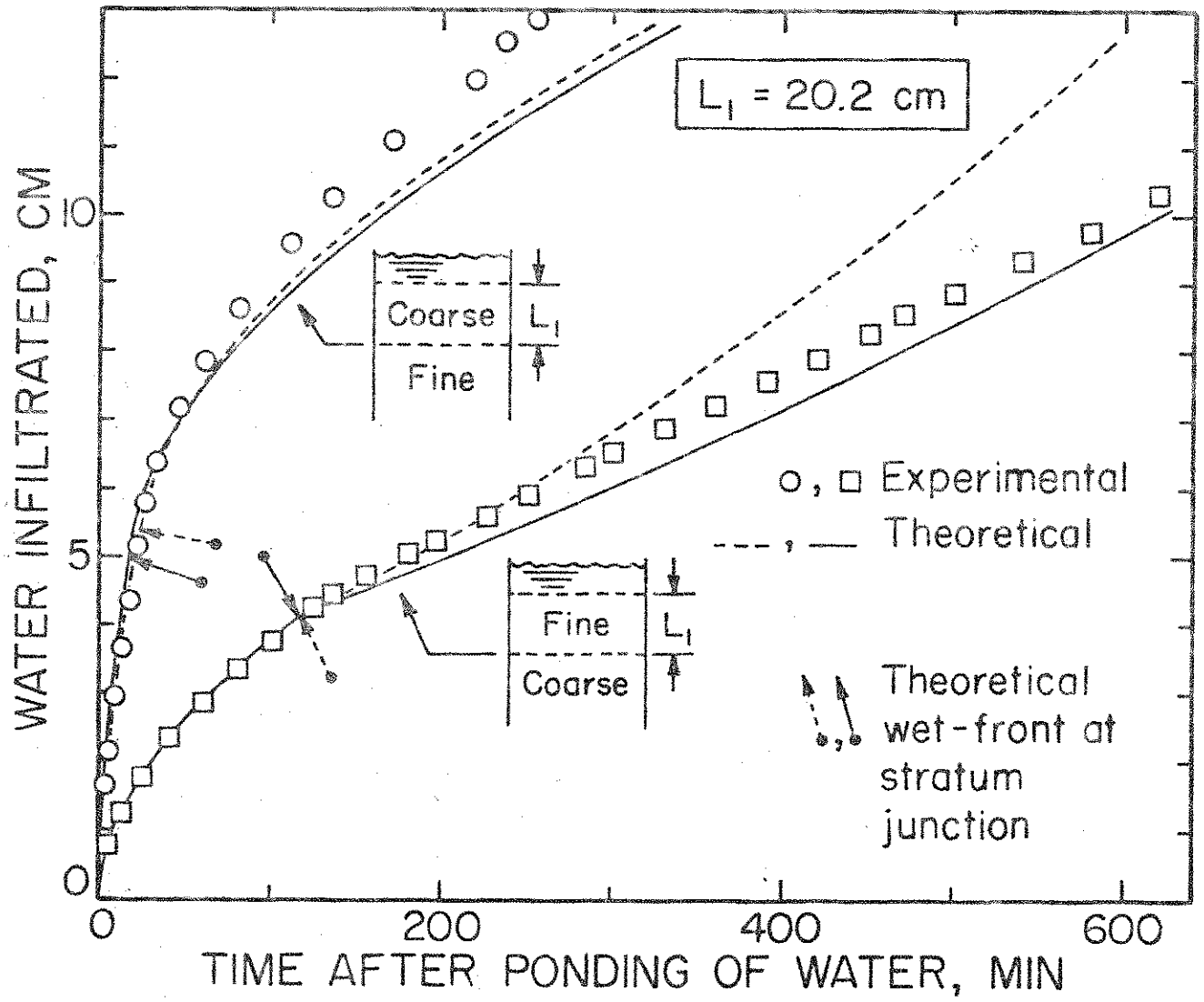

Figure 10--Water infiltrated versus time, experimental and predicted [equations (8) and (12)] for coarse-over-fine and fine-over-coarse stratifications, upper stratum L_1 = 20.2 cm. See text for explanation of theoretical curves.

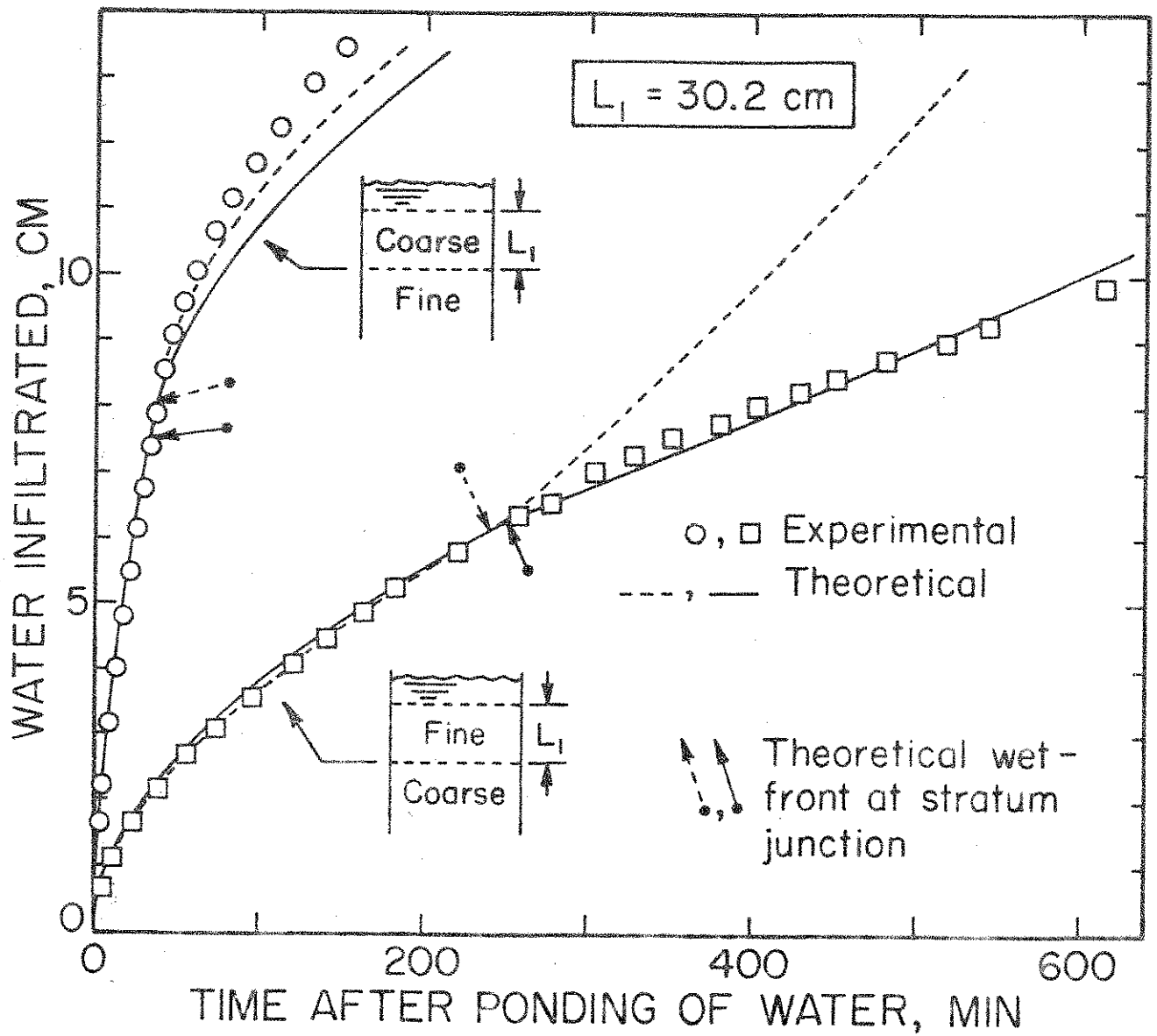

Figure 11--Water infiltrated versus time, experimental and predicted [equations (8) and (12)] for coarse-over-fine and fine-over-coarse stratifications, with upper stratum L_1 = 30.2 cm. See text for explanation of theoretical curves.

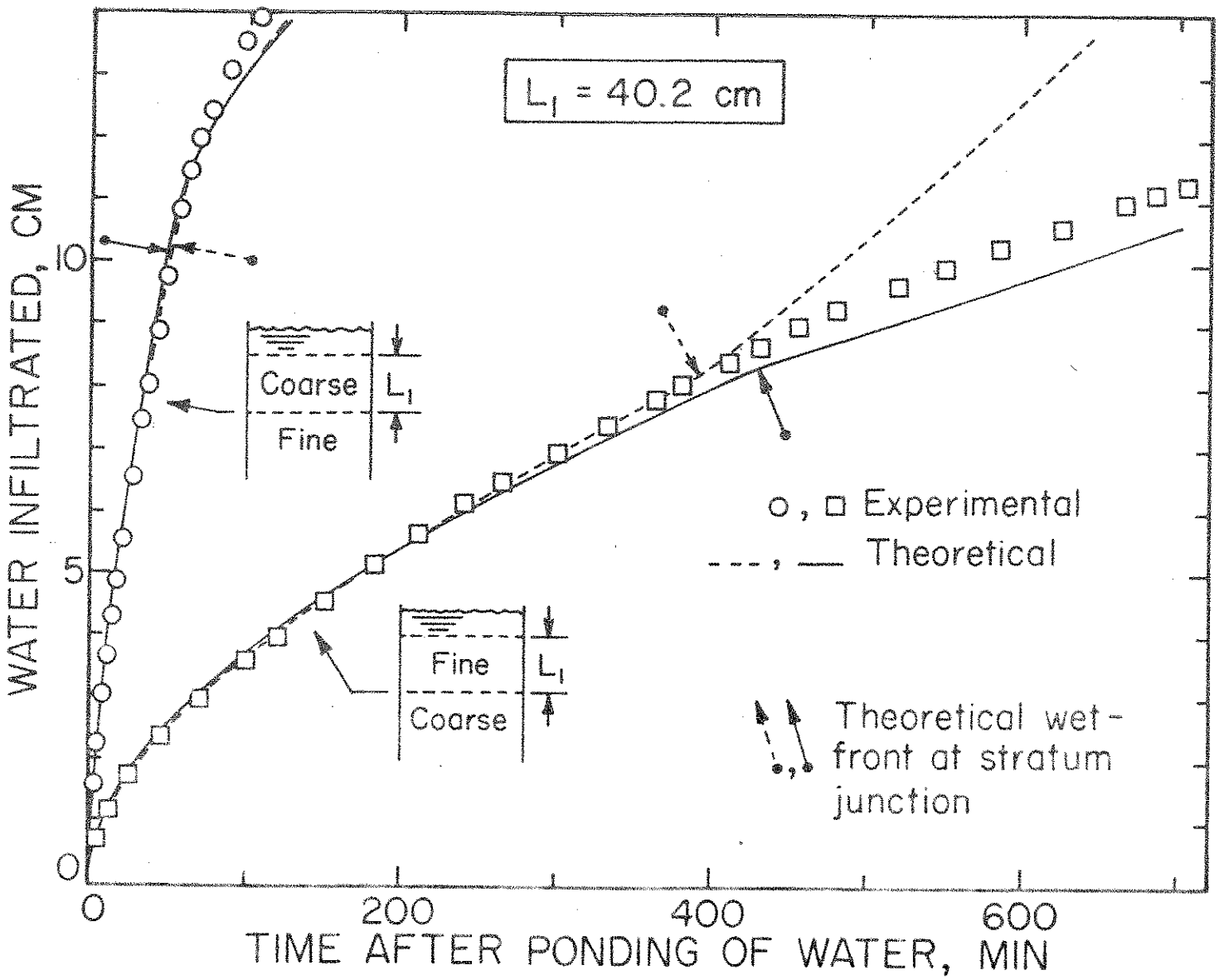

Figure 12--Water infiltrated versus time, experimental and predicted [equations (8) and (12)] for coarse-over-fine and fine-over-coarse stratifications, upper stratum L_1 = 40.2 cm. See text for explanation of theoretical curves.

what improved by the second-scheme prediction which involves more infiltration characterizations derived from the stratified columns themselves. In no instance is the second-scheme prediction poorer than the first scheme.

For fine-over-coarse cases, the agreement between experiment and first-scheme prediction is also reasonably good in three instances out of four, and for the most part the second-scheme prediction is worse than the first scheme, except that in two of these three instances (Figures 10 and 12) the experimental points fall between the two predictions when the wet front is in the lower stratum. The poorest agreement is in Figure 9 when the wet front is in the lower stratum, and again the second-scheme prediction is poorer than the first scheme. This suggests that equation (12) is least valid in fine-over-coarse systems where the fine stratum is short and the penetration of the wet front into the second stratum is a number of multiples of the length of the short upper stratum. On this basis, it might be argued that the fine-over-coarse experiments in Figures 10, 11, and 12 would become more deviant if continued to deeper wet-front penetrations, but in two of these cases the solid-line curves are actually below the data points, rather than above them as in Figure 9.

Infiltration into Media of Different Initial Water Content

Values of infiltration parameters for porous-medium columns at various initial water contents are summarized in Table 5. The first eight experiments are for the technique in which the different initial water content θ_b was obtained by mixing the dry material with pulverized ice, while the last six experiments were packed dry, wetted with water, and dewatered to various degrees on pressurized porous plates. Both coarse and fine materials were involved, but bulk densities were different in each of the three series of experiments. C_{20}, a, and P were obtained from the least-squares fit of equation (4) to the data. M could be obtained by a plot of equation (3) only for the three cases in which θ_o was zero. For the others, M was calculated by recording the value of y at which water just began to drip from the bottom end of the column, and dividing this value of y by the total length of the column. This may be the reason that $\bar{\theta}$ for a given bulk density and material, calculated as $M + \theta_o$ (since $M = \bar{\theta} - \theta_o$), is somewhat smaller for the zero initial water

Table 5. Infiltration parameters for porous columns of different initial water content.

Description	Exp. No.	θ_o	M [1]	$\overline{\theta}$	a	P	C_{20}
		cc/cc	cc/cc	cc/cc	cm	cm H_2O	10^{-3} cm/min
Uniform coarse material,	11	0	0.308	0.308	2.768	7.9	385
	12	0.046	0.318	0.364	0.174	-0.6	496
$\overline{\rho}_s$ =	13	0.082	0.282	0.364	0.221	-0.3	420
1.54 g/cc	14	0.129	0.224	0.353	0.313	0.3	332
Uniform fine material,	15	0	0.256	0.256	3.032	10.8	20.3
	16	0.066	0.246	0.312	1.948	6.8	60.3
$\overline{\rho}_s$ =	17	0.116	0.197	0.313	0.696	2.4	68.6
1.64 g/cc	18	0.152	0.159	0.311	0.280	0.7	57.4
Uniform fine material,	19	0	0.199	0.199	12.97	64.0	4.63
	20	0.078	0.156	0.234	4.32	26.6	5.54
$\overline{\rho}_s$ =	21	0.116	0.112	0.228	1.77	14.7	6.98
1.90 g/cc	22	0.126	0.096	0.222	0.80	7.2	9.71
	23	0.128	0.079	0.207	0.64	7.0	9.66
	24	0.144	0.068	0.212	1.23	16.7	6.72

[1] When $\theta_o > 0$, M is taken as the value of y when water just begins to drip from the bottom end of the column, divided by the total length of the column.

content than for the nonzero initial water contents.

For these nonzero θ_o, it is clear that $\overline{\theta}$ is remarkably similar and constant. Furthermore, even at $\theta_o = 0$ the $\overline{\theta}$ are not greatly reduced in a relative sense. Hence, it appears reasonably valid to consider $\overline{\theta}$ to be essentially independent of the initial water content for the flooding conditions here studied.

On the whole, it appears that C_{20} is also reasonably independent of θ_o, except possibly in experiment 15 where it is about one-third that of experiments 16, 17, and 18. With this exception, all of the other C_{20} for a given bulk density and material remain within, or close to, a 2-fold variation, as previously noted for Table 2 wherein all θ_o were zero.

With regard to P, however, it seems clearly to depend on θ_o, rather than remaining at some constant value conceivably specified by $\overline{\theta}$. The nature of the relationship is demonstrated graphically in Figure 13, which shows P to decrease as θ_o increases. The small negative values of P in experiments 12 and 13 are not considered significant. Examination of Figure 13 shows further that at a given θ_o, P is less for coarse material than for fine, and for a given material it increases with increasing bulk density as would be expected physically and from Table 2.

The dependence of P on θ_o is inconvenient, and tends also to reduce the practical advantage of equation (4) in comparison with equation (6). The reason for this is that the relationship between θ_o and P would need to be established for each material, and this would require experiments at different θ_o for each material. But this should not be allowed to obscure the fact that as yet there exists no simple-form stratified counterpart of equation (6). Hence, from this standpoint, the generalized Green-Ampt approach still retains some advantage, since it does provide a description of stratified conditions as embodied in equation (12).

A word of caution is in order when dealing with short columns as in experiments 19 to 24 of Tables 1 and 5. In first attempts at least-squares analysis [equations (27) and (28)]of these data, all (y,t) values were included up to the point at which water began to drip from the bottom of the column. But the fitted constants were extremely erratic, some of them behaving in the sense of equation (31) as previously discussed. Careful scrutiny of linear-scale plots of y versus t revealed in all cases that

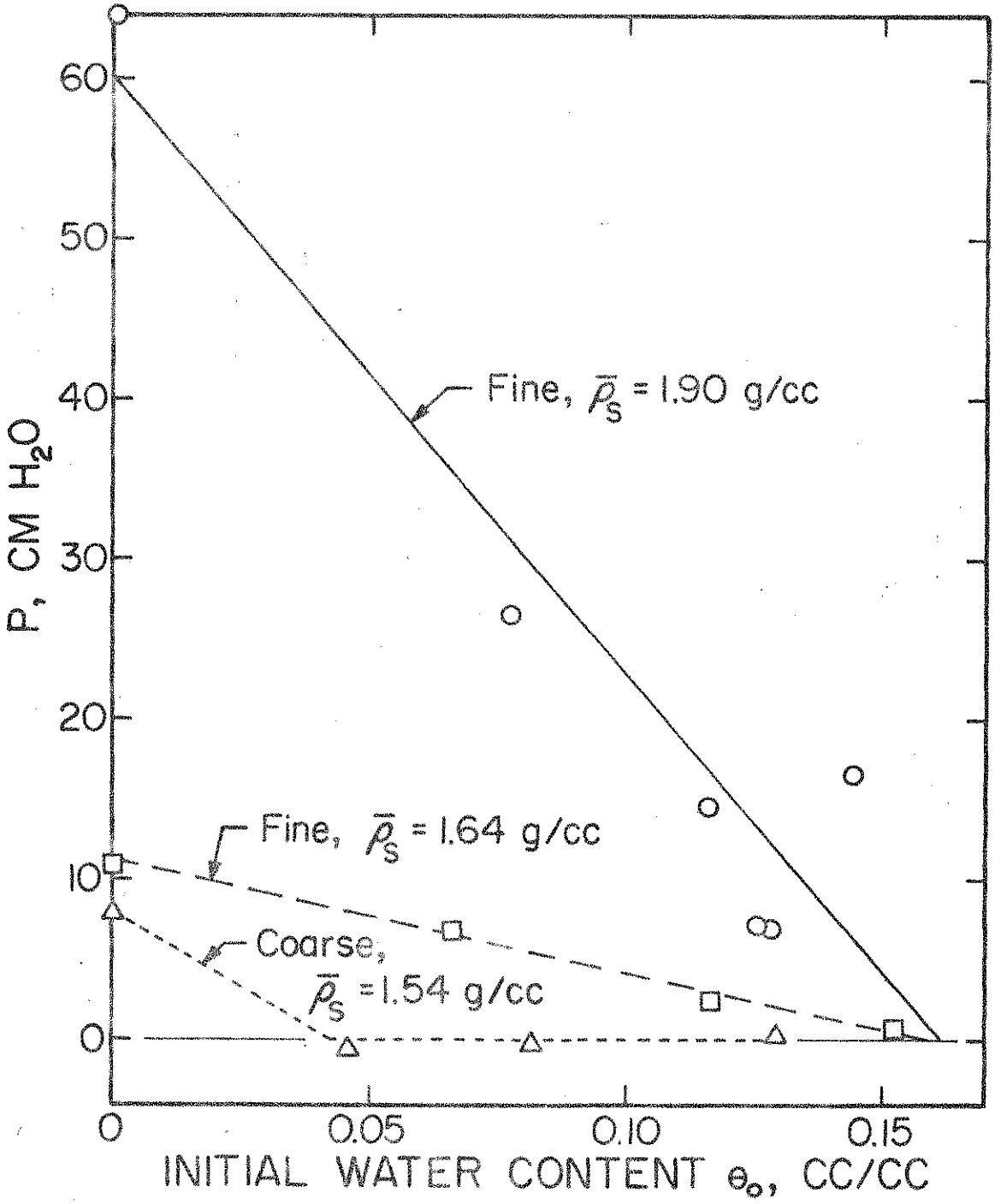

Figure 13--Variation of P with initial water content θ_o, for three bulk densities and materials.

a distinct break in the curve was occurring before water dripped from the end of the column. Hence, the range of data used for least-squares analysis was restricted to that from t = 0 up to the point of distinct break in the curve, and this is the manner in which the values reported in Table 5, experiments 19 through 24, were obtained.

Question may be raised as to whether the initial water content θ_o, obtained in the 20.2-cm columns (experiments 19-24) by placing them vertically on pressure plates, was reasonably constant, or whether the increasing suction with elevation resulted in a progressively changing θ_o with position. To investigate this, gamma-ray determinations were made at 1-cm intervals along the column, using equations (21) and (25). Within experimental error, no trend of water-content change with position could be observed. Obtainable precision for θ_o, however, was only $\pm$ 0.05, apparently caused by the 3.8-cm column diameter not providing a long enough gamma-ray path for a more precise water-content measurement.

Bulk density measurements with gamma rays were also obtained at the 1-cm intervals, using equations (22) and (24), but these appeared to be of acceptable precision, apparently since $\mu_w \rho_s$ is much larger than is the corresponding product $\mu_w \rho_w \theta$ for water. Relative variations in bulk density along the column were within a band of $\pm$ 5%, and there was no trend with position within this band. Hence, it is concluded that the increment-packing method used with air-dry material, as described earlier, did result in an acceptable level of packing uniformity, even though the sub-range variations in P and C_{20} of Table 2 might at first have suggested otherwise.

Fine-Particle Translocation

The results here involved are for experiments 25 and 26 of Table 1. First aspects to be considered will be the bulk densities determined from equations (22) and (24) by gamma-ray measurements at 0.5-cm positions along the column. Plots of bulk density versus position, both before and after infiltration, are shown in Figure 14 for the mean bulk density $\overline{\rho}_s$ of 1.80 g/cc (experiment 25). Fluctuations of bulk density both before and after infiltration are within a band of $\pm$4.4% of the mean, and there is no evidence within this band of any consistent trend with position.

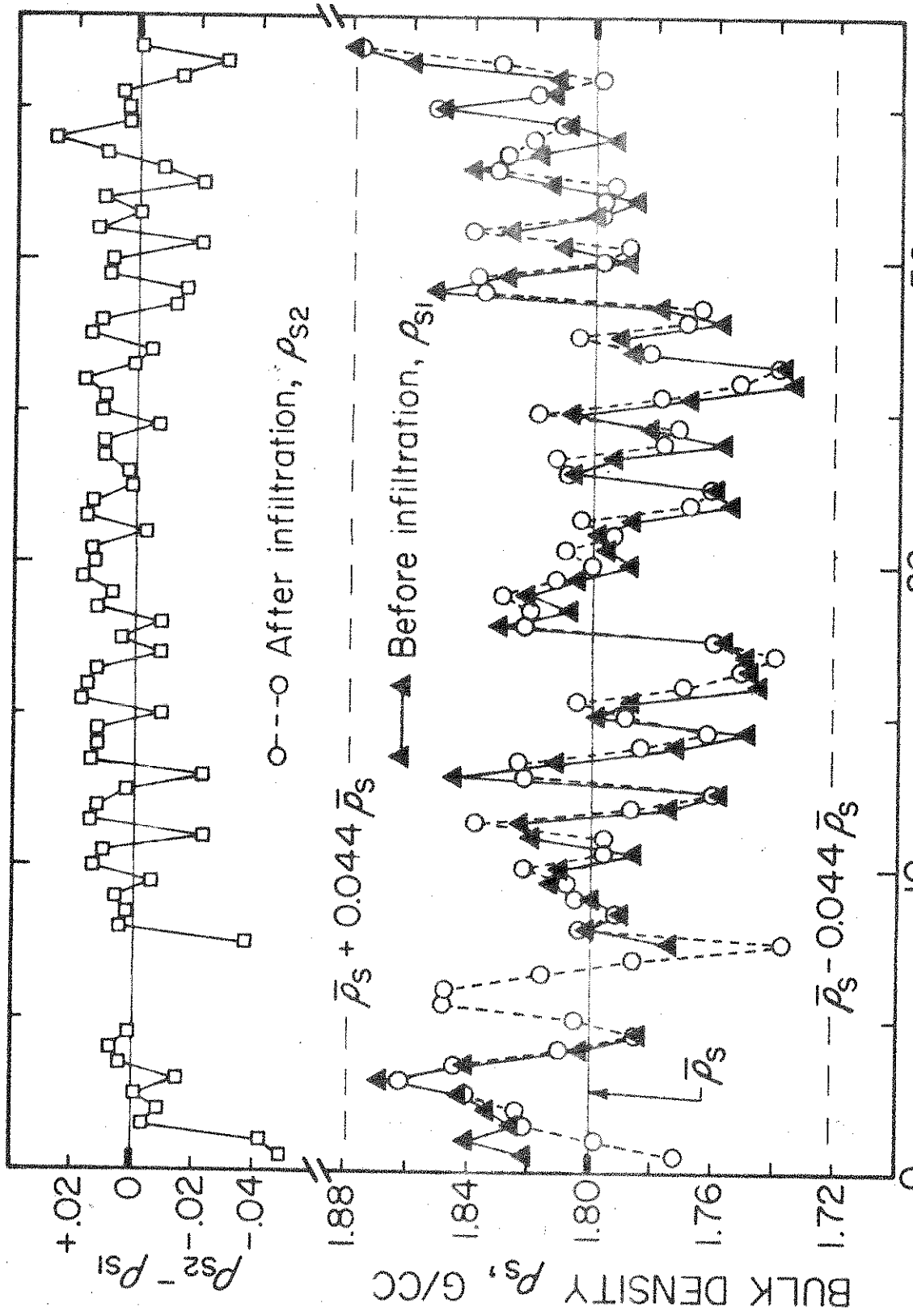

Figure 14--Bulk density versus position for fine material of mean bulk density 1.80 g/cc (experiment 25).

Hence, this again attests to a reasonable attainment of uniformity by the increment-packing method. Near the inlet end of the column, however, the bulk density after infiltration appears to be slightly reduced from its value before infiltration, consistent with the possibility that fine particles may have been translocated out of this region by infiltration. The difference is most pronounced at 0.5 and 1.0 cm, but it must also be granted that reductions of almost the same magnitude are present at 7.5 and 36.5 cm below the inlet end of the column. Even if the reductions near the inlet end are accepted as real, any redeposition of these translocated particles appears to be distributed rather evenly over the remainder of the column, since there is no subsequent part that appears to stand out as a region of bulk-density enhancement. In this respect, the gap in the pre-infiltration data from 5.0 to 7.0 cm is unfortunate. It was caused by a plexiglas supporting bracket which was judged too difficult to shift without causing possible disturbance to the column.

Graphical results for the column of mean bulk density 1.90 g/cc (experiment 26, Table 1) are shown in Figure 15. Fluctuations of bulk density are within a band of $\pm$ 5.8% of the mean, which is somewhat higher than that in Figure 14 but is nevertheless quite similar. Also, there is little evidence within the band of any consistent trend with position, thus again demonstrating an acceptable degree of uniformity in packing. There is distinctly less indication than in Figure 14 of any change in bulk density as possibly attributable to infiltration, except for the reduction at 27.5 cm which is very easily accounted for by an obvious drying-induced crack observed to be in line with the direction of the gamma-ray beam at that point. In actuality, the possibility of fine-particle translocation in this column was expected to be minimal because of the high bulk density, and the data in Figure 15 generally confirm this expectation. Unfortunately, measurements at 0.5 and 1.0 cm from the inlet end before infiltration were inadvertently omitted, so that lack of change in bulk density at these positions cannot really be established. Nevertheless, it is clear that these are the only two positions at which any significant could have occurred.

Some preliminary infiltration data taken on fine material of mean bulk density 1.80 g/cc had suggested that a plot on the basis of equation (15)

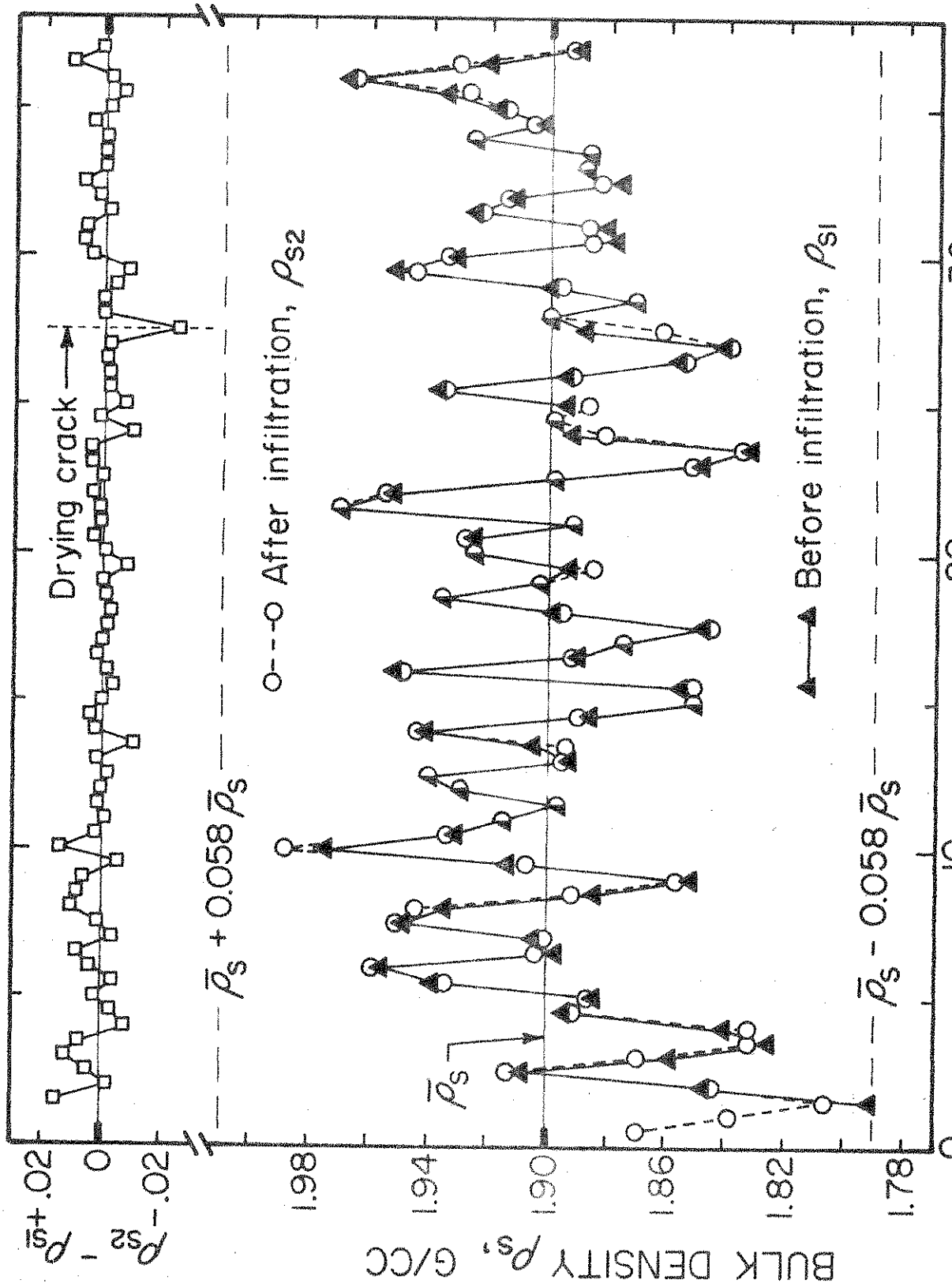

Figure 15--Bulk density versus position for fine material of mean bulk density 1.90 g/cc (experiment 26).

would show a deviating behavior, in that ydy/dt would decrease with y at small values of y rather than initially increasing with y as required by the equation. Hence, the infiltration data taken for the column of experiment 25 ($\overline{\rho}_s$ = 1.80 g/cc) were analyzed on the basis of the sliding least-squares derivative technique of equations (29) and (30). In addition, the cumulative least-square fit to equation (4) on the basis of equations (27) and (28) was also obtained. The plot of ydy/dt versus y is shown in Figure 16, and it is quite clear that there is no initial region of negative slope. Furthermore, the straight line aC + Cy [equation (15)], established from a and C determined from the least-squares fit of equation (4), goes through the points very nicely. Hence, we are left with the conclusion that if the reduction in bulk density at 0.5 and 1.0 cm in Figure 14 reflects a real translocation of fine particles, the effect is not great enough to cause anomalous infiltration deviations from equation (15). On the contrary, the first four points of Figure 16 are actually below the line specified by the subsequent points. Such behavior can be rationalized on the basis that the infinite initial dy/dt required by equation (15) cannot truly be realized physically. Rather, in starting from essential rest at t = 0, the rate dy/dt of the infiltration process will at first be less than infinite, even though it is very large. Hence, ydy/dt will initially lag the values required theoretically by the straight line pasing through the later values that are linearly conforming.

Finally, a similar graph to Figure 16 was also prepared for experiment 26 ($\overline{\rho}_s$ = 1.90 g/cc), but is not presented here because it shows essentially the same agreement between data and straight line as does Figure 16. This, of course, would have been expected, since on the basis of Figure 15 there was no real evidence of fine-particle translocation fromthe region near the inlet end of the porous-medium column.

CHAPTER 2 SUMMARY AND CONCLUSIONS

Downward infiltration into laboratory flow columns was studied for combinations of sand and silt in two different mixtures, designated as "coarse" and "fine". Packing of the columns for a given material was held uniform to within a $\pm$ 6% variation in bulk density. A relatively simple device and method were developed for applying a 1-cm depth (head) of water instantaneously to the inlet end of a porous column without

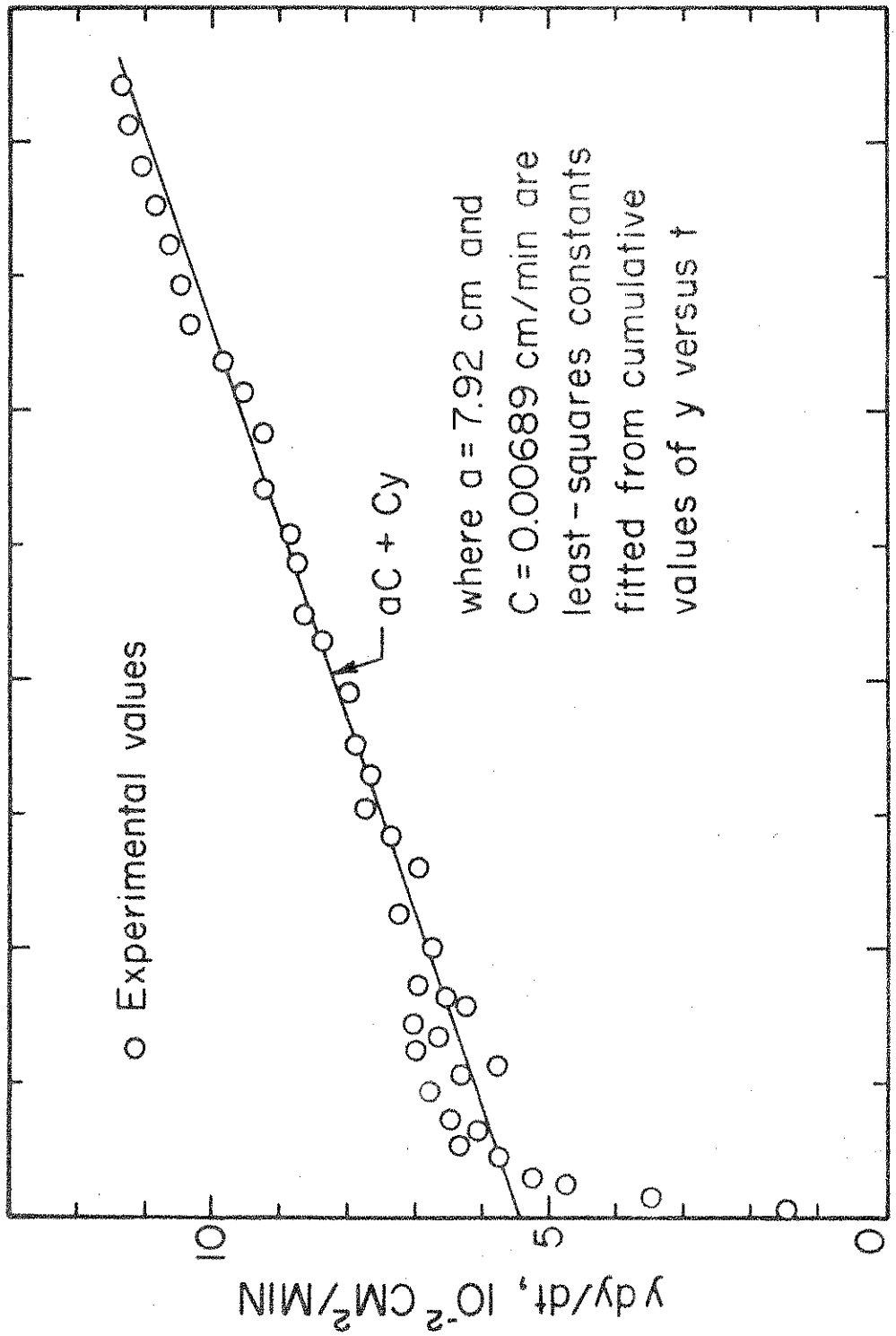

Figure 16--Plot of ydy/dt versus y [equation (15)] for a mean bulk density of 1.80 g/cc (experiment 25). Straight line aC + Cy is drawn from values of C and a obtained by a least-squares fit of equation (4) to the cumulative values y and t.

turbulent disturbance of the porous surface. Data and measurements were taken to assess the validity of infiltration equations derived by an approximate theory for both uniform and stratified columns.

For uniform columns, the equation for cumulative water infiltrated versus time accommodated the experimental data very well. The two characterizing constants C and a were fitted by least squares. C is akin to, and has units of, hydraulic conductivity, while from a it is possible to calculate a suction-head parameter P which arises from the capillarity of the porous material. Although both C and P exhibited as much as a 2-fold variation for a given porous material, their respective mean values distinguished very nicely between the coarse and fine mixtures. The physical sense also was correct, in that C decreased markedly for the fine material compared with the coarse, whereas P increased for the fine material. When the initial water content of the porous material was increased, P for a given material decreased, whereas C was not much affected.

For stratified columns initially air dry, the corresponding infiltration equation was tested by predicting water infiltrated versus time, based upon values of a, P, and C as previously determined from uniform columns. These predictions agreed acceptably with direct measurements on stratified columns when the coarse material overlaid the fine. For fine-over-coarse stratifications, however, the agreement was not always good, particularly if the wet front had penetrated into the coarse substratum relatively deeply in comparison with the thickness of the fine upper stratum. Also, the mean water content behind the wet front when in the substratum was distinctly less for fine-over-coarse than for a uniform coarse system.

For the fine material, two columns at different bulk density were investigated to determine whether the finer particles in the mixture tended to be translocated within the column as a result of the infiltration process. Some suggestion of such translocation out of the top 0.5 and 1.0 cm nearest the upper (inlet) end of the column was found for the lower bulk density (1.80 g/cc), but not for the higher (1.90 g/cc). The infiltration flow behavior, however, as analyzed by a derivative form of the approximate-theory equation for a uniform column, did not exhibit any anomalies, even for the material of lower bulk density wherein some

suggestion of fine-particle translocation had been found.

It is concluded that the approximate-theory infiltration equations have promise for uniform porous materials and for coarse-over-fine stratifications. Caution should be exercised, however, when dealing with fine-over-coarse stratifications. It should also be noted that more study is needed of the effect of the initial water content of the porous medium on infiltration. The present effort in this regard appears to be among the very first of its kind, and, although systematic, is by no means complete. The dependence of parameter P upon the initial water content implies a distinct methodological inconvenience, and it would be desirable to develop some means of circumventing or minimizing this difficulty if possible.

CHAPTER 3. MEASUREMENT OF INFILTRATION IN THE FIELD WITH A SMALL-PLOT SPRINKLING INFILTROMETER

INTRODUCTORY COMMENTS

The primary objective of this portion of the study was to measure water infiltration rates with a small-plot field instrument, to analyze and interpret these values, and to compare them with the predicted infiltration rates as determined by the procedures described in the previous chapter of this report. The predicted infiltration values were determined from cores taken at the same site as the field studies.

The unit used for making the field infiltration measurements was the Purdue Sprinkling Infiltrometer (Bertrand and Parr, 1961). The plot size for this infiltrometer is 1.16 by 1.16 m.

Some of the variables which were considered in the study were soil textural differences, initial soil-water content, and the crusting effect of the soil surface.

INSTRUMENTATION

Field Instruments

Some of the initial problems of this study involved modification of the Purdue Sprinkling Infiltrometer. The principle involved in measuring infiltration was that of taking the difference between the application and the runoff rates. It was thus imperative that the application rate be constant to attain an accurate determination of infiltration. Difficulty had been experienced in maintaining such a constant rate.

The original equipment as described (Bertrand and Parr, 1961) was designed with a centrifugal pump as the source for the constant water supply to the sprinkling nozzle. The water pressure was controlled with a series of valves through a pressure tank and then to the nozzle. This system required continual surveillance to maintain the desired sprinkling-nozzle pressure, and even then there were frequent fluctuations.

In order to correct this variation, a new system using air pressure was designed. A small gasoline-engine-driven air compressor, delivering 2.9 ft^3/min at 40 psi, was coupled to the large 700-gal water supply tank. The system is shown in Figure 17. The valve installed between the

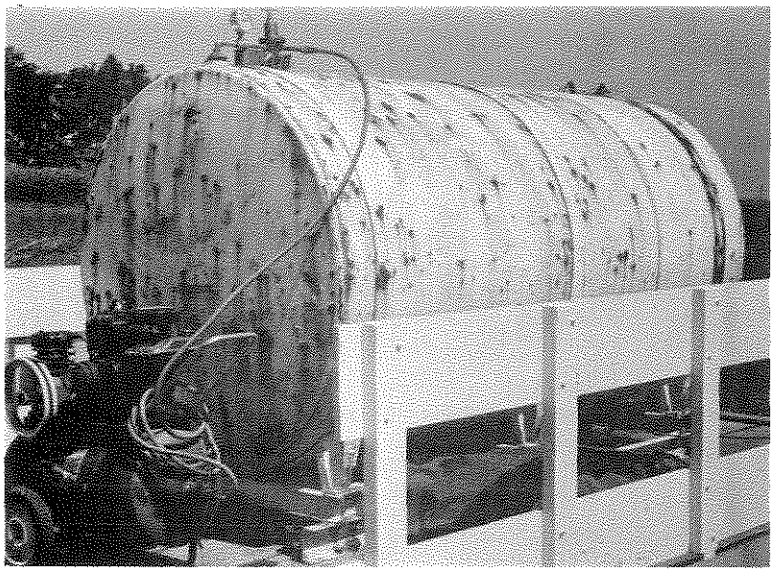

Figure 17--The redesigned water supply system for the Purdue Sprinkling Infiltrometer. Air compressor is at the left, and pressure control valve is on top of the tank and to the right of pressure gauge.

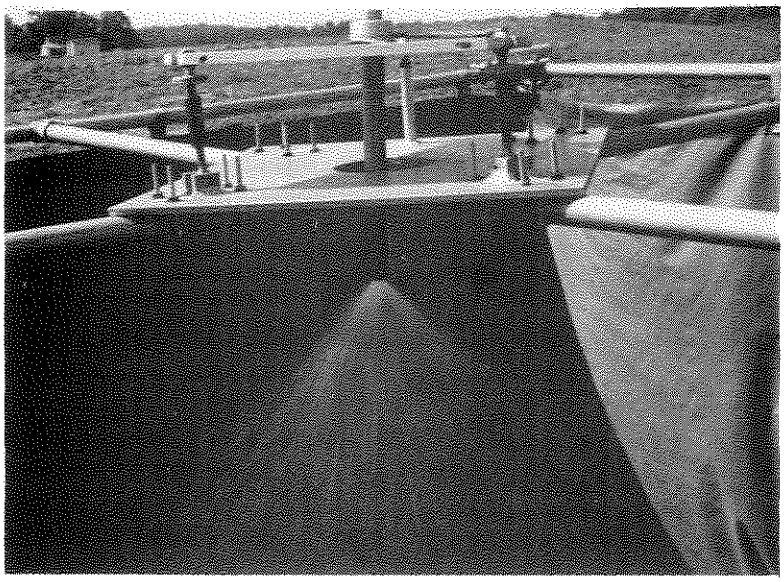

Figure 18--Apparatus for adjusting the sprinkling nozzle of the Purdue Sprinkling Infiltrometer. The two adjustable turnbuckles are in the foreground, and the stationary one is in the background.

air-pressure supply and the water tank maintained a constant pressure within the water tank. This constant pressure valve is shown (Figure 17) on the top of the tank immediately to the right of the pressure gauge. As the water level receded in the large supply tank, a slight decrease in pressure resulted at the sprinkling nozzle, but was corrected with a water-control gate valve between the water supply and the sprinkling head. By adjusting this valve, a nearly constant sprinkling-head pressure could be maintained. Measurements with this system indicated that the application rate was virtually constant.

A second change was made in the sprinkling nozzle system. The design of the infiltrometer required that the nozzle be precisely vertical in order that the spray pattern be the same each time a test was made. This required a means for adjusting the level of the nozzle. In the old system this was accomplished with some difficulty. The new design is shown in Figure 18. A floating deck is attached to a stationary deck with one stationary and two adjustable turnbuckles. By lengthening or shortening the adjustable turnbuckles, a small bullseye level located on the floating deck will indicate when the nozzle is in the vertical position.

Another change involved the redesign of the plot frames. With the old frames, the depth to which they were driven into the soil did not always prevent lateral seepage from occurring underneath the frame borders. This would result in an infiltration rate which was higher than it should have been. To alleviate this problem, the new plot frames were built 30.4 cm high, so that when installed, approximately 20.3 cm would be inserted in the soil. This depth is below the normal plow layer, and eliminated any obvious lateral seepage. Another alteration on the plot frame was the welding on of a boxed-end lip, to ensure that all the runoff water was collected in the collection flume. In the original system, runoff water could trickle by and escape. The plot frame is shown in Figure 19.

Formerly, moving the infiltrometer from one plot to another required two or more men. Detachable heavy duty cycle wheels (Figure 20) were therefore added to the infiltrometer tower frame, to make the system operable by one man.

For the laboratory experimentation it was necessary to obtain

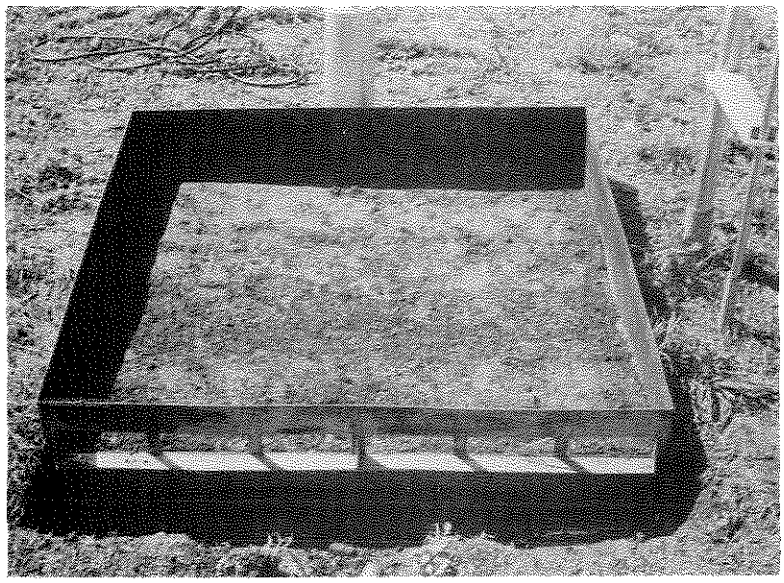

Figure 19--The plot frame for the Purdue Sprinkling Infiltrometer. The end lip, which is welded on, is shown in the foreground.

Figure 20--The tower frame of the Purdue Sprinkling Infiltrometer, showing the two cycle wheels mounted ready for movement to the next plot.

undisturbed field soil samples. To do this efficiently and with ease, a core-cutting device was designed and constructed to utilize a hydraulic coring machine. Figure 21 is a schematic drawing of the device. The 10 by 11.4 cm brass cylinders fit inside the corer, and are for the purpose of maintaining the shape of the soil core. There are two 0.6-cm brass rings which hold the larger brass cylinder in place, and also allow for trimming the ends of the soil core. Figure 22 shows the brass cylinder and the core after making the laboratory determinations.

Field soil-water content measurements were made with a neutron instrument,[4/] and gravimetrically. A two-probe density gauge[4/] (Figure 23) was tested during the field infiltration studies; however, some difficulties were experienced with its operation. With this instrument, it was hoped that the wet front of infiltrating water could be followed, thus providing a means for comparison with the laboratory determinations on core samples taken from the same plot. Further work will be conducted on this portion of the study.

Laboratory Instruments

In making the laboratory measurements for accumulative infiltration on the field core samples, the procedure developed and also described in the previous chapter (pages 13-15) was followed. The apparatus was similar, except that the diameter of the applicator was larger so as to accommodate the field core samples (Figure 24). Another procedural difference was in following the wet front in the core. The cores were initially measured when at field water-content conditions, which in itself would make it difficult to follow the progress of the wet front; also, the cores were encased in the brass cylinders which made it impossible to observe wet front movement visually. Therefore, the only possible wetting observation to be made was when water appeared at the bottom of the core as noted by a

---

[4/] Both instruments are supplied by Troxler Laboratories, Raleigh, North Carolina. The neutron instrument is the Model 1257 Depth Moisture Gauge, with neutron source of 100 mc of Americium-Beryllium. The Model 1376 Two-Probe Density Gauge has a 5-mc source of Cesium 137.

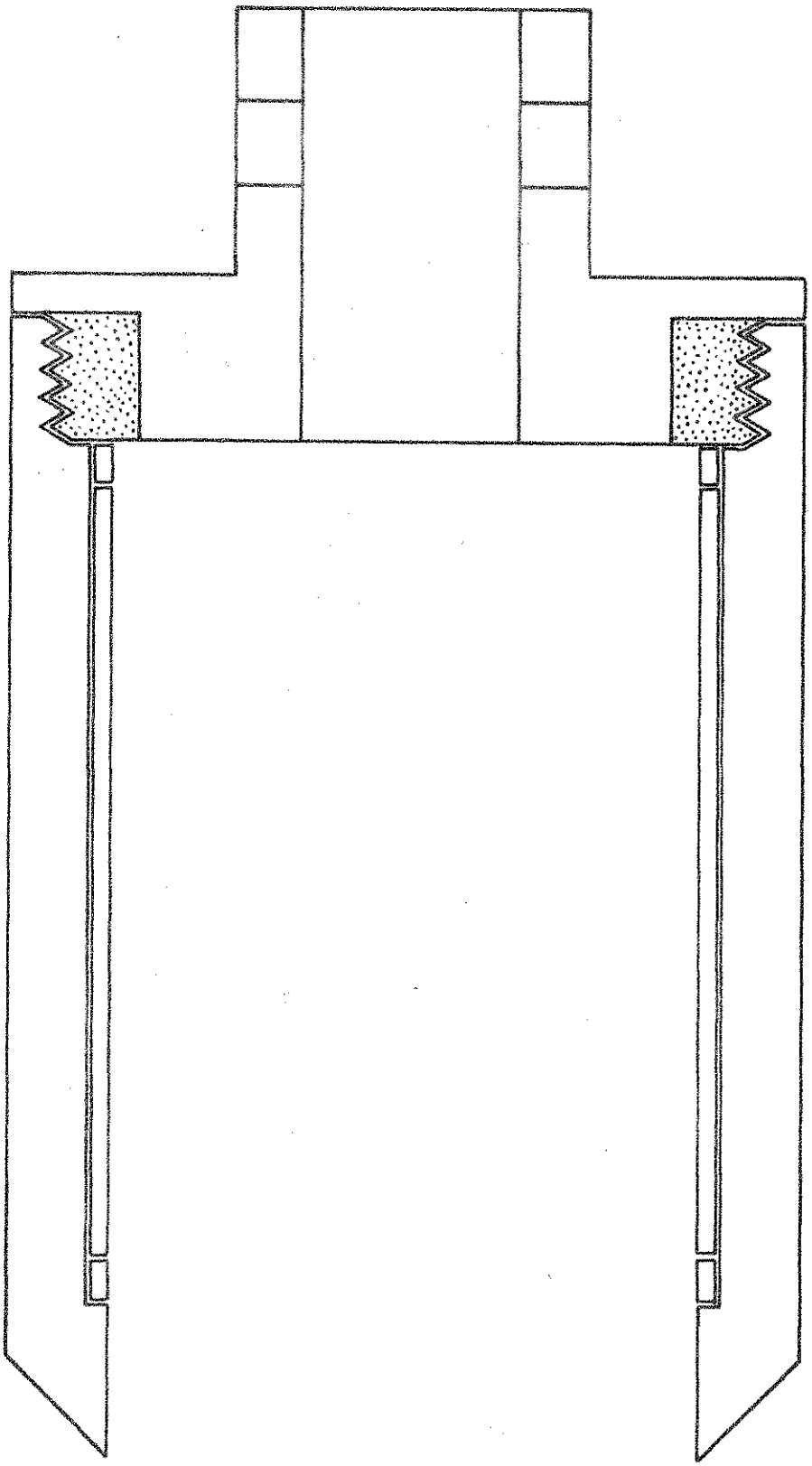

Figure 21--Sectional diagram of the soil core sampler, with view of the three inner brass cylindrical rings and the outer cutting case constructed primarily of aluminum. Dotted portion is stainless steel.

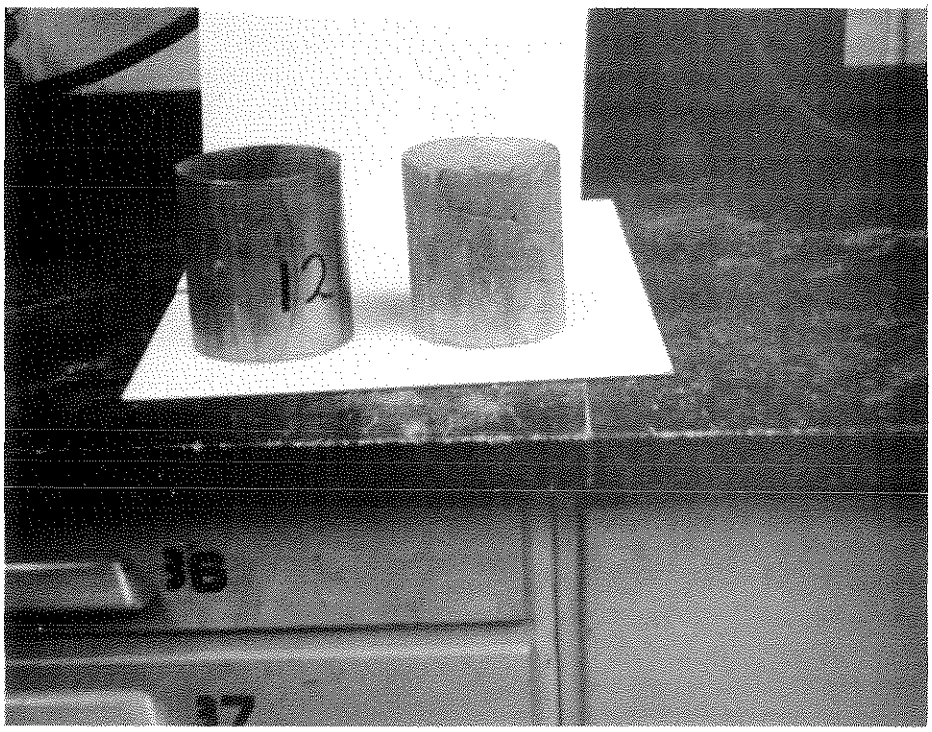

Figure 22--The brass cylinder used for taking the soil core samples, and a core which was removed after making the laboratory measurements.

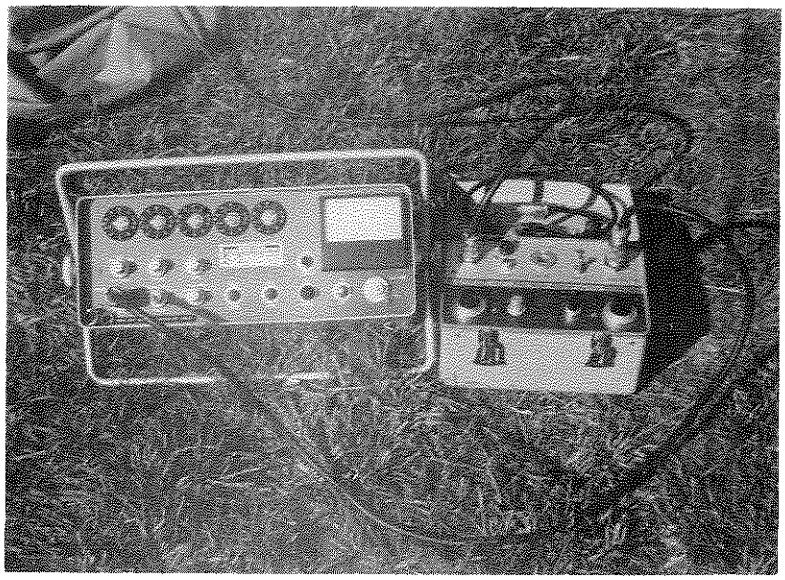

(A)

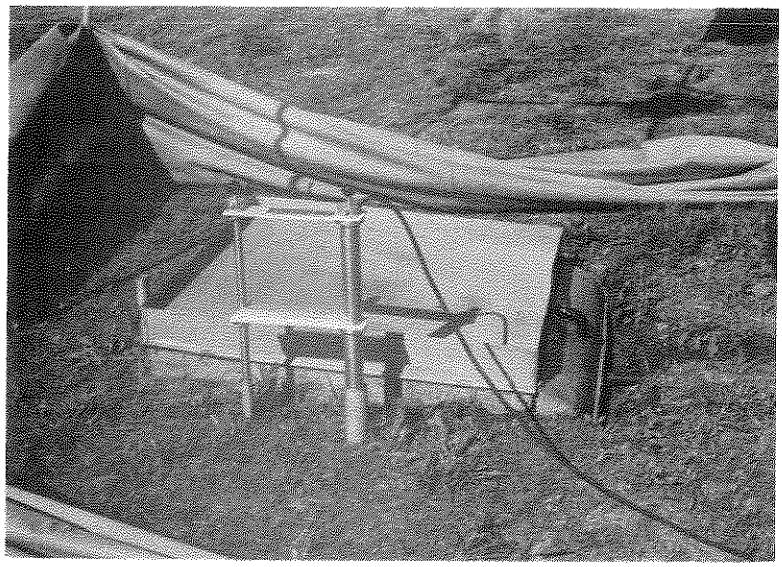

(B)

Figure 23--The two-probe density gauge. In (A) the scaler is on the left and the pulse-height analyzer on the right. In (B) the tube on the left contains the radioactive source, while the tube on the right has the detector.

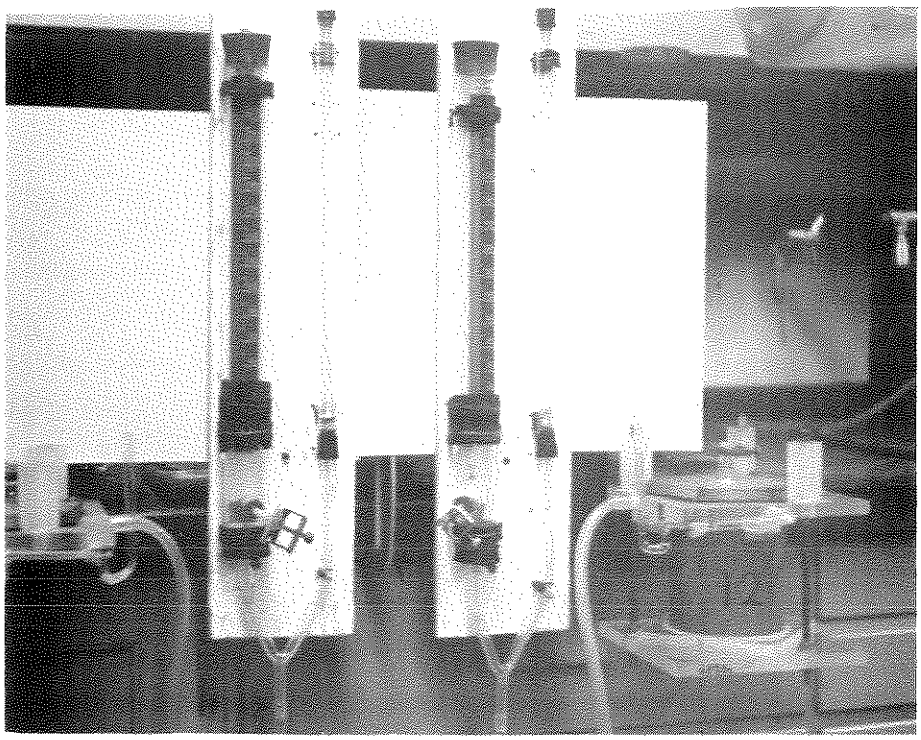

Figure 24--The apparatus used for making the laboratory measurements on the field core samples.

sparkle or glistening effect. This procedure provided the information for estimating M of equation (3), the estimate being taken as y at the point of sparkle or glistening, divided by the length of the column.

FIELD INFILTRATION MEASUREMENTS WITH VARYING SURFACE SOIL CONDITIONS

The infiltration characteristics of a soil are known to be influenced by the surface conditions of that soil (Mannering, 1967). In order that a prediction procedure could be developed whereby field infiltration was estimated by laboratory determinations from representative sample cores, some information was necessary to ascertain to what extent surface conditions must be considered in the laboratory.

Preliminary field tests also were made to study soil texture and soil roughness, and their influence on the infiltration rate.

When field testing with the sprinkling infiltrometer, the normal operation is to make one run at a soil-water content prevalent to the area at the time of testing. This is referred to as the "dry run", although surface soil-water content may vary from very dry or below the wilting percentage to relatively more wet. Twenty-four hours after the "dry run", a second run is made at the exact same location, and is called the "wet run". The results of the "wet runs" are usually more comparable from one plot to the next, since the soil-water contents are more nearly the same. The method and operation of the infiltrometer did not have any special aspects in these experiments but were essentially as given in the bulletin by Bertrand and Parr (1961). The measurements were made in all cases for 60 min.

Textural Variation of the Surface Soil

This experiment was conducted on a Russell loam soil. The plots were prepared by installing the plot frames, and then carefully removing the surface 2.5 cm of soil. In the removal of the top soil, an attempt was made to maintain the natural porosity in the soil below the removed 2.5 cm.

From the original top soil, five textural treatments were established. The top soil had been collected, dried, and passed through a 2-mm sieve. Treatment 1 consisted of replacing the 2.5 cm of top soil with the original

dried and sieved soil; 2 was a combination of 75% by dry weight top soil and 25% silica sand; 3 was 50% soil and 50% sand; 4 was 25% soil and 75% sand; and 5 was 100% sand. The laboratory textural analysis for the varying combinations is as given in Table 6.

Table 6. Textural classification for the surface 2.5 cm of soil from the infiltration experimental plots.

Treatment No.	% Field Soil	% Silica Sand	Textural Percentage			Textural Classification
			Sand	Silt	Clay	
1	100	0	43.8	44.6	11.6	loam
2	75	25	46.0	43.0	11.0	loam-sandy loam
3	50	50	66.9	25.4	7.7	sandy loam
4	25	75	80.8	14.9	4.3	loamy sand
5	0	100	100.0	0	0	sand

The experiment had been designed to have 4 plot replications of each treatment. Unfortunately, due to time limitations, only two replications were made for the dry run of treatment 4 (25% soil and 75% sand) and the wet run of treatments 2 (75% soil and 25% sand) and 4 (25% soil and 75% sand). On treatments 1, 2 and 5 the complete four replications on both dry and wet runs were made. The results of the dry run are shown in Figure 25, while those for the wet run are in Figure 26.

In the dry run, the infiltration rates for the various treatments were in the order one would anticipate, in other words, the coarser the texture of the top soil the higher the infiltration rate. However, treatments 2 and 3 had very little effect over treatment 1 on infiltration, and not until the texture attained a loamy sand (over 80% sand) was there much apparent increase in the rate. The terminal infiltration rate for the 100% sand top soil was about four times that for the natural top soil.

In Figure 26, the wet runs of the same plots as above, the infiltration rates are in general lower than in the previous figure. The only exception is with treatment 2 (mixture of 75% soil and 25% sand) which

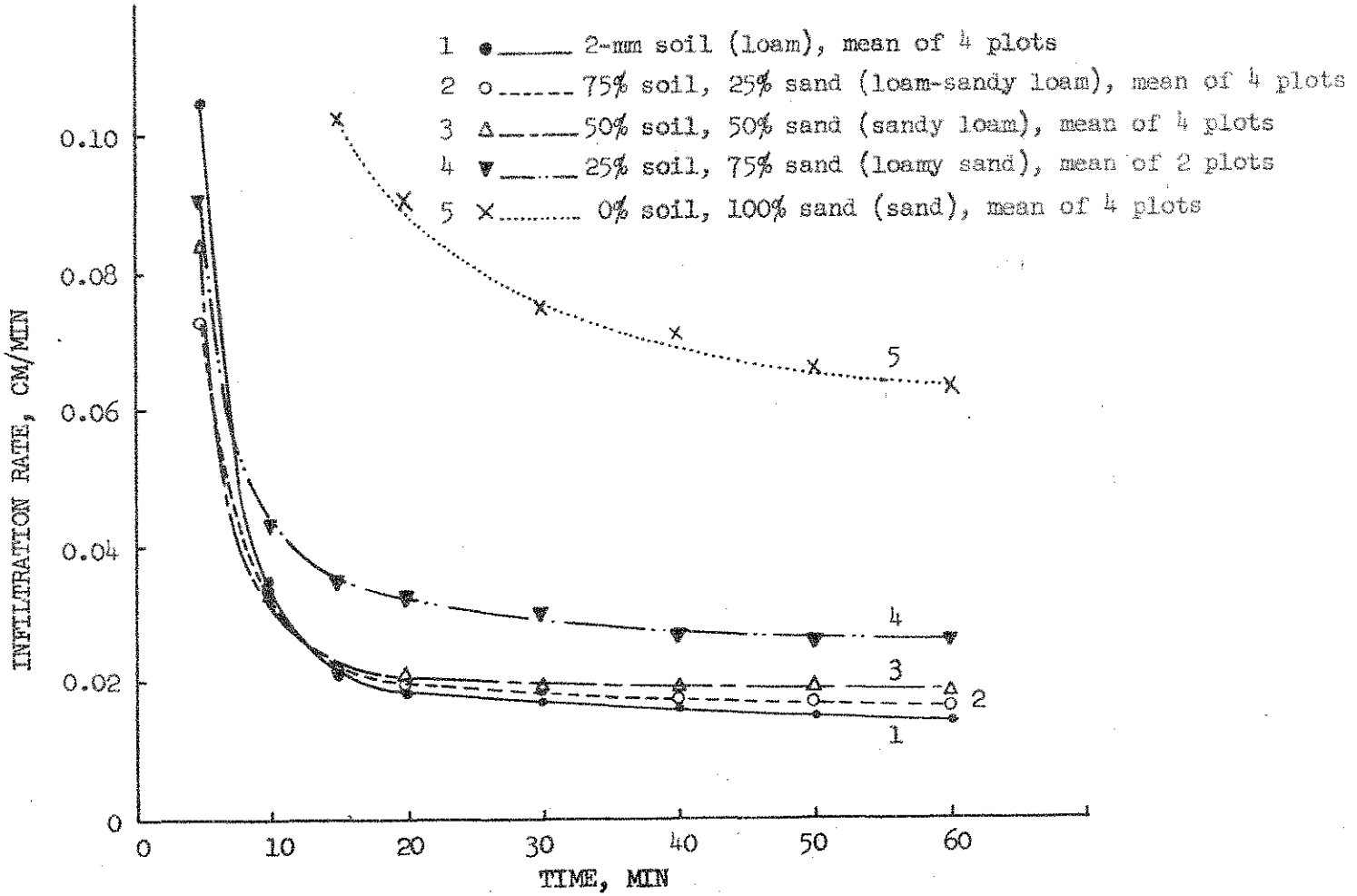

Figure 25--Infiltration rate curves for the dry run of the five different-textured surface soils, ranging from loam to sand.

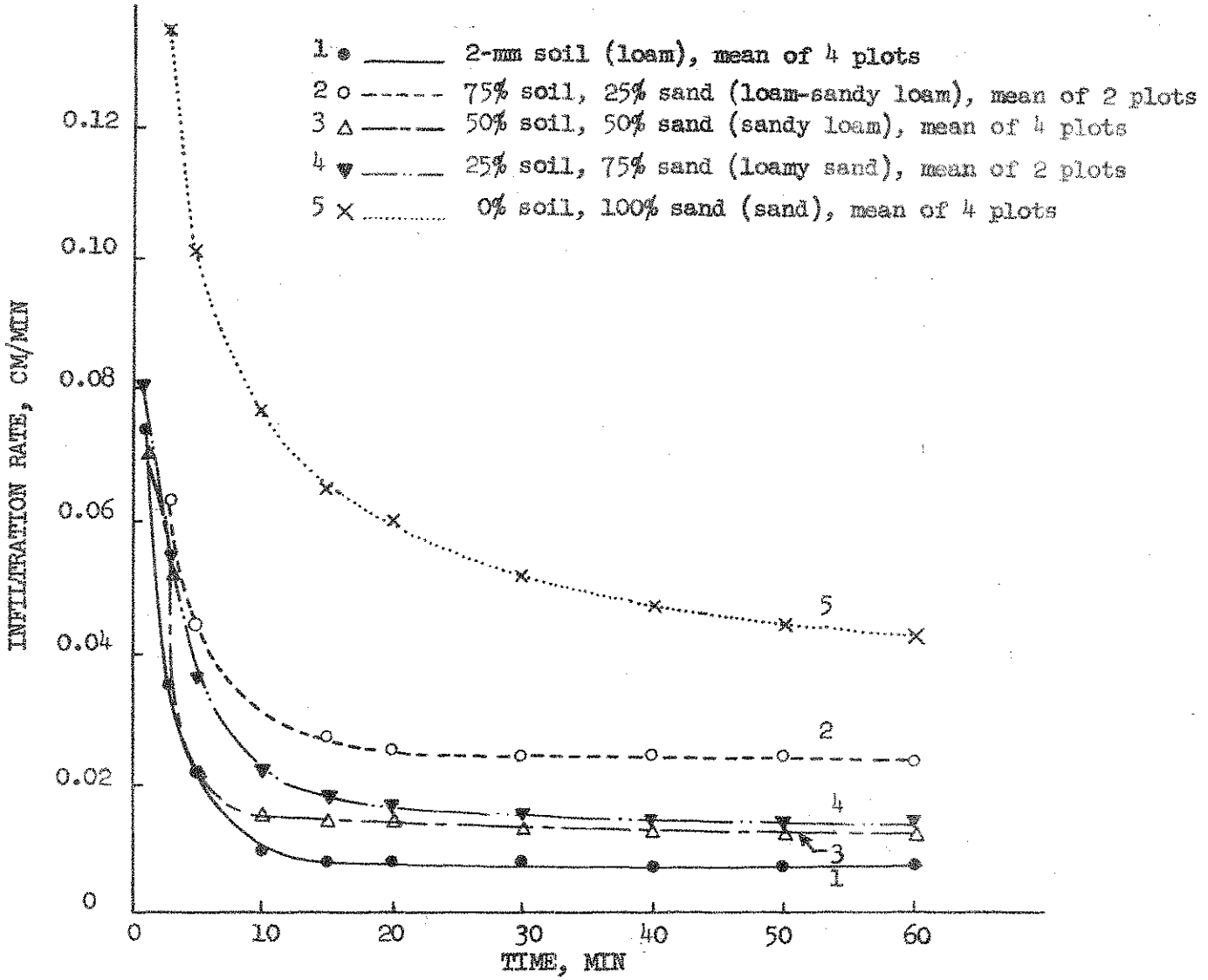

Figure 26--Infiltration rate curves for the wet run of the five different-textured surface soils, ranging from loam to sand.

increased from a terminal rate of 0.016 cm/min to 0.023 cm/min. Also, treatment 2 would seem out of order, as it would be normally anticipated that this treatment would be intermediate between 1 and 3. No logical reason for this can be offered at present. All the other treatments on the wet run show a distinct decrease in water intake from the dry run. Table 7 summarizes the data given in Figures 25 and 26.

Table 7. The effect of surface soil texture on infiltration.

Treatment No.	Textural type	Total infiltration in 1 hr		Terminal rate after 60 min		Decrease in rate from dry to wet run	
		Dry run	Wet run	Dry run	Wet run	Absolute	Percentage
		cm	cm	cm/min	cm/min	cm/min	
1	loam	1.80	0.63	0.014	0.007	0.007	50
2	loam-sandy loam	1.71	1.89	0.016	0.023	--	
3	sandy loam	1.93	1.04	0.018	0.012	0.006	33
4	loamy sand	2.07	1.23	0.026	0.014	0.012	46
5	sand	5.39	3.66	0.063	0.042	0.021	33
Bluegrass		6.51	3.63	0.050	0.025	0.025	50

The results of a non-replicated run on a bluegrass plot which was adjacent to the experiment are also given in Table 7. It is noteworthy that infiltration with bluegrass was quite similar to that with 100% sand surface texture.

Analyses of variance of the terminal 60-min infiltration rates shows that with the dry runs the differences between treatments are highly significant. However, when the Duncan test is applied, the only treatment which is significantly different is treatment 5, or that with 100% sand surface texture. There were no significant differences between the other 4 treatments. In the analyses of variance for the wet runs, there were significant differences between treatments; however, when the Duncan test was applied, these statistical differences did not hold.

Although the surface texture varied, the soil below the 2.5 cm layer was the same for all treatments. The soil-water content of this sub-surface layer was very nearly the same for all the dry runs, and was considered the same for the wet runs, since these were all made 24 hr after the initial 60-min application. It can be assumed, therefore, that the hydraulic conductivity of the soil below the top layer would have been essentially the same for all treatments. It is further assumed that there were no structural changes with the 100% sand-surface texture to cause any decrease in conductivity of this layer, at least such changes would have been minimal. The similarity between the infiltration for this treatment and the bluegrass plot would tend to verify this.

There does appear to be an increase in both total infiltration and terminal rate as the surface texture becomes coarser; however, only when there is 100% sand (treatment 5) does this increase become statistically significant. With the exception of treatment 2 (loam-sandy loam), all the treatments had a distinct decrease in total infiltration and terminal rate when comparing the wet with the dry runs. Although there were some variations, the percentages of this decrease in the terminal rates were reasonably similar. It would appear, then, that the differences in infiltration which did occur could be attributed to the change in the hydraulic conductivity of the surface soil, presumably caused by the beating action of the falling water drops. This change in hydraulic conductivity of the surface is sometimes referred to as "surface sealing". From the data presented, this decrease in conductivity of the surface soil seemed to occur in all soils, even those having a low percentage of silt and clay.

If the assumption is made that the hydraulic conductivity of the soil below the surface layer is the same for all treatments, and that the hydraulic conductivity of the 100% sand surface does not change because of alteration in its physical characteristics, then the rate curves for this experiment would indicate that the surface texture of a natural soil does not greatly influence infiltration. Further, the curve for 100% sand shows that the hydraulic conductivity of the lower layer of soil does permit the water to flow through at a rate near 0.06 cm/min, whereas the rate of the other treatments with silt and clay top soil is much lower.

Also, the curves for the soil mixture treatments decrease much more rapidly after the beginning of water application, which would tend to indicate that this change in the hydraulic conductivity of the surface soil begins very soon after initiation of impact energy from the falling water. This is not to deny that silt- and clay-containing textures do have reduced infiltration rates when compared with the pure sand, but it does imply that variations in silt or clay content in themselves have slight effects.

Although the range of soil textures used in this experiment is not great; that is, there logically should have been included clay or silty clay textures, the relatively small difference in infiltration rates with soils containing any silt or clay gives evidence that surface texture alone is probably not a dominant factor when considering the infiltration rate of a watershed. It would seem that surface sealing is taking place, but that its effect does not vary greatly with changes in soil texture.

Surface Configuration and Infiltration

Various surface-soil conditions are normally encountered over a watershed area. Each of these conditions may influence the water intake, and in turn the runoff. A fallow or bare soil will usually be expected to have a lower infiltration rate than the same soil covered with vegetation. Furthermore, the smoothness or roughness of the surface of a fallowed soil also can conceivably alter the rate. Agricultural practices are sometimes used to specifically maintain a degree of patterned roughness to influence the overall hydrology of a field or area. The tests described in this section were designed to study ridging effects on the infiltration rate.

The study was done on a Russell loam soil with about a 5% slope. The Russell is the well drained soil of the Russell catena. The area had been fallowed for several years and was bare of any vegetation. The runoff collection was on the downslope side of the plot.

Comparisons were made of a smooth fallow surface, a smooth fallow surface which had been crusted by prior storms, fallow ridges perpendicular to the slope, and fallow ridges parallel to the slope. The ridges were hand constucted within the plot frames, and were 10 cm high and 20 cm apart

from crest to crest. Dry and wet runs as described earlier were made for all these determinations. Figures 27, 28 and 29 give the data for this portion of the study, which is further summarized in Table 8.

Table 8. Effect of surface configuration on infiltration.

Treatment	Infiltration rate after 60 min		Total infiltration during the 60 min	
	Dry	Wet	Dry	Wet
	cm/min	cm/min	cm	cm
Fallow - smooth	0.011	0.008	1.83	0.79
Fallow - smooth - crusted	--	0.004	--	0.69
Fallow - ridges perpendicular to the slope	0.005	0.008	1.61	0.81
Fallow - ridges parallel to the slope	0.004	0.002	1.04	0.54

In the trial testing the cross-slope (perpendicular) ridges, water collected behind the ridges until it overtopped and began to run off into the collection flume. As it overtopped, the ridges were rapidly eroded, which allowed much of the surface-stored water to accumulate at the collection point. This accounts for the unique appearance of the curve for the dry run in Figure 28. For a period, the runoff is greater than the application rate, which would indicate a negative infiltration. However, after the excess stored water is accumulated, a uniform infiltration rate is maintained. The curve does show that cross-slope ridges will delay the time of initial runoff; however, in storms where the rainfall rate continues to be greater than the infiltration rate, this advantage may be lost and even impaired by excess soil erosion, when the water begins to break out of the storage areas.

An analysis of variance considering the infiltration rate after 60 min of the wet run for the above treatments showed no statistically significant differences. In the cases studied, there certainly is no evidence that

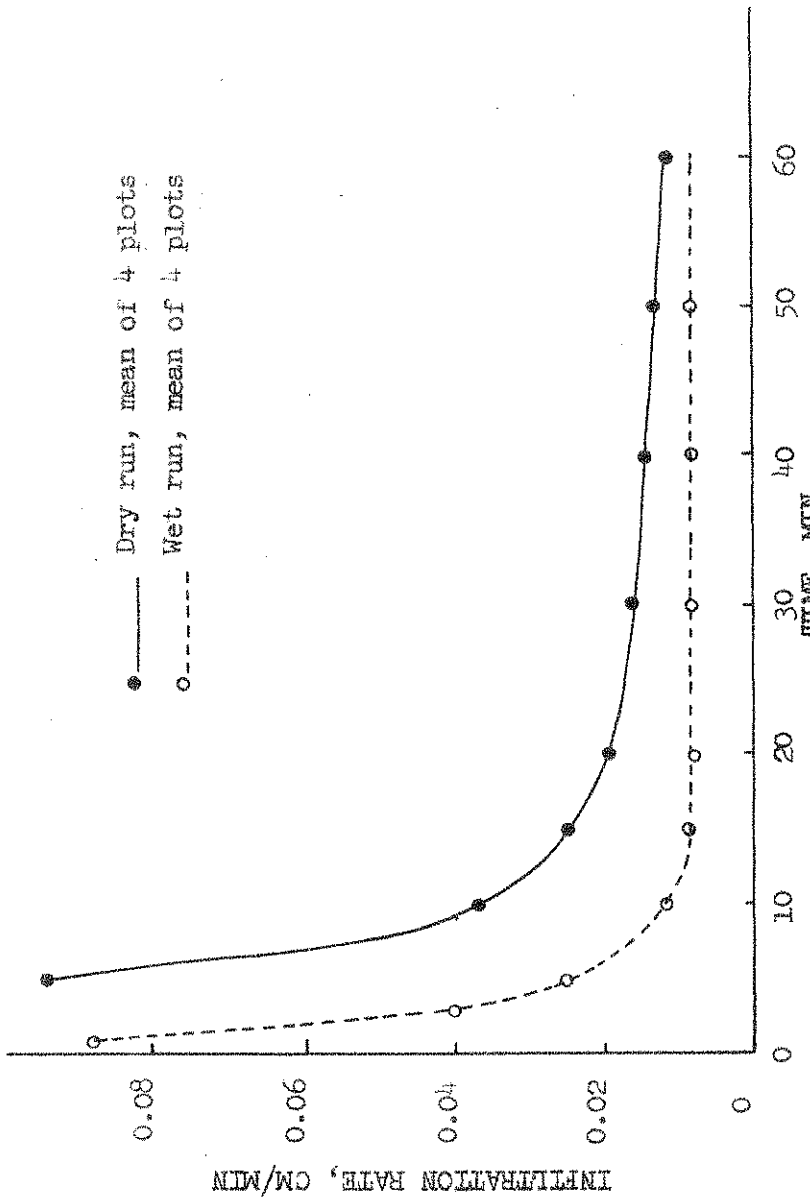

Figure 27.--Infiltration rate for Russell loam with a smooth fallow surface.

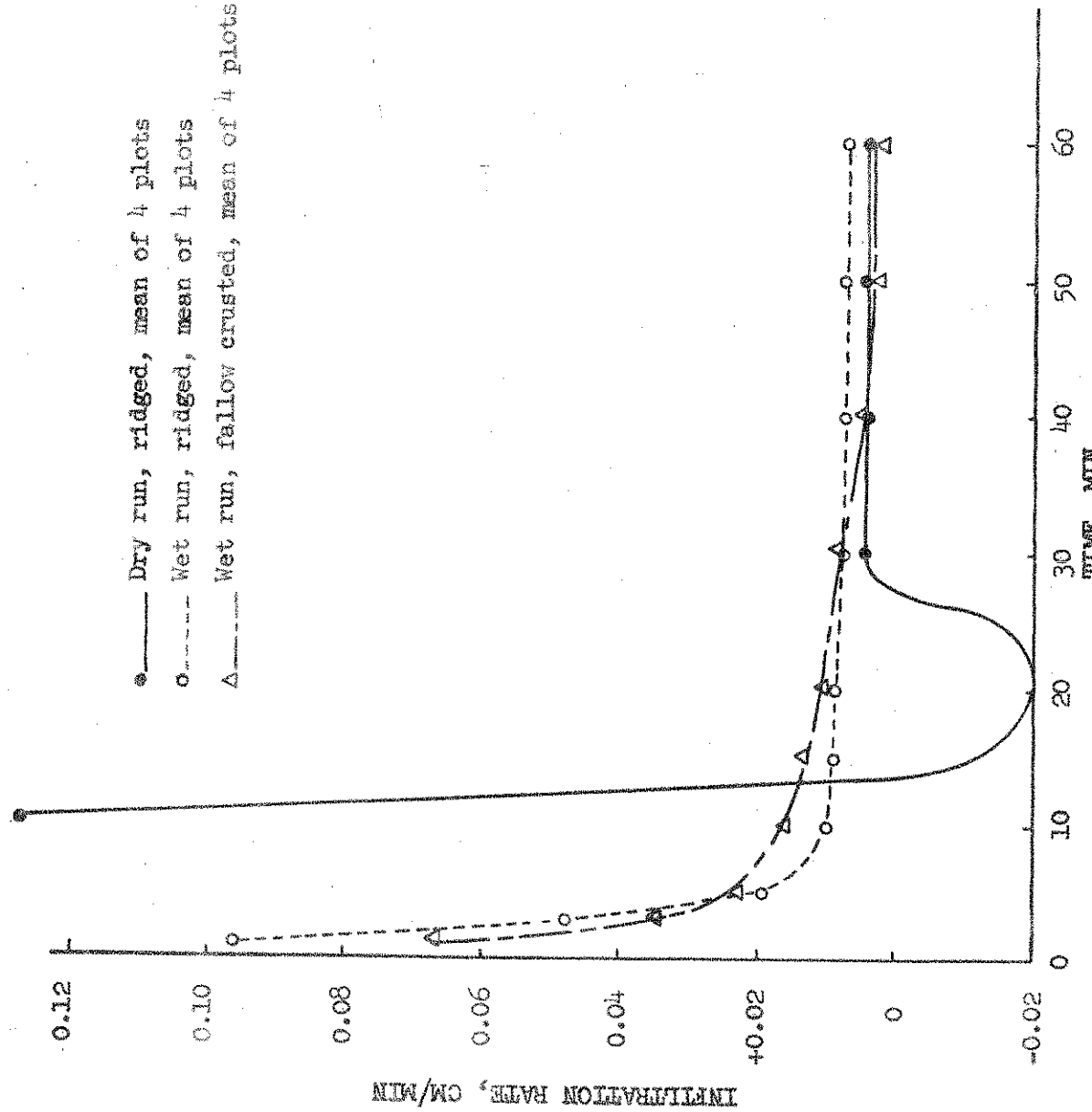

Figure 28--Infiltration curves, dry and wet runs, for plots with 10-cm ridges perpendicular to the slope. Also, for comparison, wet runs of fallow crusted plots. Soil is Russell loam.

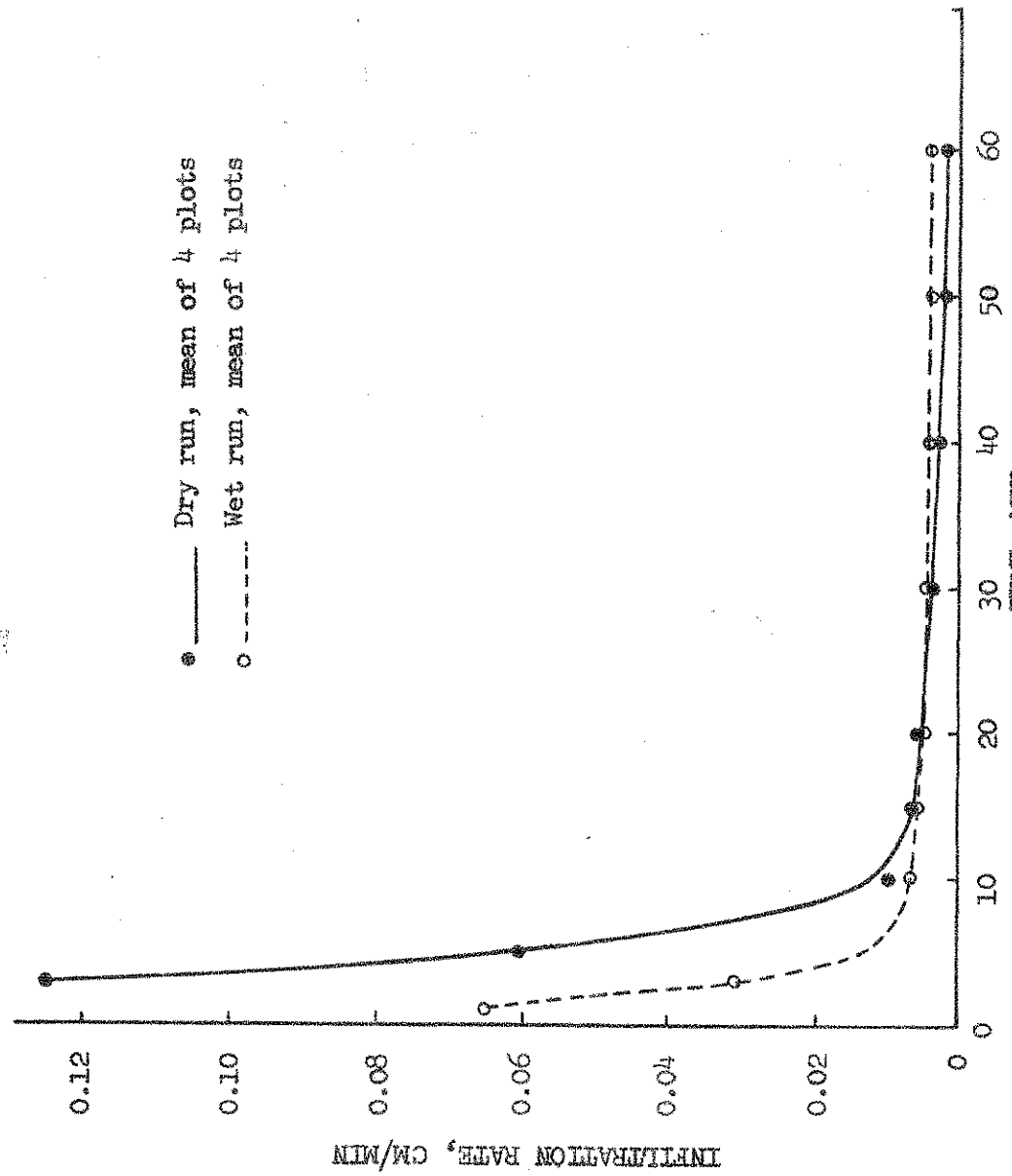

Figure 29--Infiltration curves, dry and wet runs, for plots with 10-cm ridges parallel to the slope, on Russell loam.

ridging the soil, either perpendicular to the slope (cross) or parallel to the slope (up and down), had any beneficial effect on infiltration, when compared with the smooth fallow surfaces. The data do give some indication, however, that the plots with ridges parallel to the slopes have a lower infiltration rate. This latter treatment is not considered a good soil and water conservation practice.

There was no attempt to measure the amount of soil removed from the plots by the water. However, as noted before, the overtopping of the perpendicular slopes did cause considerable visible erosion. It would be anticipated that the plots with parallel-to-slope ridges would have excessive soil loss, because of increased runoff and velocity of the water flow.

INFILTRATION ON UNDISTURBED SOILS

The field studies described heretofore did not include the correlated determinations in the laboratory by the procedure given in Chapter 2 of this report. The study now to be reported contains the initial trials comparing the infiltration rate measured by the sprinkling infiltrometer with that predicted from the laboratory cores taken from within the field plots.

The site tested originally was a bluegrass sod which had been in natural vegetation for some period of time. This virtually eliminated any effects of an artificial stratum such as a plow-layer of a cultivated field. The soil was a Fincastle silt loam, with distinct A_1, A_2, and B horizons. The A_2 horizon was not thick enough to make a complete core with the sampler used.

To make the laboratory infiltration measurements with the apparatus as previously described, it was necessary that the soil-core surface be free from vegetation and mulch. In the preparation of the field site, after the plot frames were installed, the top 2.5 cm of grass mulch was carefully removed. This grass mulch was replaced by a layer of fiberglass to simulate the protective action of the bluegrass sod. After the field trials, four core samples were taken from within each of the plots.

In addition to the usual dry and wet run on each plot, on four of the twelve wet runs the fiberglass protective cover was removed after

60 min, and operation of the infiltrometer was continued for another 30 min. On four other trials, the bare surface was permitted to dry and crust for a period of four days, after which infiltration was again measured with the infiltrometer. The fiberglass cover was used on the field plots to protect the soil surface for making it comparable with that of the core samples.

Core-sample infiltration was measured in the laboratory as described on pages 60 and 65, and least-squares fitting (pages 25-27) to equation (4) was attempted, but without complete success. Hence, the directly measured field-core infiltration was taken as the prediction, and it is in this special and less rigorous sense that "predicted" is used in the remainder of the present Chapter 3. The data are summarized in Table 9,

Table 9. Infiltration, field-plot values by sprinkling infiltrometer, and field-core values by laboratory measurement.

Treatment	Infiltration rate after 40 min		Total infiltration during 40-min period	
	Dry	Wet	Dry	Wet
	cm/min	cm/min	cm	cm
Fiberglass cover	0.084	0.059	6.02	4.68
Bare soil-crusted	0.018	0.018	1.68	1.33
Fiberglass removed (60-90 min)	--	0.017	--	0.80
Predicted from field cores	0.022	--	2.48	--
Bluegrass	0.066	0.029	5.13	3.21

while a more complete graphical presentation is given in Figure 30. The points on the curves are the mean values of the number of trials indicated in the legend of the figure.

The field-core (predicted) curve is for only 40 min, the reason

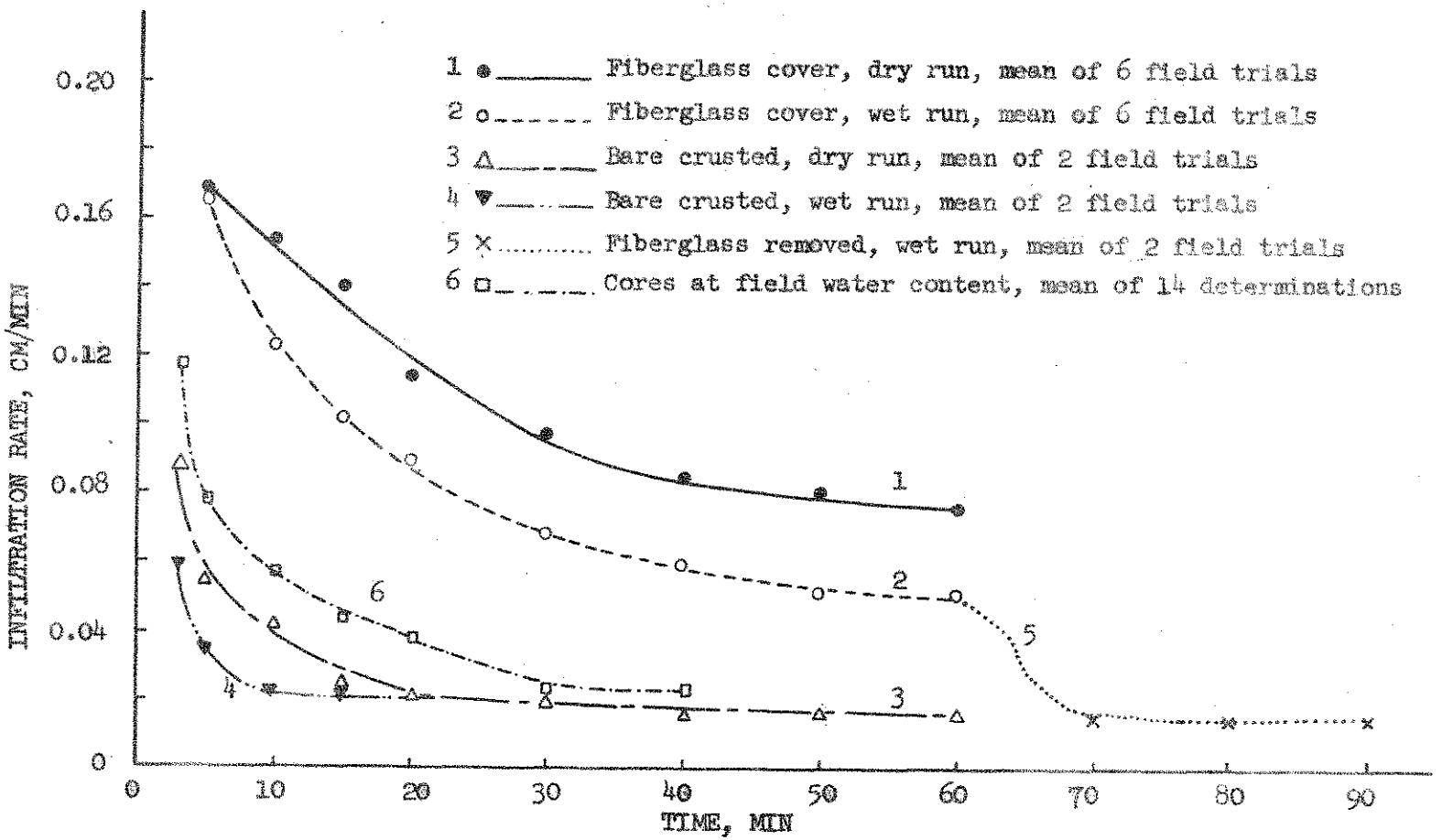

Figure 30--Comparison of infiltration rate curves of plots with fiberglass covers, bare crusted, and fiberglass removed, with that of infiltration into field cores, all on Fincastle silt loam.

being that the wet front reached the bottom of the core by that time. The data in Table 9 are based on 40 min instead of 60 min, so that comparisons could be made of the field-core values with those observed in the field.

As a means of checking the effect of the fiberglass cover, the data from some adjoining bluegrass plots are also given in Table 9. Although there is some difference in infiltration between the bluegrass and the fiberglass plots, the bluegrass being 15 to 25% lower than the fiberglass, the assumption that fiberglass is affording protection to the soil surface similar to a bluegrass mulch does seem to have validity.

The cores were of course taken at field soil-water content, and in this sense were comparable to the dry run of the fiberglass-cover plot (curve 1, Figure 30). Therefore, the field-core infiltration rates, curve 6, should be an estimate of or bear a similarity with curve 1, or even possibly curve 2 which is the wet run of the fiberglass plots. However, as can be noted in Figure 30 and also in Table 9, the field-core infiltration is much more nearly that of the bare-cursted soil, and of that after the fiberglass layer was removed. Subsequent results of further experiments as reported in the next section tend to bear out this same kind of finding, and possible reasons for it will be reported there.

LABORATORY MEASUREMENTS WITH FIELD CORES

Comparisons of laboratory-determined field-core infiltration rates with rates measured by the sprinkling infiltrometer were made on two soils, namely a Russell loam and an Oaktown sandy loam. The field cores were taken from within the respective plots, and after the infiltrometer runs were made.

In those plots where comparisons were made, the grass mulch was removed and replaced by a fiberglass layer. On another sequence of trials, the fiberglass layer was removed, thus permitting the impact energy of the water drops to act on the soil surface.

Before taking the core samples, the thin crusted layer, resulting from the falling water drops, was carefully shaved off. It was thus considered that the surface of the cores would have the same characteristics as that of the soil which had been measured with the infiltrometer.

Russell Loam

The results of these experiments are presented in Figures 31 and 32. The rate curves in Figure 31 are those of a bluegrass sod plot before the grass mulch was removed. This was intended for comparison with curve 3, Figure 32, which had the mulch removed but protected with the fiberglass layer. This latter curve was for the dry run only; however, the soil was approximately at 28.9% water by volume. The field cores, taken about one week after the infiltrometer trials, had a mean water content of 26.7% by volume when infiltration measurements were made in the laboratory. The rates for these cores could only be determined for 40 min, since the water front reached the bottom of the core by that time. After the laboratory infiltration measurements were completed on the cores at the field water content, they were placed in a pressure-membrane cell, and water was extracted at the 15-bar suction. Infiltration measurements were then repeated on the cores at this lower water content, as given in curve 2, Figure 32. The data are further summarized in Table 10.

Table 10. Comparison of field-core infiltration rate with that measured by the sprinkling infiltrometer, for Russell loam.

Treatment [1]	Terminal infiltration rate after 40 min	Terminal infiltration rate after 60 min	Total infiltration after 40 min	Total infiltration after 60 min
	cm/min	cm/min	cm	cm
1	0.006	--	1.58	--
2	0.012	0.048	1.70	1.96
3	0.058	0.048	4.10	5.17
4	0.014	0.014	1.07	1.33
5	0.016	0.008	1.51	1.77
Bluegrass sod, dry run	0.065	0.050	5.43	6.53

[1] Treatments: 1, cores at field water content; 2, cores at 15-bar suction; 3, sprinkling infiltrometer in the field, with fiberglass cover; 4 and 5, sprinkling infiltrometer in the field, fallow crusted.

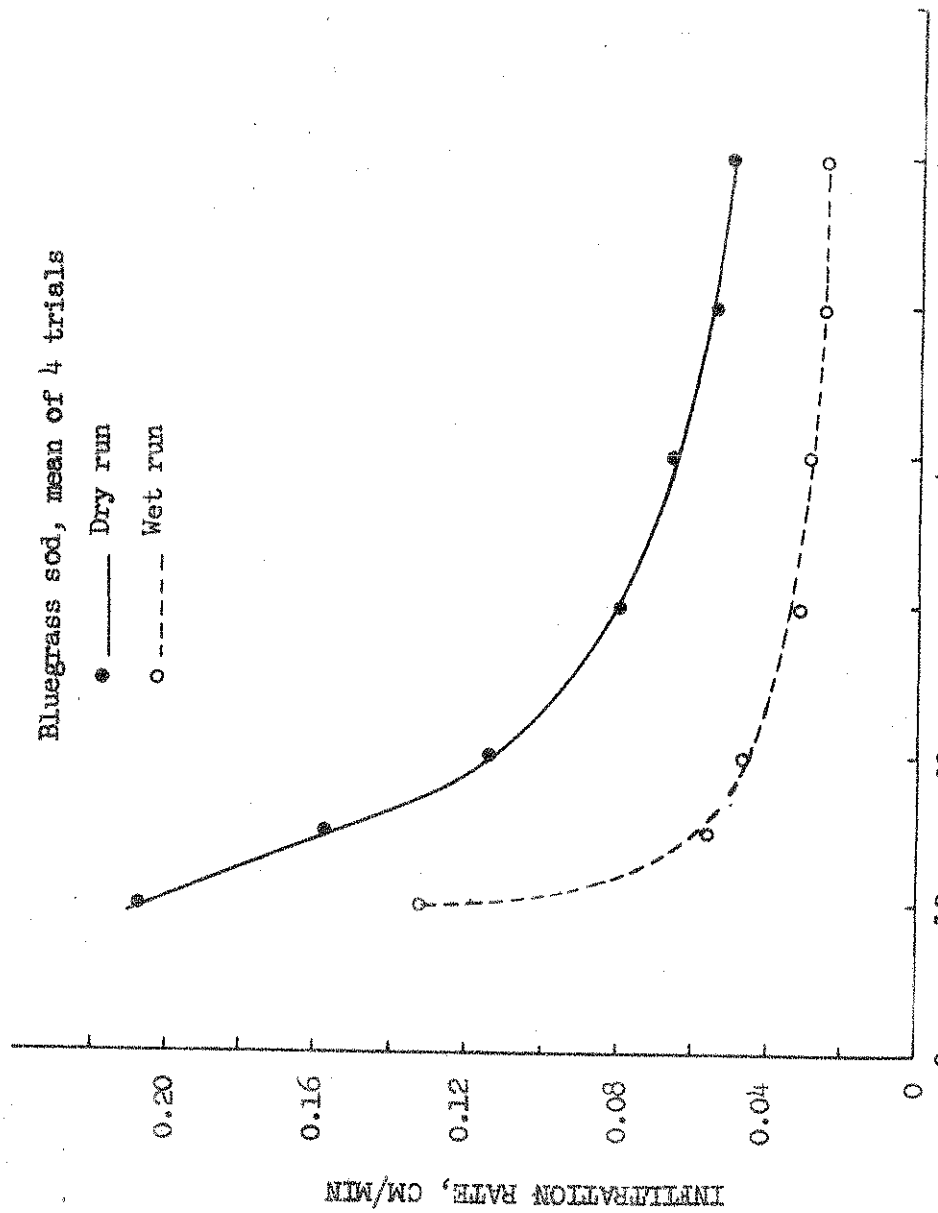

Figure 31--Infiltration rate curves for a bluegrass sod on Russell loam.

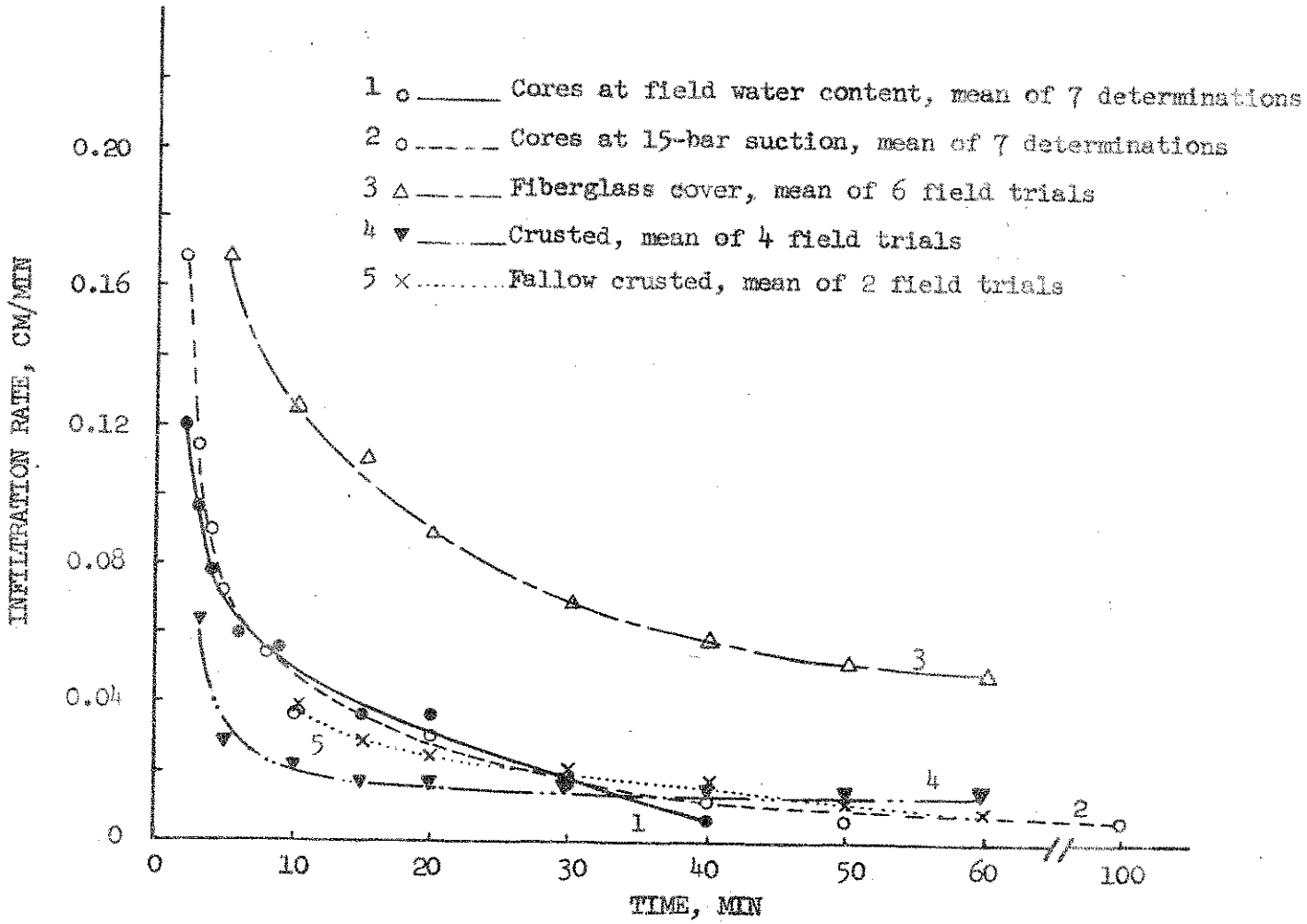

Figure 32--Infiltration rate curves for comparison of field and laboratory measurements on Russell loam.

If the dry-run curves for the bluegrass plots and the field fiberglass cover were placed on the same graph, the infiltration rates would appear very similar, with the bluegrass plots slightly higher. This difference is about 14% after 20 min and only about 2% at 60 min. However, when analyzed statistically the rates at 60 min are significantly different but the total infiltration for 60 min is not. Although the evidence does not permit a definite statement to the effect that the infiltration characteristics of the two treatments are the same, their similarity again gives credence to the assumption that the fiberglass cover does afford very nearly the same kind of surface protection as a bluegrass mulch.

By inspection of the infiltration rates given in Figure 32, only curve 3 for the fiberglass cover appears to be much different from the others. This would tend to indicate that the laboratory core samples would most accurately estimate the crusted and fallow-crusted conditions in the field. However, by the method used for field sampling, if the theoretical procedure was to show promise, it was anticipated that there would be similarity between curves 1 and 3; that is, the cores at field water content and the field infiltrometer determinations with the fiberglass cover. It would further be expected that because of the lower initial water content, the cores at the 15-bar suction would have a higher predicted infiltration rate than the cores at field water content. However, the cores for both initial water contents were quite similar to field measurements on plots where the surface had been subjected to the sealing effect of water-drop impact.

This would lead one to suspect that in the field core-sampling procedure, when removing the thin crusted layer, a layer of reduced hydraulic conductivity was formed near the surface. Upon inspection of some cores after they had air dried, it was found that the soil immediately below the surface did have considerably more structure and pore space than did the surface soil directly in contact with the applied water. It appeared that in the preparation of the field cores at a water content of about the field value, the surface layer was altered. Further work will need to be done to clarify this potential problem, and, if indeed it is a problem, a method of core sampling to preserve the original structure and porosity of the soil-core surface must then be developed.

Oaktown Sandy Loam

To test a range of soil porosity, laboratory measurements of infiltration were also made on a sandy loam soil. The results are given in Figure 33. Bromegrass cover and fiberglass cover were again compared with the measurements on field cores. The only situation wherein the field-plot surface soil was subjected directly to the impact energy of the water drops was in the wet run of the fiberglass cover plots, where, after 50 min, the fiberglass was removed and the surface soil was exposed.

As usually is the case with the field plots, the wet runs were consistently lower in infiltration rates than the dry runs. As noted in Figure 33, the infiltration rate with the fiberglass cover was considerably below the rate with bromegrass cover. One might again ask about the possibility of having destroyed the natural porosity when removing the grass mulch. There again was a distinct drop in infiltration rate when the fiberglass cover was removed; however, the drop was not as drastic as in a previous trial (Figure 30).

If curve 5 (Figure 33) for infiltration into field cores were extrapolated, the terminal rate after about 60 min might be nearly that of the field infiltrometer measurements with the surface exposed. Of most significance, the field-core rate is again well below the rates for bromegrass and fiberglass cover, and with the procedure used it was hypothesized that the estimated rates should have compared with curves 1 and 3. These results would again point out the possibility of changes or sealing on the surface of the field cores by the sampling procedure used.

Examination of curve 5 points out another problem with the field-core procedure as presently outlined. The last observation point occurred at 10 min, at which time the bottom end of the core had already begun to glisten, indicating that the "wet front" had reached the bottom. A better characterization of infiltration behavior would require more observations within the 10-min period, or a longer core sample, or perhaps both.

CHAPTER 3 SUMMARY AND CONCLUSIONS

The Purdue Sprinkling Infiltrometer, as modified, provides a means of measuring infiltration in the field. However, one must recognize that

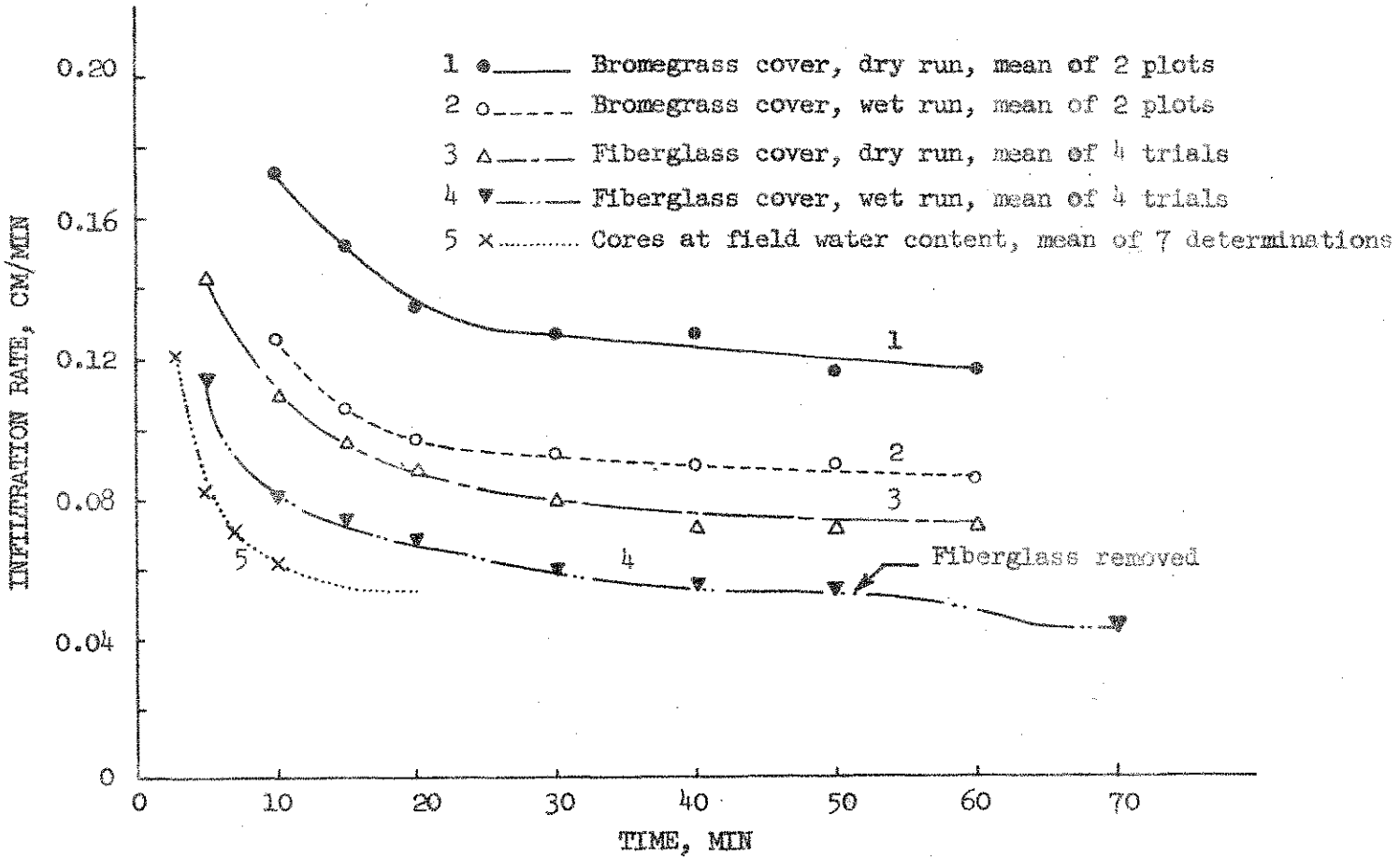

Figure 33--Infiltration rate curves for comparison of field and laboratory measurements on Oaktown sandy loam.

the small size of the plots utilized may or may not be representative of an area or watershed.

In this particular study, the infiltrometer was used in making infiltration measurements in the field, and these measurements were compared with laboratory determinations of infiltration into field cores of undisturbed soils.

Field experiments showed that within the range of surface-soil textures from sandy loam to loam, the infiltration characteristics did not vary greatly. Also, ridging of the soil or making it other than smooth did not have any significant effect. However, when the surface was protected, such as with a grass mulch, a fiberglass cover, or a 100% sand layer, the infiltration rates were significantly higher than in instances when the natural surface soil was exposed to the impact energy of the water drops.

In experiments where laboratory-determined infiltration rates into field cores were compared with the field-determined infiltrometer rates, the field-core rates were closer to those of soils which had been subjected to the impact energy of falling water drops, rather than comparing well with protected-surface values. It was anticipated that the field-core rate would estimate the rate in the field for the protected soil surfaces. The possibility is suggested that the preparation of field cores creates a soil surface in which the hydraulic conductivity is lowered similarly to that of bare or exposed soils.

If, as postulated, the procedure for taking the soil core-samples does in fact produce this surface impediment for infiltration, it would seem that the theoretical procedure for estimating infiltration rates in the field does still hold promise. Further work will be conducted in sampling procedures and evaluation.

CHARACTERIZATION of the RATE of WATER INFILTRATION into SOIL

continued

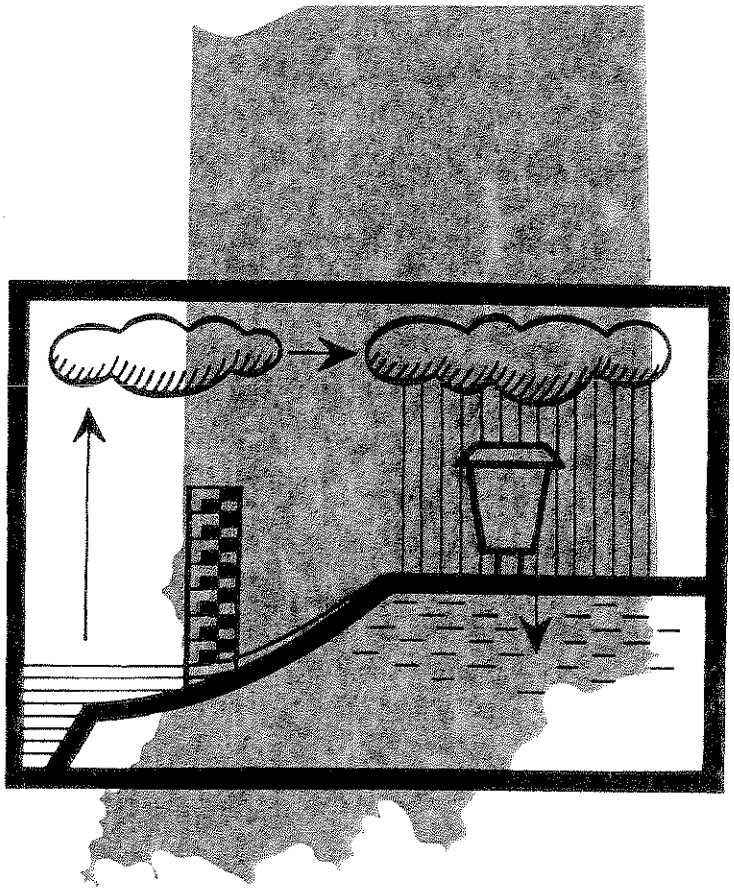

by
D. Swartzendruber
R. W. Skaggs
D. Wiersma

December, 1968

PURDUE UNIVERSITY
WATER RESOURCES RESEARCH CENTER
LAFAYETTE, INDIANA

CHAPTER 4. EVALUATION OF INFILTRATION EQUATIONS FROM LARGE-PLOT RAINFALL-SIMULATOR FIELD DATA

Many situations arise in hydrology where it is desirable to evaluate infiltration of water into the soil under rainfall conditions. An example is in the prediction of rate of surface runoff. During a given storm rainfall intensities in excess of infiltration rates produce surface runoff. Since a large percentage of the rainfall usually infiltrates into the soil, the accuracy with which the surface runoff can be predicted is heavily dependent on the accurate evaluation of infiltration. It is desirable to evaluate infiltration rates or accumulative infiltration volumes rapidly with a small number of input parameters. Often these parameters are the coefficients of algebraic equations which relate the infiltration rate to time or soil-water content.

A number of algebraic infiltration equations have been proposed. The four most widely used equations were presented by Green and Ampt (1911), Horton (1940), Philip (1957a), and Holtan, England and Shanholtz (1967). The present chapter reports an effort to evaluate these equations on the basis of large-plot field data, and to obtain numerical values for the parameters in the four equations for several different soils at varying initial moisture contents and surface conditions.

PUBLISHED INFILTRATION EQUATIONS

The so-called exact approach for the solution of the flow equations for infiltration of water into soil has been considered briefly at the beginning of Chapter 2. Numerical solution techniques have been presented by Klute (1952), Philip (1957c), Hanks and Bowers (1962), and Rubin (1966 a, b) for many of the boundary conditions of interest. Perhaps a greater barrier to numerically solving the general flow equations for applied problems is the large amount of computer time necessary to determine infiltration for the variable conditions existing within a watershed. This barrier could be overcome by the concise closed-form infiltration equations that have arisen from both theoretical and empirical origin. However, a lack of knowledge of the equation parameters for different soils and conditions makes the use of these equations difficult.

An algebraic infiltration equation originally presented by Green and Ampt (1911) and further treated by Philip (1954) was discussed in detail in Chapter 2. Assuming a deep homogeneous soil with a uniform initial soil-water content and water ponded on the surface, an expression for infiltration rate can be obtained by differentiating equation (4) with respect to time to obtain

$$f = C(1 + a/y) \tag{33}$$

where $f = dy/dt$ is the infiltration rate. The other symbols are just as defined in Chapter 2; namely, y is the cumulative volume of water infiltrated per unit cross sectional area, t is the time, and C and a are the constants which characterize the infiltration properties of the soil. Fok and Hansen (1966) analysed infiltration as predicted by equation (33), and presented graphical techniques of determining parameters a and C.

Probably the infiltration equation which has previously been the most widely used in hydrology is the one presented by Horton (1940) of the form

$$f = f_c + (f_o - f_c)\, e^{-k_f t} \tag{34}$$

where f_c is the final (or steady-state) infiltration rate, f_o is the initial infiltration rate (at time $t = 0$), and k_f is a constant dependent on the soil and its surface conditions. Horton proposed that the transporting properties of the soil surface were affected by the impact energy of the falling raindrops, so that factors f_c and k_f in equation (34) were also dependent on rainfall intensity. This equation seems to fit infiltration data well, but requires three parameters (f_o, f_c and k_f) to be evaluated from results of field experiments.

Philip (1957c) presented a rapidly converging numerical technique for solving the flow equation for a homogeneous, deep soil with a uniform initial water content and a water-ponded surface. His solution may be written for infiltration rate as an infinite series in powers of $t^{1/2}$ where the coefficient of each term is ultimately dependent on the soil-water diffusivity, conductivity, and water-content characteristics, and must be determined by numerical methods. Philip (1957a) proposed that the first two terms of his series solution be used as a concise infiltration equation. This equation was discussed in Chapter 2 where it was shown that the coefficients could be approximately matched with those in the Green-

Ampt equation. Differentiating equation (6) yields the following relationship for the infiltration rate

$$f = S/2t^{1/2} + G \tag{35}$$

For very large times the infiltration rate should equal the hydraulic conductivity, K. Equation (35) would agree with this if G = K. However, Philip notes that this equality does not exist and that equation (35) theoretically fails for large times.

Philip (1957a) compared results obtained with various concise infiltration equations to results obtained using his series solution. Equations (33) and (34) gave values within 5% of those predicted by the detailed analysis while Horton's equation (34) predicted values in error by as much as 82% for small times. However, it should be noted that Philip's solution was obtained for fairly restrictive boundary conditions, and that its applicability to field situations, where the soil is likely to be nonhomogeneous and its surface properties time variant under rainfall conditions, may not be more reliable than other prediction equations. Indeed, the theoretical origin of the equation may be misleading for rainfall infiltration.

Rubin (1966b) used numerical techniques to solve the general flow equation, and obtained theoretical infiltration rate relationships for a soil wherein the surface was subjected to rainfall at rates initially lower than the infiltration rate. The results showed that the infiltration rate-time relationship depended on the rainfall rate, and was quite different than that for water-ponded surface condition--even when assuming no change in surface properties due to raindrop impact and surface sealing. Consequently, it should not be surprising if theoretically based equations that have been derived for a water-ponded surface do not perform as well under rainfall conditions.

An empirical equation based on a water-storage concept has been proposed by Holtan (1961) and Holtan, England, and Shanholtz (1967), which expresses the infiltration rate as

$$f = m(S_t - y)^n + f_c \tag{36}$$

where S_t is the storage potential of the soil above the impeding stratum (total porosity minus the antecedent soil water expressed in units of length), and m and n are constants specified by soil type, and surface and cropping conditions. The use of y instead of t as the independent variable offers advantages in watershed hydrology simulation. For example, difficulties are not encountered in computing the infiltration rate at any time during a storm event, even when the water supply does not exceed the infiltration rate. By assuming a relationship between drainage and soil-water content, equation (36) can be used to predict the recovery of infiltration rate as the result of a temporary interruption in rainfall.

Huggins and Monke (1967) used the following rearranged form of Holtan's equation to describe infiltration data taken with a sprinkling infiltrometer

$$f = \lambda[(S_t - y)/N]^n + f_c \qquad (37)$$

where N is the total storage available for infiltrated water and is equal to the product of total porosity and the effective depth. Since $(S_t - y)/N$ never exceeds unity, the constant λ represents the maximum possible increase in infiltration rate over the final steady-state rate, f_c. The constant n dictates the steepness of the infiltration curve at the beginning of infiltration. A major difficulty with equations (36) and (37) is the evaluation of the control depth on which to base N and S_t. Holtan and Creitz (1967) suggested using the depth to the first impeding layer; however, Huggins and Monke (1967) found that the effective depth was highly dependent on both the surface condition and the cultural practices used in preparing the seedbed.

Watson (1959) compared the predictions for infiltration rate by Horton's and Philip's equations [equations (34) and (35) respectively] with experimental results obtained with a sprinkling infiltrometer. He showed that Philip's equation would best fit the experimental data in the early portion of the test, but the agreement was good over the entire 90-minute test. Horton's equation showed considerable deviation during the early part of the test, but accurately characterized the latter part where the infiltration rate approached a constant value.

PROCEDURE

Field Experiments

The experimental data used in this study were obtained from erosion experiments conducted by the Agricultural Research Service, U. S. Department of Agriculture, at Purdue University. The rainfall simulation equipment and its operation were discussed by Meyer and McCune (1958). The data were runoff hydrographs obtained for simulated storms of 60- and 30-minute durations.

This source of infiltration data was attractive for several reasons. The size of the plots was large (12 by 35 feet) and generally representative of natural field conditions. Available data involved a large variety of soil types, crops, and cultural practices. A regular soil survey report, the soil-water contents at the beginning of each test, and various physical properties of the soil, such as porosity, bulk density, and organic matter content were available for most of the tests.

Simulated rainfall was applied at an intensity of about 2.5 in/hr, with a drop-size distribution and velocity near that of natural rainfall. The kinetic energy at impact was approximately 80% of that corresponding to natural rainfall. Another important advantage of these data for infiltration analysis was the availability of runoff sediment content measurements. This made it possible to correct the runoff rate for sediment, a source of error in other methods used for experimentally studying infiltration under rainfall.

The data here analyzed were obtained from two erosion studies conducted by the Agricultural Research Service at selected sites throughout Indiana. One of these was an investigation of the effect of physical properties of soils on erosion and runoff; from it, infiltration data were obtained for replicated experiments on 12 different fallow soils. The second study was an investigation of the influence of runoff and soil loss on the fate of surface-applied nitrogen; from it, infiltration data were obtained for two series of replicated tests on both fallow and fescue sod plots on a Zanesville silt loam soil. Table 11 gives the data that were used in addition to the runoff hydrographs.

Table 11. Description and supplementary data for field plots for which rainulator hydrographs were analyzed.

Code [1]	Soil type	Cover	Porosity	Initial water content, wt. basis		Slope	Rainfall	Sediment wt. basis
				Depth 0-5 in	Depth 5-10 in			
			%	%	%	%	in/hr	%
008 162 2	Avonburg si.l.	Fallow	49.1	14.1	17.6	10.3	2.62	15.0
008 162 5	" "	"	49.1	14.1	17.6	10.3	2.82	16.0
008 262 5	" "	"	49.1	20.7	20.4	10.3	2.73	11.5
014 162 3	Russell si.l.	"	54.0	18.2	19.8	8.8	2.69	9.5
014 162 6	" "	"	54.0	18.2	19.8	8.8	2.55	10.0
014 262 6	" "	"	54.0	25.9	21.9	8.8	2.63	10.0
033 162 5	Miami sandy l.	"	53.8	10.5	13.0	11.1	2.68	11.5
033 162 6	" "	"	53.8	10.5	13.0	11.1	2.51	7.5
035 162 3	Warsaw sandy l.	"	55.0	14.8	16.7	9.8	2.54	2.0
035 162 5	" "	"	55.0	14.8	16.7	9.8	2.28	1.5
035 262 3	" "	"	55.0	19.7	19.0	9.8	2.41	4.0
037 164 4	Miami si. l.	"	50.9	9.5	14.2	8.7	2.68	7.5
037 164 6	" "	"	50.9	9.5	14.2	8.7	2.62	7.2
037 264 4	" "	"	50.9	23.4	18.1	8.7	2.59	7.5
038 164 4	Morley si. l.	"	52.0	13.9	17.5	9.6	2.25	6.0
038 164 6	" "	"	52.0	13.9	17.5	9.6	2.66	7.3
038 264 4	" "	"	52.0	25.6	20.4	9.6	2.55	6.5
038 264 6	" "	"	52.0	25.6	20.4	9.6	2.62	7.0
043 164 4	Morley loam	"	45.3	13.5	16.9	10.1	2.23	6.0
043 264 4	" "	"	45.3	20.1	20.3	10.1	2.42	7.5
045 164 4	Morley c.l.	"	43.2	13.8	17.8	10.0	2.54	5.0
045 164 6	" "	"	43.2	13.8	17.8	10.0	2.56	4.0
045 264 4	" "	"	43.2	21.9	21.9	21.1	2.58	5.5
045 264 6	" "	"	43.2	21.9	21.1	10.0	2.58	5.3
046 165 1	Cincinnati si. l.	"	46.0	21.6	24.2	7.0	2.39	9.0
046 165 3	" "	"	46.0	21.6	24.2	7.0	2.62	9.0
048 165 5	Frederick si. l.	"	43.9	21.8	21.7	12.2	2.73	10.0
048 265 5	" "	"	43.9	24.2	23.4	12.2	2.37	7.0
048 265 4	" "	"	43.9	24.2	23.4	12.2	2.26	7.5
049 165 4	Grayford si. l.	"	53.0	23.4	23.9	7.9	2.56	9.5
049 165 6	" "	"	53.0	23.4	23.9	7.9	2.68	10.0

Table 11. (Continued)

Code [1]	Soil type	Cover	Porosity	Initial water content, wt. basis		Slope	Rainfall	Sediment wt. basis
				Depth 0-5 in	Depth 5-10 in			
			%	%	%	%	in/hr	%
051 165 2	Penbroke si. l.	Fallow	46.8	19.2	22.5	7.1	2.55	6.0
051 165 6	" "	"	46.8	19.2	23.5	7.1	2.39	6.0
051 265 2	" "	"	46.8	24.1	22.9	7.1	2.26	5.0
051 265 6	" "	"	46.8	24.1	22.9	7.1	2.39	5.5
802 165 1 [2]	Zanesville si. l.	"	52.1	25.5	24.9	13.0	2.38	6.0
802 265 1	" "	"	52.1	32.1	27.0	13.0	2.48	5.0
804 165 3	Zanesville si. l.	"	52.9	25.4	26.3	13.0	2.38	6.0
804 265 3	" "	"	52.9	30.7	28.6	13.0	2.38	5.5
802C165 1	" "	Crusted	52.1	29.0	26.8	13.0	2.44	5.5
802C265 1	" "	fallow	52.1	32.7	28.3	13.0	2.42	4.3
804C165 3	" "	"	52.9	25.5	26.9	13.0	2.36	5.5
804C265 3	" "	"	52.9	28.6	27.6	13.0	2.36	4.0
801 165 5	Zanesville si.l.	Fescue	43.8	11.0	13.6	13.0	2.47	0.2
801 265 5	" "	sod	43.8	26.8	23.7	13.0	2.51	0.1
803 165 2	" "	"	41.4	14.9	15.1	13.0	2.43	0.3
803 265 2	" "	"	41.4	26.4	24.3	13.0	2.43	0.03
801C165 5	Zanesville si.l.	"	43.8	26.3	24.9	13.0	2.43	0.01
801C265 5	" "	"	43.8	30.0	28.0	13.0	2.43	0.01
803C165 2	" "	"	41.4	24.6	24.6	13.0	2.43	0.01
803C265 2	" "	"	41.4	30.2	29.4	13.0	2.43	0.01

[1] Code example: (802C165 1) 802 - Treatment; C - crusted surface (a second series of tests conducted three days after the very wet run); 1 - run number (1 - dry, 2 - wet, 3 - very wet); 65 - year of run; 1 - flume number.

[2] The initial moisture contents for the 800 series were determined for depths of 0-6 in and 6-12 in.

The procedure of preparing the experimental plots and conducting the rainulator tests for the fallow conditions was described by Olson, Mannering, and Johnson (1962). Briefly, the plot preparation consisted of plowing in the spring followed by five diskings to keep the plots fallow until the rainulator tests were conducted in July and August. The plots were covered to keep off natural rainfall between the time of the last disking and the initial rainulator run.

The plots were subjected to three simulated storms at a rainfall intensity of about 2.5 in/hr. The storms consisted of an initial or dry run of 60 min, followed 24 hr later by a wet run of 30 min, followed 15 min later by a very wet run of 30 min. The runoff hydrographs were obtained with a calibrated flume and a FW-1 waterstage recorder. Water content was determined by gravimetrically sampling the upper 10 in of the soil profile prior to the dry and wet runs.

The experimental procedure in the second study was described in detail by Moe, Mannering, and Johnson (1967). The fallow plots were prepared in the same manner as before. However, a second series of tests was run 3 days after the very wet run. This permitted observation of the so-called surface-sealing effect on the infiltration characteristics of this soil. The fescue sod plots were clipped to a height of 2 in and the infiltration runs were similar to those for the fallow condition.

Determination of Infiltration Rate

The first step in the analysis of the rainulator data with respect to infiltration was to record the runoff records in digital form. Points from the stage records were recorded at intervals such that the record was described by straight lines connecting them. This data transfer was rapidly and accurately accomplished by using an analog/hybrid computer in conjunction with a chart-reading apparatus.

Water applied to an experimental plot in excess of the infiltration rate produces runoff. Therefore, for a steady state situation, the infiltration rate may be determined by taking the difference between the application and runoff rates. However, in the initial stages of rainfall there is storage on the plot surface and the flow of water from the plot may be termed, "unsteady overland flow". The equation of continuity applied to the entire plot may be written for the determination of in-

filtration rate in the following form

$$f = R - Q - \dot{s} \tag{38}$$

where f is the infiltration rate as before, R is the rainfall rate, Q is the runoff rate, and $\dot{s}$ is the storage rate on the plot surface.

R and Q were obtained in the experiments; thus, to obtain infiltration data for the tests, it was necessary to characterize the storage rate, $\dot{s}$. Water is stored on the plot as retention storage, water ponded in depressions on the plot surface, and as surface detention storage. Since measurements of the water surface profiles were not made, it was necessary to evaluate storage rates by some other technique.

Foster, Huggins, and Meyer (1968) analyzed the flow of surface water on rainulator plots. They showed that the runoff could be described by assuming overland flow conditions and a model based on the kinematic wave theory. Governing equations were the continuity and uniform flow equations, namely

$$\partial q/\partial x + \partial Z/\partial t = \sigma \tag{39}$$

$$Z = f_1 \overline{V}^2/8gS_o \tag{40}$$

where q is the discharge per unit width, x is the distance from the upstream end of the plot, Z is the depth of water on the plot at point x, t is the time, $\sigma = R - f$ is the rainfall excess, f_1 is the Darcy-Weisbach coefficient of friction, $\overline{V}$ is the average downslope velocity at point x, g is the acceleration due to gravity, and S_o is the slope of the plot.

Foster, Skaggs, and Huggins (1969) presented techniques using the method of characteristics to solve equation (39) and a more general form of equation (40), in reverse fashion such that the storage rate, $\dot{s}$, could be obtained directly. For the initial stages of runoff, the equations were solved exactly for rainfall excess (thus infiltration rate) by using the slope of the runoff hydrograph. However, for times greater than 2 to 5 min after the beginning of runoff, the solution required the assumption that the discharge at any point, x, was given by

$$q_x = (x/L)Q_E \tag{41}$$

where L is the length of the plot, and Q_E is the discharge at the end of the plot. Use of equation (41) allowed evaluation of the storage rate $\dot{s}$ which was then used in equation (38) to evaluate infiltration rates. Foster,

Skaggs, and Huggins (1969) analyzed extreme cases of both rapidly and slowly varying infiltration rates, and showed that the error in the evaluation of infiltration rates due to the use of equation (41) was less than 2%. Thus, the stage hydrograph, sediment content, plot slope, measured rainfall application rate, and the coefficient of friction, f_1, were used as input data for digital computer programs to solve equations (39) and (40) and the consequent evaluation of $\dot{s}$ in equation (38).

Selection of the coefficient of friction was difficult. Foster, Huggins, and Meyer (1968) showed that f_1 dictated the steepness of the rising limb of the runoff hydrograph. Using the methods suggested by Foster, Skaggs, and Huggins (1969), ten field hydrographs were simulated for a wide range of f_1 for several assumed infiltration relationships. The results of those simulations indicated that, as far as the evaluation of infiltration and storage rates was concerned, the roughness of the fallow plots could be adequately described by using values for the friction factor of 1.5 for the dry runs and 0.75 for the wet runs.

Evaluation of the storage and infiltration rates required the numerical differentiation of field runoff hydrographs. Discontinuities in the slopes of the field hydrographs caused the storage-rate calculation for that point to also be discontinuous. To minimize the effect of these discontinuities, calculated storage and infiltration rates were plotted and a smooth curve drawn through the points to define the infiltration rate-time relationship for a test. The runoff, storage, and infiltration relationships are shown in Figures 34 and 35 for dry and wet runs on fallow Morley silt loam. Note that the storage rate is high for the wet run (Figure 35) where the runoff hydrograph is steep, and lower for the dry run (Figure 34) where the runoff hydrograph slopes are more moderate.

Analysis of Data

A least-squares regression analysis was chosen to evaluate the ability of the infiltration equations to describe the experimental data, and to determine values of the equation parameters for different soils and antecedent conditions. The infiltration curve was recorded in digital form such that the volume of infiltration between successive points was constant. Fifty points were recorded for each hydrograph and the infiltration equa-

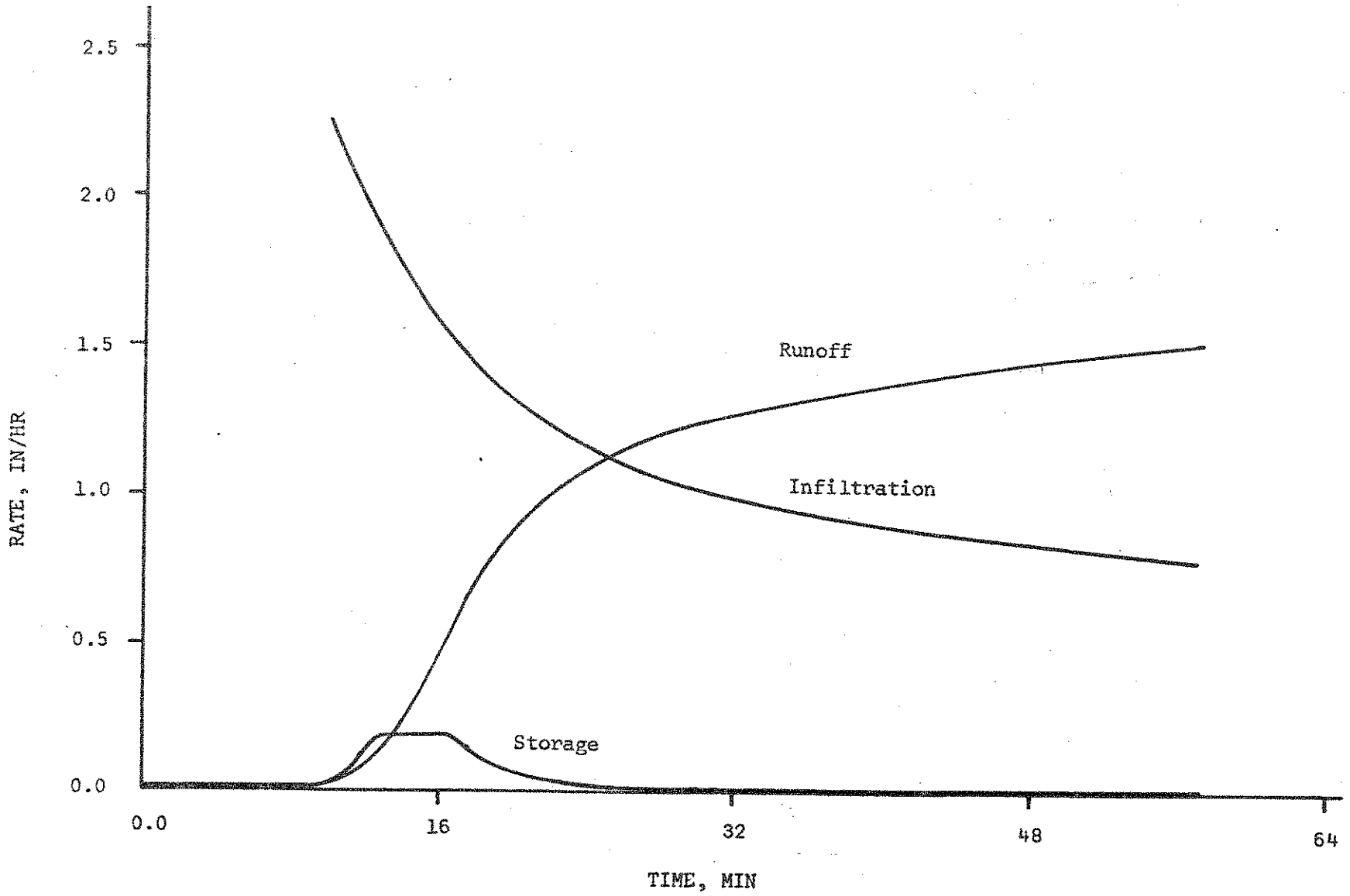

Figure 34 -- Runoff, storage, and infiltration relationships for a dry run on fallow Morley silt loam.

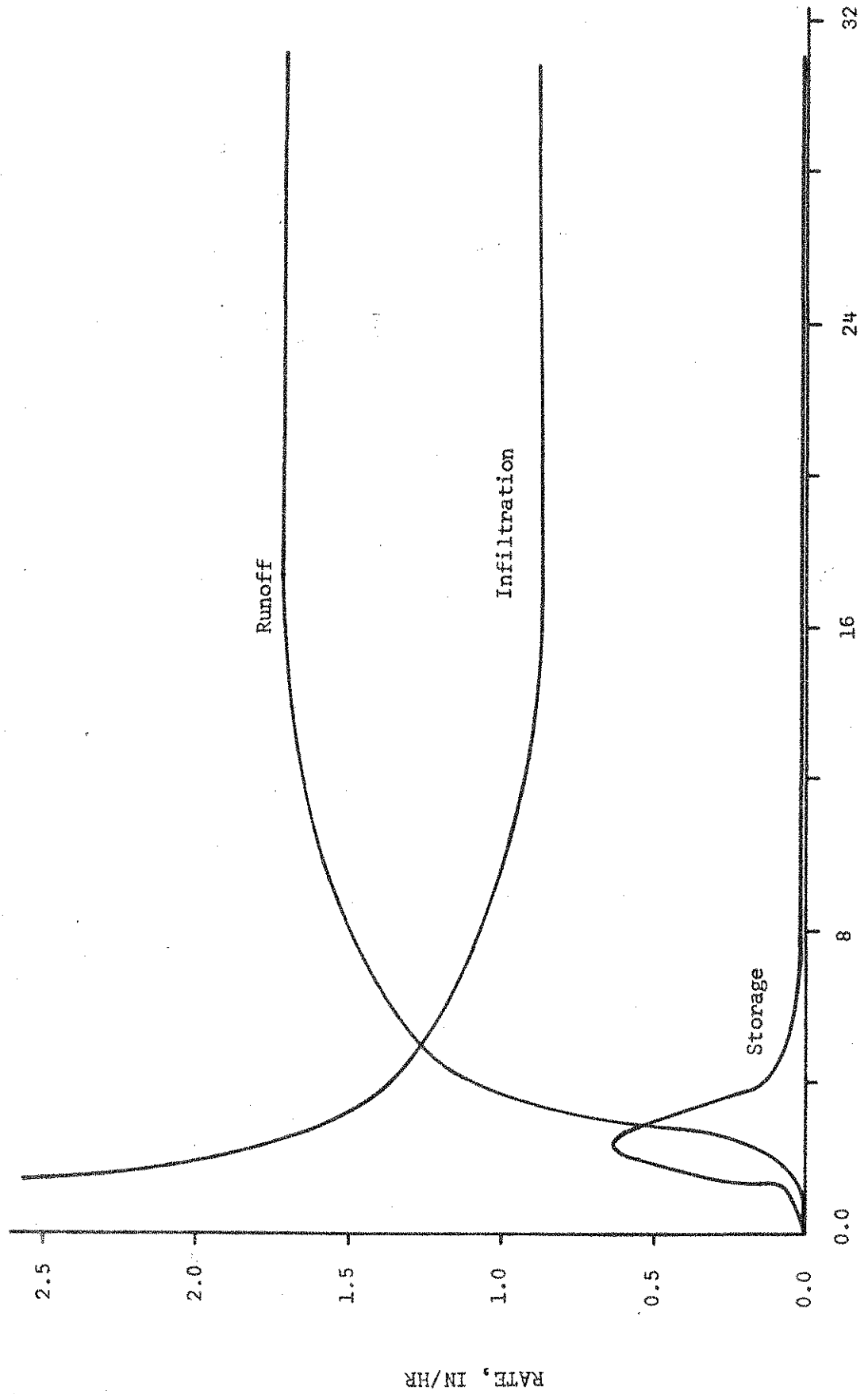

Figure 35 -- Runoff, storage, and infiltration relationships for a wet run on fallow Morley silt loam.

tions were fitted to these data by regression.

To facilitate the regression analysis, equation (33) was written in the form

$$f = C + A/y \qquad (42)$$

where $A = aC$. The accululative infiltration, y, was determined by numerically integrating the infiltration rate with respect to time. Then, by redefining the independent variable as $1/y$, the constants C and A were obtained by linear regression. In equation (35), taking $t^{-1/2}$ as the independent variable allowed the use of linear regression to determine constants S and G.

Equations (34) and (35) are nonlinear equations; thus, their parameters cannot be determined by linear regression without transforming the dependent variable. To avoid transformations, a nonlinear regression program, available in the SHARE program library (SHARE program #3094), was used to determine the appropriate coefficients in equations (34) and (35).

RESULTS AND DISCUSSION

The results of least-squares fitting of the equations of Green and Ampt, Philip, and Horton to the experimental data are given in Table 12. Corresponding results for Holtan's equation [equation (36)] are presented in Table 13. A two-parameter form of Holtan's equation, obtained by setting $n = 1.4$ in equation (36), was fitted to the data by linear regression. The results of the fit of this equation are also given in Table 13.

Graphical representations of the fit of each of the equations to the data are exemplified by Figures 36 and 37. These plots are for dry and wet runs on Morley silt loam; the fits are typical of those obtained for other soils in this study.

From these figures and the correlation index (R^2) in Tables 12 and 13, it may be observed that all five of the equations give close fits to the infiltration data in the time range that was tested. An indication of the comparative ability of the equations to fit the experimental data is given by the means of the R^2 values in Tables 12 and 13.

Table 12. The results of regression fits to the Green-Ampt, Philip, and Horton equations.

Code	Green-Ampt			Philip			Horton			
	R^2	C	A	R^2	G	S	R^2	f_e	f_o-f_c	k_f
		in/hr	in^2/hr		in/hr	$in/hr^{1/2}$		in/hr	in/hr	1/hr
008 162 2	.984	- .83	1.58	.954	-1.07	2.86	.998	0.60	6.40	6.77
008 162 5	.954	-5.00	4.65	.824	-2.68	4.52	.989	0.22	43.85	13.25
008 262 5	.953	-0.61	0.22	.990	-0.81	1.02	.987	0.15	3.33	16.88
014 162 3	.970	-0.37	1.01	.943	-0.67	2.18	.997	0.68	5.52	8.35
014 162 6	.949	-0.56	1.12	.897	-0.70	2.20	.999	0.67	8.38	10.06
014 262 6	.980	-0.56	0.45	.945	-0.69	1.40	.998	0.54	5.23	17.64
033 162 5	.949	0.39	0.72	.970	-0.13	1.86	.991	0.92	3.32	5.75
033 162 6	.960	0.09	0.85	.941	-0.32	2.00	.993	0.85	4.46	7.16
035 162 3	.978	0.57	1.40	.996	-0.16	2.80	.997	1.04	3.00	2.69
035 162 5	.974	0.99	0.84	.992	0.45	1.92	.994	1.12	1.88	1.97
035 262 3	.966	0.32	0.10	.995	0.08	0.60	.998	0.68	3.00	28.84
037 164 4	.908	-1.14	3.40	.888	-1.55	4.56	.995	1.03	49.17	9.59
037 164 6	.955	-0.41	1.97	.988	-1.24	3.76	.994	0.53	4.50	3.28
037 264 4	.972	0.46	0.22	.945	0.13	0.90	.993	0.95	3.59	2.05
038 164 4	.992	0.05	0.86	.970	-0.37	2.06	.997	0.81	4.08	6.11
038 164 6	.941	0.07	1.06	.976	-0.61	2.52	.985	0.73	3.81	4.64
038 264 4	.984	0.59	0.11	.949	0.36	0.56	.980	0.90	2.62	25.71
038 264 6	.982	0.53	0.11	.945	0.31	0.56	.976	0.85	2.69	26.83
043 164 4	.781	0.03	0.92	.908	-0.84	2.68	.950	0.12	3.38	2.53
043 264 4	.962	0.06	0.15	.927	-0.12	0.74	.998	0.61	4.02	30.40
045 164 4	.988	-1.61	4.11	.970	-2.40	5.98	.990	0.64	10.87	4.51
045 164 6	.922	0.02	1.92	.978	-0.98	3.82	.998	-0.21	4.02	1.40
045 264 6	.972	0.52	0.12	.949	0.25	0.62	.998	0.86	2.91	25.48
045 264 4	.929	0.48	0.11	.982	0.12	0.68	.995	0.72	2.50	18.29
046 165 1	.962	-0.17	0.98	.918	-0.46	2.10	.998	0.83	7.07	8.95
046 165 3	.887	-0.92	1.20	.837	-0.75	2.06	.983	0.057	1.68	14.20
046 265 3	.925	0.29	0.12	.988	-0.07	0.72	.995	0.53	2.52	16.26
048 165 5	.912	0.22	0.87	.872	-0.14	1.90	.983	1.03	6.47	9.92
048 265 5	.933	0.45	0.10	.887	0.27	0.52	.995	0.78	3.38	34.17
048 265 4	.996	0.43	0.07	.986	0.22	0.48	.950	0.66	1.79	20.10
049 165 4	.974	0.58	0.36	.998	0.19	1.18	.991	0.87	2.31	6.20
049 165 6	.929	0.28	0.77	.891	0.005	1.62	.964	1.02	6.46	10.29

Table 12. (Continued)

Code	Green-Ampt			Philip			Horton			
	R^2	C	A	R^2	G	S	R^2	f_c	f_o-f_c	k_f
		in/hr	in^2/hr		in/hr	$in/hr^{1/2}$		in/hr	in/hr	1/hr
051 165 2	.929	-0.35	0.53	.925	-0.56	1.56	.985	0.46	4.47	10.52
051 165 6	.941	-0.51	0.75	.889	-0.56	1.72	.999	0.55	6.83	11.64
051 265 2	.750	0.27	0.15	.918	0.36	0.98	.993	0.09	2.68	7.50
051 265 6	.667	0.53	0.23	.850	-0.28	1.28	.962	0.02	3.05	4.72
802 165 1	.994	0.13	1.29	.998	-0.46	2.68	.999	0.93	3.97	4.34
802 265 1	.986	0.64	0.08	.984	0.38	0.50	.977	0.86	2.11	24.01
804 165 3	.970	0.18	1.37	.996	-0.55	2.94	.999	0.69	3.18	2.67
804 265 3	.927	0.27	0.14	.889	0.11	0.64	.974	0.72	3.77	29.11
802C165 1	.889	0.50	0.15	.848	0.31	0.68	.992	0.79	3.67	22.66
802C265 1	.863	0.31	0.09	.824	0.18	0.50	.997	0.69	5.24	53.55
804C165 3	.933	0.21	0.17	.916	0.03	0.78	.998	0.57	3.22	17.79
804C265 3	.950	0.35	0.12	.859	0.18	0.58	.990	0.78	5.08	40.08
801 165 5	.946	1.22	0.98	.962	0.86	1.78	.960	1.02	2.11	2.53
801 265 5	.960	0.95	0.61	.978	0.25	1.82	.972	1.54	8.60	11.21
803 165 2	.953	1.34	0.86	.982	0.78	1.86	.997	2.13	1.86	2.25
803 265 2	.956	0.86	0.69	.925	0.26	1.78	.993	1.60	9.99	13.00
801C165 5	.814	-0.54	2.27	.927	-1.89	4.84	.974	-2.63	6.50	0.83
801C265 5	.966	-1.32	1.47	.996	-2.20	3.64	.961	-0.20	3.69	4.18
803C165 2	.878	-0.24	1.84	.953	-1.24	3.86	.986	-1.40	4.83	0.96
803C265 2	.941	-1.14	1.24	.988	-2.00	3.26	.991	-0.08	4.91	5.09
$\bar{R}^2$	.935			.936			.987			

Table 13. The results of regression fits to two forms of Holtan's equation.

Code	Control depth	Holtan				Holtan (1.4 exponent)			
		R^2	m [1]	n	f_c	R^2	m [1]	n	f_c
	in				in/hr				in/hr
008 162 2	3.01	.999	4.60	1.67	0.64	.994	3.88	1.4	0.59
008 162 5	2.60	.983	18.30	1.62	0.17	.978	13.90	1.4	0.10
008 262 5	0.93	.980	31.50	1.60	0.07	.988	23.30	1.4	0.0012
014 162 3	2.68	.981	5.53	2.19	0.68	.954	3.54	1.4	0.57
014 162 6 [2]	2.97	.998	6.87	3.31	0.66	.868	2.78	1.4	0.44
014 262 6 [2]	1.79	.997	51.50	3.12	0.52	897	8.06	1.4	0.23
033 162 5	3.25	.987	1.31	2.66	0.92	.918	1.46	1.4	0.68
033 162 6	2.21	.996	3.76	1.73	0.89	.984	3.01	1.4	0.85
035 162 3 [2] [2]	4.75	.997	0.89	1.54	1.27	.996	0.93	1.4	1.24
035 162 5 [2]	4.65	.991	0.60	1.37	1.40	.990	0.60	1.4	1.40
035 262 3	0.93	.997	358.00	4.18	0.67	.802	8.13	1.4	0.52
037 164 4 [2]	4.32	.992	2.99	3.37	1.03	.876	2.05	1.4	0.79
037 164 6 [2]	3.86	.993	1.95	1.39	0.70	.992	1.98	1.4	0.72
037 264 4	1.72	.992	45.80	2.26	0.95	.861	5.31	1.4	0.81
038 164 4 [2]	3.19	.996	2.28	2.50	0.83	.945	1.74	1.4	0.69
038 164 6 [2]	3.66	.983	1.88	1.90	0.78	.968	1.94	1.4	0.63
038 264 4	1.27	.984	163.00	3.78	0.90	.857	6.48	1.4	0.82
038 264 6	1.21	.982	221.00	3.84	0.85	.852	7.17	1.4	0.77
043 164 4	3.81	.946	2.35	1.03	0.42	.929	2.34	1.4	0.56
043 264 4	1.57	.993	842.00	5.47	0.55	.736	6.56	1.4	0.33
045 164 4	6.25	.995	2.51	1.58	0.75	.992	2.38	1.4	0.66
045 164 6 [2]	6.15	.998	1.60	0.96	0.78	.978	1.45	1.4	1.01
045 264 4	1.93	.994	43.40	3.09	0.71	.893	6.65	1.4	0.55
045 264 6	1.89	.999	156.00	4.18	0.86	.805	5.60	1.4	0.73
046 165 1 [2] [2]	5.01	.999	2.65	4.56	0.82	.870	1.89	1.4	0.60
046 165 3 [2]	4.20	.993	21.60	4.96	0.55	.794	3.13	1.4	0.26
046 265 3	1.97	.998	38.20	2.71	0.52	.929	8.61	1.4	0.34
048 165 5	3.88	.987	5.51	1.69	1.05	.982	4.47	1.4	1.03
048 265 5	1.17	.997	304.00	3.03	0.65	.901	13.10	1.4	0.74
048 265 4	2.10	.964	216.00	5.23	0.79	.785	4.08	1.4	0.43
049 165 4	3.79	.992	1.76	2.78	0.89	.925	1.49	1.4	0.72
049 165 6	4.30	.970	2.65	4.56	0.95	.810	1.30	1.4	0.84

Table 13. (Continued)

Code	Control depth	Holtan R^2	Holtan m [1]	Holtan n	Holtan f_c	Holtan (1.4 exponent) R^2	Holtan (1.4 exponent) m [1]	Holtan (1.4 exponent) n	Holtan (1.4 exponent) f_c
	in				in/hr				in/hr
051 165 2	2.46	.970	11.66	2.51	0.44	.899	4.97	1.4	0.27
051 165 6	2.30	.999	1.37	2.02	0.55	.974	6.69	1.4	0.50
051 265 2 [2]	1.69	.991	7.46	1.10	0.95	.982	10.10	1.4	0.26
051 265 6 [2]	2.52	.959	4.70	0.98	0.26	.939	5.94	1.4	0.51
802 165 1 [2]	6.11	.999	1.28	2.05	1.00	.978	1.30	1.4	0.88
802 265 1 [2]	2.17	.984	1.82	5.17	0.85	.769	4.00	1.4	0.67
804 165 3 [2]	5.86	.999	1.30	1.40	0.93	.998	1.37	1.4	0.18
804 265 3	1.65	.982	80.80	4.96	0.72	.764	5.85	1.4	0.61
802C165 1	1.45	.987	58.8	2.67	0.79	.910	9.02	1.4	0.76
802C265 1	1.10	.998	11540.00	4.94	0.68	.753	13.30	1.4	0.62
804C165 3	1.52	.995	36.3	2.30	0.57	.949	9.85	1.4	0.53
804C265 3	1.89	.995	8740.00	8.93	0.77	.599	3.60	1.4	0.55
801 165 5 [2]	10.00	.982	0.61	1.09	1.55	.931	0.60	1.4	1.45
801 265 5 [2]	10.00	.971	0.38	5.85	1.24	.889	1.80	1.4	1.37
803 165 2 [2]	10.00	.996	0.49	1.20	1.67	.992	0.46	1.4	1.72
803 265 2 [2]	10.00	.994	0.32	6.59	1.60	.914	1.70	1.4	1.53
801C165 5 [2]	10.00	.979	10.00	1.59	-0.78	.943	2.26	1.4	0.82
801C265 5 [2]	10.00	.996	3.87	1.41	-2.04	.994	7.17	1.4	0.56
803C165 2 [2]	10.00	.986	2.31	0.65	-0.02	.962	1.93	1.4	0.91
803C265 2 [2]	10.00	.991	6.73	0.72	-3.54	.963	7.92	1.4	0.62
$\overline{R}^2$		.988				.905			

[1] The dimension of m depends on the value of the exponent n which is dimensionless.

[2] The infiltration rate did not reach steady state for these runs.

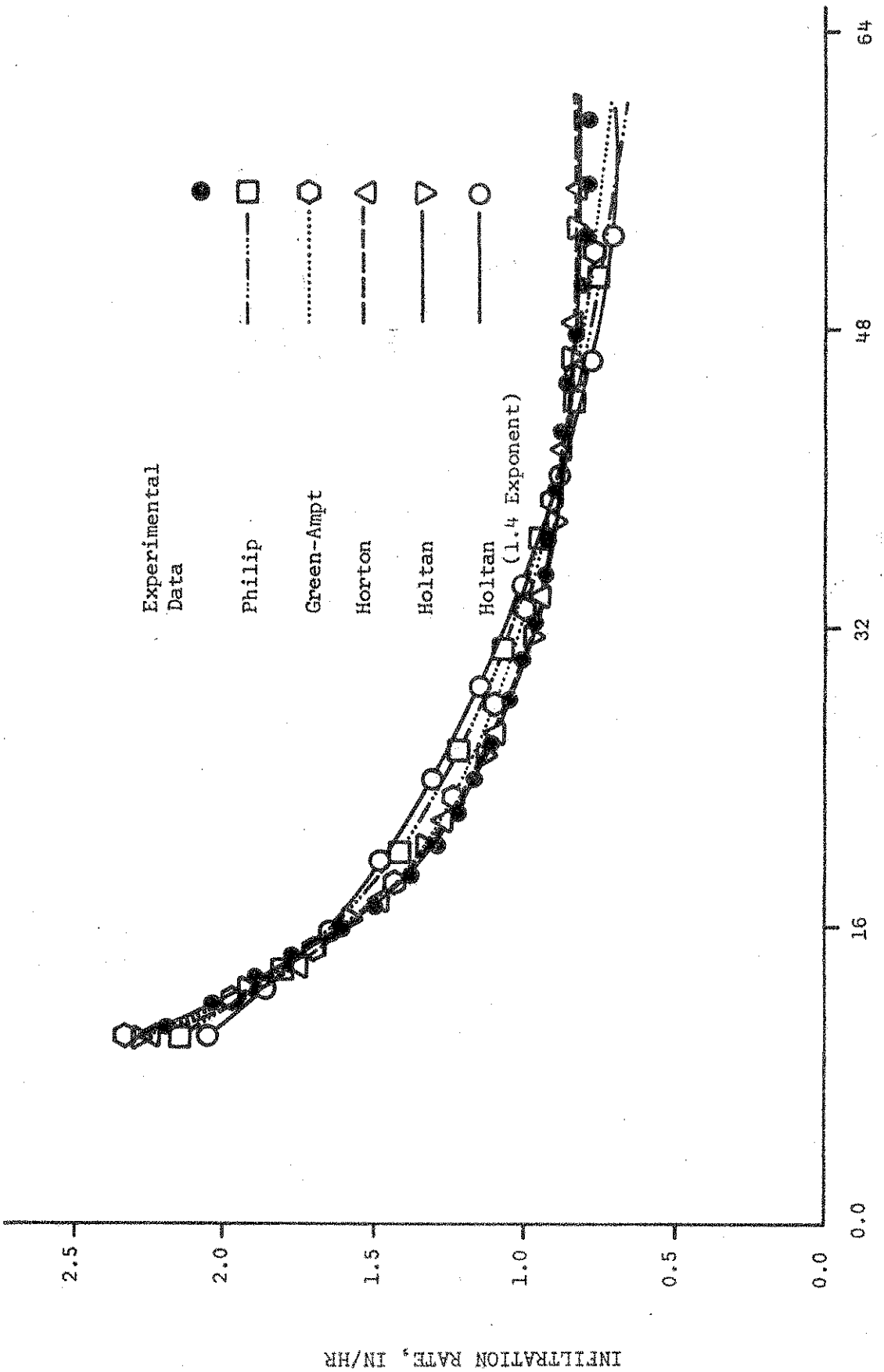

Figure 36 -- Fit of infiltration equations to experimental data obtained for a dry run on fallow Morley silt loam.

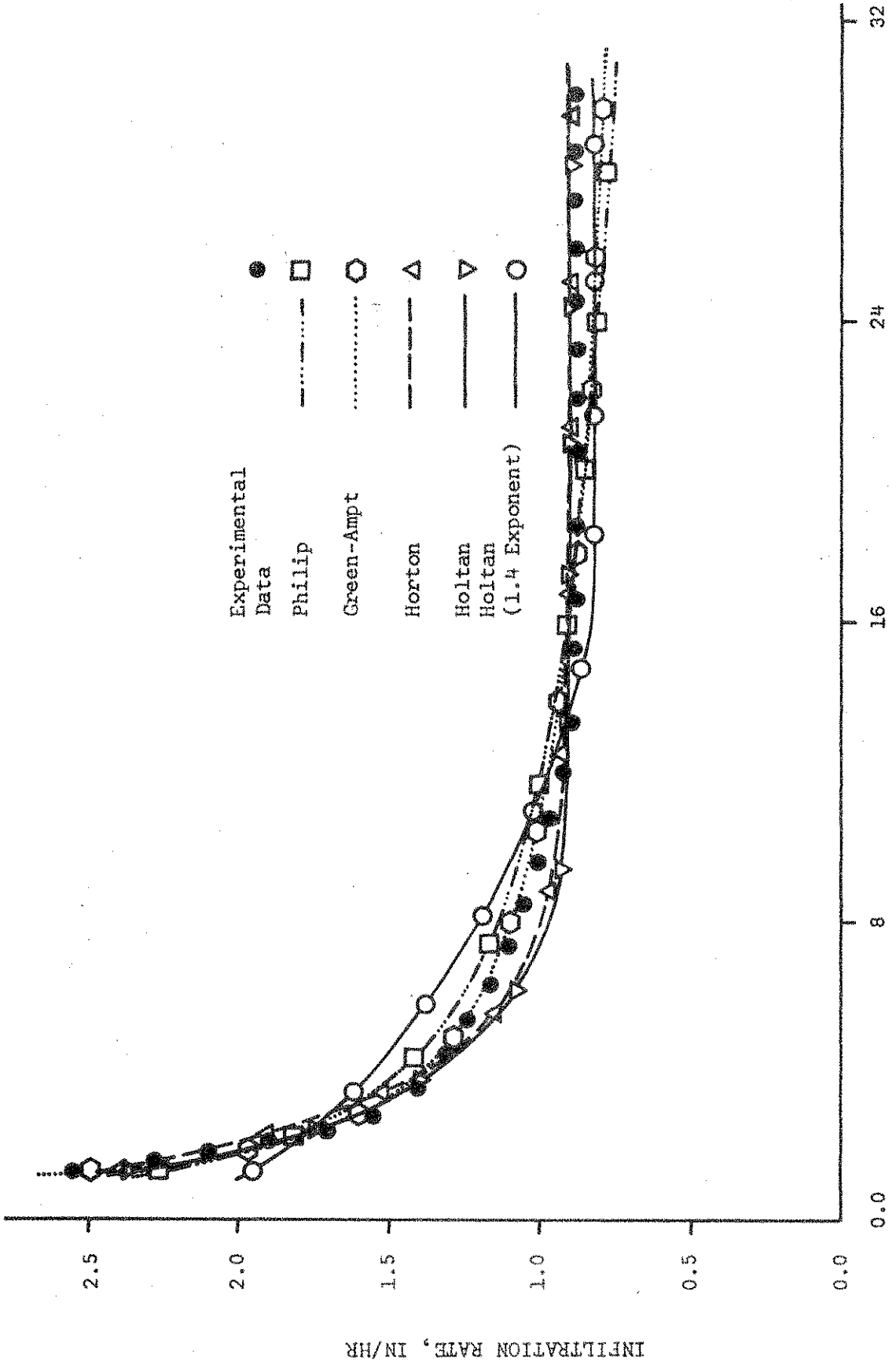

Figure 37 -- Fit of infiltration equations to experimental data obtained for a wet run on fallow Morley silt loam.

A characteristic common to the Green-Ampt and Philip equations for most of the cases analyzed was that, even though the infiltration rate diminished to a constant rate during the run, the predicted infiltration rate continued to decrease at the end of the run. This characteristic is shown in Figures 36 and 37. Also, it is reflected in Table 12 by the negative values for some of the constants C and G. Although this occurred for both equations, the difference in the apparent steady-state infiltration rate as obtained from the data and the constants C and G was consistently greater for the Philip equation. Thus, the use of these equations with parameters that have been determined by regression will likely cause predicted infiltration rates to be too low for times greater than the duration of the experimental test. The regression could be weighted such that the steady state infiltration rates would be more closely approximated by the equations; however, this would cause a greater disagreement between predicted and experimental values during the initial states of the run.

Horton's three-parameter equation (34) fit the data well over the entire run with a mean R^2 value of 0.987. The steepness of the initial portion of the infiltration curve is reflected in the magnitude of k_f. Thus, the k_f values were, in general, larger for the wet runs and for the runs on crusted soil than for those on cultivated and sod plots. The parameter f_c, with few exceptions, agreed closely with the steady-state infiltration rate and was dependent on the soil type.

From the results in this study it appears that poor fits reported in the literature for Horton's equation during the early part of infiltration tests may have been due to the method used for determining the parameters. Horton (1940) suggested that the parameters be determined by plotting ln $(f - f_c)$ versus t and obtaining k_f as the slope of a straight line drawn through the data, and $(f_o - f_c)$ as the intercept of the line. This procedure minimized the squared deviations of ln $(f - f_c)$, thereby weighting values close to f_c heavier than the larger values occurring in the initial stages of the run. The nonlinear regression used in this study minimized the squares of the deviations of the dependent variable, f, and consequently the equation closely fit the data during the entire run.

To determine the parameters in Holtan's equation (36), it was necessary to assign a control depth on which to base S_t. For fallow soils, this depth

was computed from the initial soil-water content, the soil porosity, and the volume of water that had infiltrated at the time the infiltration rate reached a constant value. If the infiltration rate did not reach a constant value, the volume of water that had infiltrated by the end of the test was used. This method of defining control depth gave much better fits to the infiltration data than the use of the depth to the B horizon suggested by Holtan and Creitz (1967). For the sod plots, the slope of the infiltration-time relationship was quite steep at the termination of both the dry and wet runs. The top of the B horizon was used as the control depth for this case.

Defining the control depth in the above manner, Holtan's equation gave an excellent fit to the experimental data with a mean R^2 for all the runs of 0.988. The agreement between the steady-state infiltration rates and the f_c parameter in equation (36) was exact for many of the tests on fallow soil. Although the method used to define S_t permitted the equation to closely fit the data, the parameter m varied quite drastically between the dry and wet runs. The wide variation was mainly due to differences in control depth and could be reduced by using the form of equation (37). However, either form of the equation requires that $y = S_t$ before the predicted infiltration rate becomes constant. Therefore, it is necessary that S_t be estimated accurately to obtain reliable predictions using Holtan's equation.

The control depths for the wet runs had a range of 0.93 to 2.52 in with a mean of 1.64 in. This agreed closely with the mean of 1.67 in for the control depths of dry runs on the crusted soils, tests 804C and 802C. The range for the dry runs on soils with a freshly cultivated surface was 2.21 in to 6.25 in with a mean of 3.81 in. Thus, the control depths for the runs analyzed in this study for fallow soils were less than the distance to the top of the B horizon (7 to 10 in for these soils). Furthermore, the effective control depth was dependent on the condition of the surface, being less for a crusted than for a cultivated surface.

Of the equations tested, the two-parameter form of Holtan's equation gave the poorest fit to the data. The mean R^2 for all the runs was 0.905. The predicted steady-state infiltration rate was, in general, less than the observed values. However the variation in the parameter m was considerably

less than in the three-parameter form of the equation.

Examination of the infiltration equation parameters given in Table 12 for the different soil types and conditions shows considerable variation from one case to another. Part of this variation is due to initial soil-water conditions. The parameters a, S, G, and f_o in the Green-Ampt, Philip, and Horton equations are, by definition, dependent on initial soil-water content. However, the amount of variation of these parameters between tests at different initial water contents cannot be explained by initial water-content differences alone. Furthermore, the parameters C, f_c and k_f in the Green-Ampt and Horton equations and all the parameters in Holtan's equation are supposed to be independent of initial soil-water content; yet Table 12 shows considerable variation of these parameters with initial water content. It is not clear from these results whether the variation of parameters is due to soil-water differences or to the surface compaction and crusting which accompanied the higher water contents.

Much of the variation noted above can be explained by differences in the surface conditions of the soils resulting from natural variations that occur between field plots. Natural variation of the infiltration characteristics of field plots is exemplified by Figure 38, which shows experimental infiltration data for two test plots on the same soil with the same surface and initial water-content conditions. The difference in the infiltration curves, which is typical for the runs analyzed in this study, is reflected in the equation parameters.

Infiltration data for Zanesville silt loam soil with four different surface conditions is shown in Figure 39. The initial water contents were not equal for all cases; however, comparison of the dry and wet runs on the cultivated soil with the dry run on the crusted soil surface indicates that the difference in the curves in Figure 39 is heavily dependent on surface conditions. Thus, the differences in surface conditions are also reflected in the equation parameters.

CHAPTER 4 SUMMARY AND CONCLUSIONS

An investigation was conducted to experimentally evaluate infiltration equations proposed by Green and Ampt, Horton, Philip, and Holtan. Experimental data for 13 soils were obtained from erosion studies con-

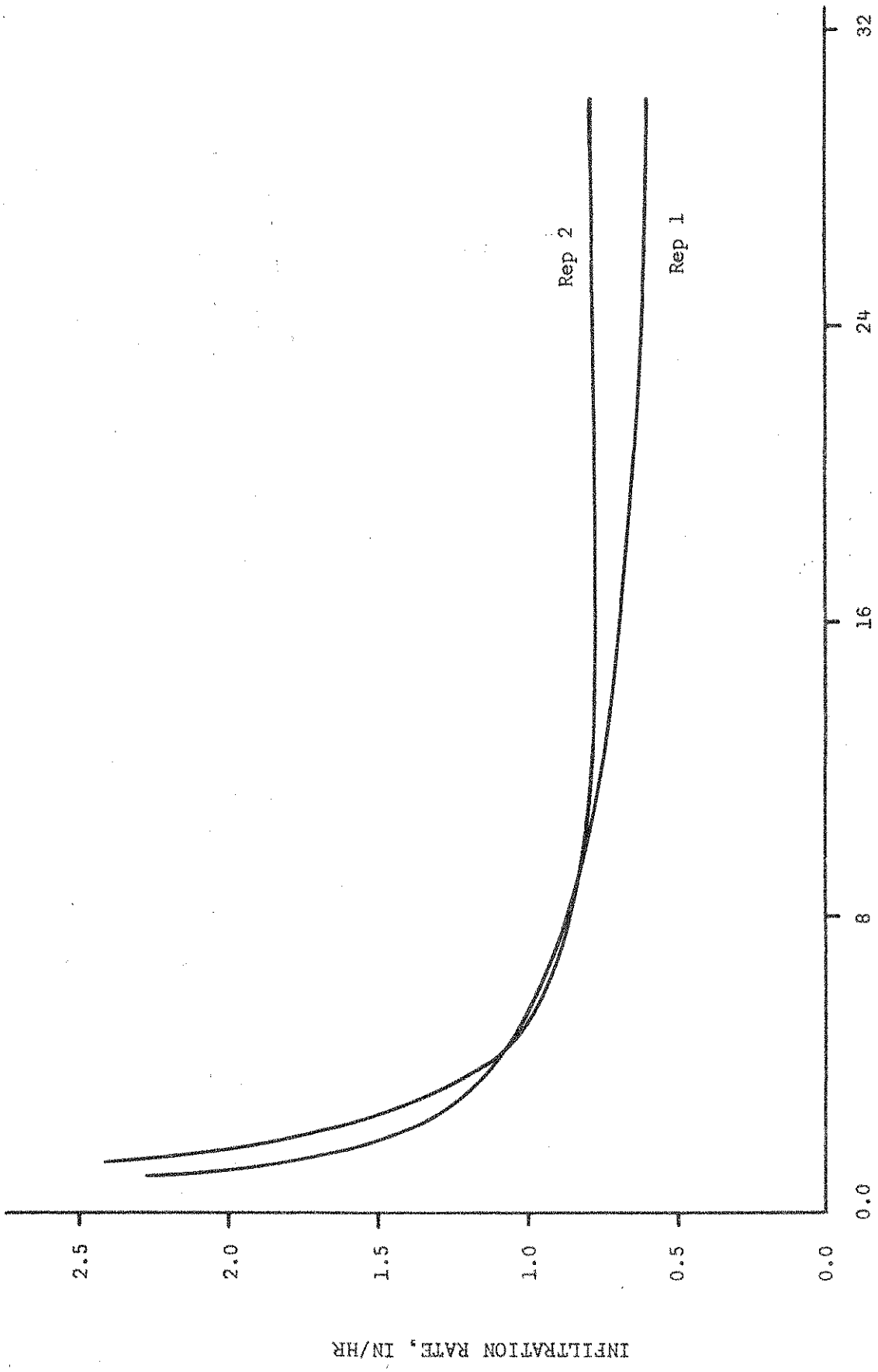

Figure 38 -- Two replications for wet runs on fallow Fredrick silt loam.

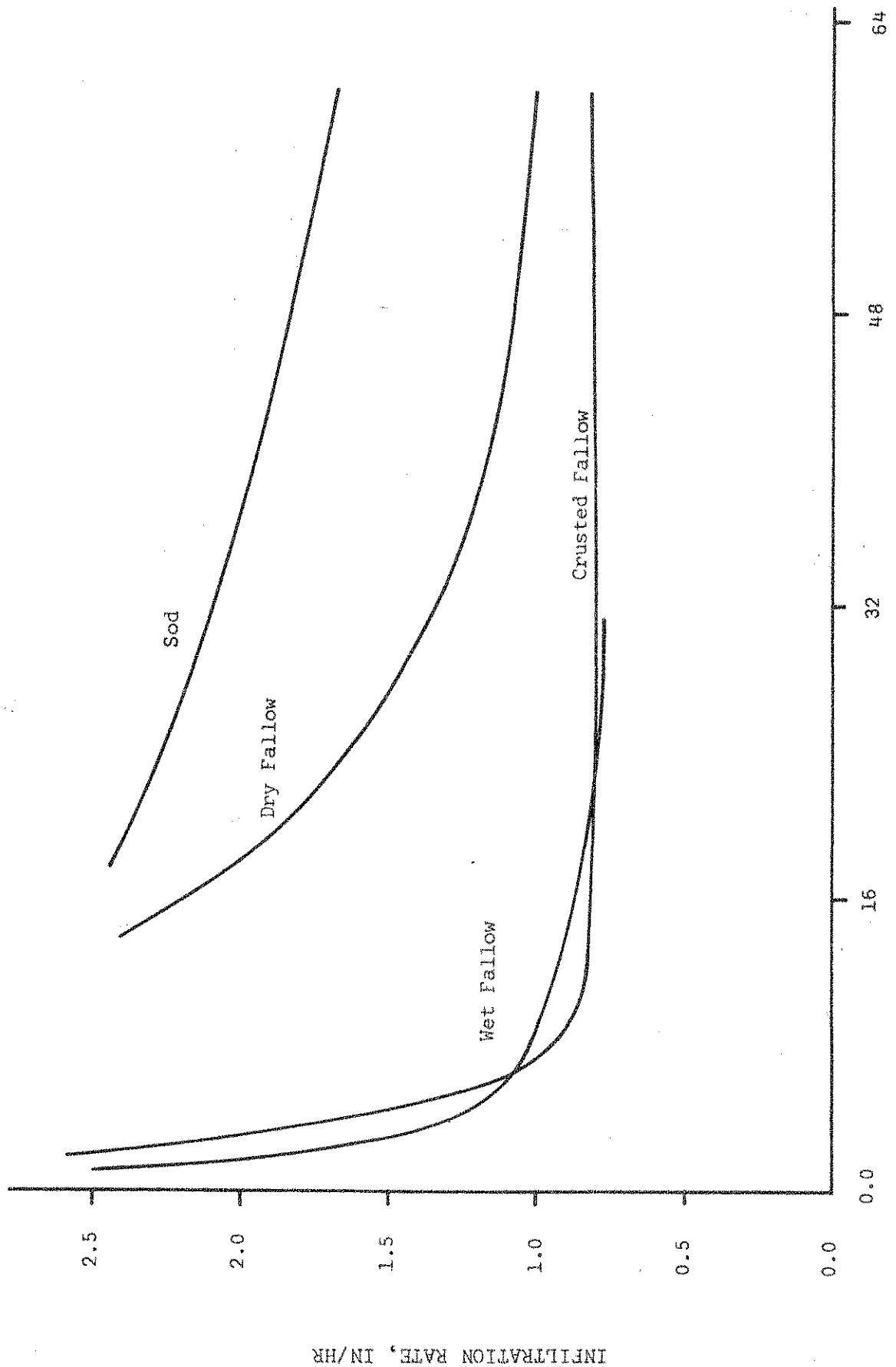

Figure 39 -- Infiltration relationships for different surface conditions and initial water contents for Zanesville silt loam.

ducted by the Agricultural Research Service using the rainulator, a plot-sized rainfall simulator. Infiltration rate-time relationships were determined from these studies by making overland flow analyses to approximate the storage rates on the plot surface. The parameters in the four equations, plus those from a simplified form of Holtan's equation, were obtained by performing regression analyses on the infiltration data. Values of equation parameters and the correlation index for each of the 52 runs analyzed are presented.

On the basis of the results obtained from the above study, the following conclusions were formulated:

Experimental infiltration rate-time relationships can be obtained from rainulator data. Due to the size of the plots, it is necessary to evaluate the surface storage rates to obtain reliable infiltration relationships. For fallow and sod plots, these rates can be approximated by an overland flow analysis.

Adequate fits to experimental infiltration data can be obtained by any of the four equations tested. However, the Philip and Green-Ampt equations obtained by regression predict infiltration rates that are too low for times greater than the duration of the experimental test from which the equation parameters are obtained.

Very good representations of the infiltration rate-time relationships can be obtained from the three-parameter equations of Holtan and Horton. Both equations predict steady-state infiltration rates that agree closely with experimental values. For Holtan's equation, it is necessary to make a reliable estimate of the control depth on which the parameter S_t is based, in addition to the three equation parameters. This control depth is affected by surface compaction and crusting and, for fallow soils, is generally much less than the depth to the B horizon.

Differences in soil-surface conditions and initial soil-water content, as well as natural variation between field plots, cause the parameters obtained for the infiltration equations to vary widely. In view of this variation and the requirement of a control-depth evaluation in Holtan's equation, it appears that the infiltration data analyzed in this study can best be described by Horton's equation [equation (34)].

The tendency toward a slight superiority of Horton's equation over

the other infiltration equations might appear at first thought to be at odds with the findings of Chapter 2, wherein the Green-Ampt approach appeared to be reasonably adequate. Considerable caution should be exercised, however, when comparing the behavior of the laboratory columns of Chapter 2 with that of a relatively large infiltration field-plot which is being subjected to simulated rainfall. First of all, in a laboratory column under water-ponded conditions, it is possible to obtain a good measurement of infiltration for a relatively localized region of soil surface. On a field plot, in contrast, the effect of surface storage of water under transient conditions is troublesome, even though the present approach as embodied in equations (38) through (41) is felt to be valid and useful. Beyond this, however, soil variations, crusting-sealing effects, nonuniform initial soil-water contents, and initially unponded applications of water may very well induce important changes from the behavior of a reasonably well controlled, water-ponded column of sand. From this point of view, it is not necessarily surprising if the more empirical Horton equation, with its three characterizing constants, turns out in some respects to provide a more adaptable fit to field data which are not necessarily conforming to the simpler conditions involved in the Green-Ampt approach.

CHAPTER 5. GENERAL SUMMARY AND CONCLUSIONS

Water infiltrated into soil is of important consequence to the water economy of an area, since the water taken in by the soil is used for plant growth and evapotranspiration, for baseflow in streams, and for addition to groundwater storage. Furthermore, the non-infiltrated water that becomes runoff has a potentiality for excessive erosion and destructive flooding. Runoff can occur when the rainfall intensity exceeds the infiltration capability of the soil. In humid areas which have on the order of 36 to 42 in of annual rainfall, about two-thirds of the water is infiltrated, while the remaining one-third constitutes the runoff.

The infiltration capability of a soil is strongly affected by such factors as inherent soil properties, soil-water content, and vegetative cover, and these factors frequently are subject to change with time. Vegetative cover, for example, may range seasonally from bare soil initially to the eventual complete cover of a fully grown crop, or vice versa when a farming or tillage operation changes a vegetatively protected surface to a bare-soil condition. Soil-water content obviously fluctuates under the competing influences of rainfall and evapotranspiration. The impact energy of raindrops on bare soil can reduce the permeability of the soil surface, with a resultant decrease in infiltration rate. Instruments are available for measuring the infiltration rate at a given site and time, but as yet it is extremely difficult to make enough measurements for various sites and conditions to enable a precise infiltration characterization over an area of extensive size.

Important features of the infiltration process were here studied from the standpoint of describing them mathematically and experimentally, to be followed by an attempt at integrating the various factors into a workable prediction scheme which would supplement the present methods of on-site field measurements. To be practicable, the prediction scheme would require development to the point of being more rapid and flexible than the performing of the required large number of on-site infiltration measurements as presently conducted. The approach used was to examine theoretical and empirical mathematical expressions which had been developed

previously, and to relate these to the infiltration phenomenon as it occurs both under laboratory and field conditions. The stages in which the study was carried out were first to develop the necessary theoretical considerations, and then to test these on laboratory soil columns, to relate the results to small (10-cm diameter) undisturbed field cores, and to extend the results to small field plots (1.16 by 1.16 m) and then to larger field plots (12 by 35 ft). An ultimate step would have been to characterize infiltration on a watershed, but, because of the obvious complexity involved, this step was considered to be outside the scope of the present study.

Four infiltration equations were considered, two of them (Green-Ampt and Philip) arising out of approximate infiltration theory, with the other two (Horton and Holtan) being empirical in origin. The specific forms are:

Green-Ampt:	$y/a - \ln(1 + y/a) = Ct/a$
Philip:	$f = S/2t^{1/2} + G$
Horton:	$f = f_c + (f_o - f_c)\, e^{-k_f t}$
Holtan:	$f = m(S_t - y)^n + f_c$

Here y is the volume of water infiltrated per unit cross sectional area, t is the time, $f = dy/dt$ is the infiltration rate, and the remaining quantities in the equations are the infiltration-characterizing constants. In the Green-Ampt equation, C is similar to a hydraulic conductivity and has the same units, while $a = (\overline{\theta} - \theta_o)(H + P)$, where $\overline{\theta}$ is an average volumetric soil-water content, θ_o is the initial volumetric soil-water content, H is the depth of water ponded on the soil surface, and P is a suction-head parameter related to the capillarity of the soil. In the Philip equation, S is the so-called sorptivity, while G is very similar to the C of the Green-Ampt equation. In the Horton equation, f_c is the final infiltration rate reached at large times, f_o is the initial infiltration rate (at $t = 0$), while k_f is a constant dependent on the soil and its surface characteristics. In the Holtan equation, m and n are empirical constants specified by soil type and surface and cropping conditions,

f_c is the final infiltration rate just as in the Horton equation, and S_t is a water-storage potential of the soil as specified by the total porosity and antecedent soil-water content above a so-called control depth in the soil.

Under carefully controlled experimental conditions in the laboratory, the Green-Ampt approximate-theory equation showed considerable promise for predicting the infiltration into uniform porous materials and coarse-over-fine stratifications, but was not quite as successful for fine-over-coarse stratifications. It was also shown that the Philip equation is quite similar to the Green-Ampt; however, the fact that some of the parameters in the Green-Ampt equation are less complicated makes it somewhat simpler to use.

Originally, it was hoped that the approximate theoretical approach could be made applicable to the prediction of infiltration under field conditions. Such a possibility was indicated by experimental laboratory measurements on undisturbed field cores when compared with results from the sprinkling infiltrometer on small plots, but certain difficulties were encountered. It was expected that the infiltration rates measured on the field cores in the laboratory would compare most nearly with the field plots having an effective protective cover. In actuality, however, the field-core rates in the laboratory were more nearly those of a bare soil which was subjected to the beating action of the water drops falling from the sprinkling infiltrometer. It was suggested that in taking the field cores, a partial surface seal was somehow created so as to cause an infiltration reduction similar to that produced on bare soil by water-drop impact.

With the sprinkling infiltrometer, it was further shown that surface texture (or particle size distribution) does not significantly affect the infiltration rate on a bare soil, unless the texture is of an extreme nature that provides unusually good protection against falling water-drop action. It was suggested that the surface-sealing effect on infiltration becomes an important factor when the soil is unprotected. It was also shown that altering the surface configuration by ridging a bare soil had little effect on the infiltration rate.

The two approximate-theory and the two empirical equations were evaluated experimentally on large field plots by the use of rainfall simulator equipment. Over an extended time course, the empirical equations were found to be somewhat better than the approximate-theory equations. With the two empirical equations, however, differences in soil-surface conditions, initial soil-water content, and natural variation between field plots caused the fitted infiltration-equation parameters to vary rather widely. Because these variations were somewhat less with Horton's equation than with Holtan's, and because of the somewhat troublesome control-depth evaluation in Holtan's equation, it appears that the Horton equation is preferable for describing the infiltration rates on the larger field plots of this study.

It may appear that the conclusions of this study are somewhat at variance with each other, in that the Green-Ampt approximate-theory approach was found adequate for the laboratory columns, whereas the empirical equations were preferable for the larger-scale field plots. But it should be noted that in the laboratory a water-ponded condition was employed, and that measurements were made on a relatively localized region of soil surface. With the larger-scale plots in the field, the water was applied as simulated rainfall rather than by ponding, and overland flow and surface roughness were present also even though explicit attempts were made to separate out their effects. Whether in the field or the laboratory, however, the results of the study show that surface crusting and sealing effects, initial soil-water contents, and natural soil variations are dominant factors in the infiltration process.

LITERATURE CITED

Bazargani, J. I. 1964. Transient water flow characteristics of unsaturated soils. Ph.D. Thesis, Purdue University, Lafayette, Indiana.

Bertrand, A. R., and J. F. Parr. 1961. Design and operation of the Purdue Sprinkling Infiltrometer. Purdue Univ. Agr. Exp. Sta. Res. Bull. 723, 16 pp.

Childs, E. C. 1967. Soil moisture theory. Advan. Hydrosci. 4:73-117.

Davidson, J. M., D. R. Nielsen, and J. W. Biggar. 1963. The measurement and description of water flow through Columbia silt loam and Hesperia sandy loam. Hilgardia 34:601-617.

Fok, Y. S., and V. E. Hansen. 1966. One dimensional infiltration into homogeneous soil. Amer. Soc. Civ. Eng. Proc. 92:35-48, No. IR3.

Foster, G. R., L. F. Huggins, and L. D. Meyer. 1968. Simulation of overland flow on short field plots. Amer. Geophys. Union, 49th Annual Meeting, Washington, D. C., Paper H30.

Foster, G. R., R. W. Skaggs, and L. F. Huggins. 1969. Kinematic analysis of overland flow with unsteady lateral inflow. Water Resources Res. 5, manuscript submitted.

Gardner, W. H. 1965. Water content. In "Methods of Soil Analysis" (C.A. Black, ed.), Part 1, pp. 82-127. Amer. Soc. Agron., Madison, Wisconsin.

Gardner, W. R. 1967. Development of modern infiltration theory and application in hydrology. Trans. Amer. Soc. Agr. Eng. 10:379-381, 390.

Green, R. E., R. J. Hanks, and W. E. Larson. 1964. Estimates of field infiltration by numerical solution of the moisture flow equation. Soil Sci. Soc. Amer. Proc. 28:15-19.

Green, W. H., and G. A. Ampt. 1911. Studies on soil physics: I. Flow of air and water through soils. J. Agr. Sci. 4:1-24.

Hanks, R. J., and S. A. Bowers. 1962. A numerical solution of the moisture flow equation for infiltration into layered soils. Soil Sci. Soc. Amer. Proc. 26:530-534.

Holtan, H. N. 1961. A concept for infiltration estimates in watershed engineering. USDA-ARS Publication 41-51, 25 pp.

Holtan, H. N., and N. R. Creitz. 1967. Influence of soils, vegetation and geomorphology on elements of the flood hydrograph. Proc. Symp. Floods and Their Computation, Leningrad.

LITERATURE CITED (Continued)

Holtan, H. N., C. B. England, and V. O. Shanholtz. 1967. Concepts in hydrologic soil grouping. Amer. Soc. Agr. Eng. Trans. 10:407-410.

Horton, R. E. 1940. An appraoch toward physical interpretation of infiltration capacity. Soil Sci. Soc. Amer. Proc. 5:399-417.

Huggins, L. F., and E. J. Monke. 1967. The mathematical simulation of the hydrology of small watersheds. Tech. Rept. No. 1, pp. 38-47. Purdue Water Resources Research Center, Lafayette, Indiana.

Jackson, R. D., C. H. M. van Bavel, and R. J. Reginato. 1963. Examination of the pressure-plate outflow method for measuring capillary conductivity. Soil Sci. 96:249-256.

Kirkham, D., and C. L. Feng. 1949. Some tests of the diffusion theory, and laws of capillary flow, in soils. Soil Sci. 67:29-40.

Klute, A. 1952. A numerical method for solving the flow equation for water in unsaturated materials. Soil Sci. 73:105-116.

Mannering, J. V. 1967. The relationships of some physical and chemical properties of soils to surface sealing. Ph.D. Thesis, Purdue University, Lafayette, Indiana.

Meyer, L. D., and D. L. McCune. 1958. Rainfall simulator for runoff plots. J. Agr. Eng. 39:644-648.

Moe, P. G., J. V. Mannering, and C. B. Johnson. 1967. Loss of fertilizer nitrogen in surface runoff water. Soil Sci. 104:389-394.

Olson, T. C., J. V. Mannering, and C. B. Johnson. 1962. The erodibility of some Indiana soils. Proc. Indiana Acad. Sci. 72:319-324.

Philip, J. R. 1954. An infiltration equation with physical significance. Soil Sci. 77:153-157.

Philip, J. R. 1957a. The theory of infiltration: 4. Sorptivity and algebraic infiltration equations. Soil Sci. 84:257-264.

Philip, J. R. 1957b. The theory of infiltration: 5. The influence of the initial moisture content. Soil Sci. 84:329-339.

Philip, J. R. 1957c. Numerical solution of equations of the diffusion type with diffusivity concentration-dependent. II. Australian J. Phys. 10:29-42.

Philip, J. R. 1958. The theory of infiltration: 7. Soil Sci. 85:333-337.

Rubin, J. 1966a. Numerical analysis of ponded rainfall infiltration. Paper presented at Symp. Water in the Unsaturated Zone, Wageningen, Netherlands.

LITERATURE CITED (Continued)

Rubin, J. 1966b. Theory of rainfall uptake by soils initially drier than their field capacity, and its applications. Water Resources Res. 2:739-749.

Swartzendruber, D. 1960. Water flow through a soil profile as affected by the least permeable layer. J. Geophys. Res. 65:4037-4042.

Swartzendruber, D. 1966. Soil-water behavior as described by transport coefficients and functions. Advan. Agron. 18:327-370.

Swartzendruber, D. 1968. The applicability of Darcy's law. Soil Sci. Soc. Amer. Proc. 32:11-18.

Swartzendruber, D., and T. C. Olson. 1963. Rate of change as determined graphically with an equilateral glass prism. Soil Sci. Soc. Amer. Proc. 27:108-110.

van Duin, R. H. A. 1955. Tillage in relation to rainfall intensity and infiltration capacity of soils. Neth. J. Agr. Sci. 3:182-191.

Watson, K. K. 1959. A note on the field use of a theoretically derived infiltration equation. J. Geophys. Res. 64:1611-1615.

PROJECT PUBLICATIONS

Several portions of this report are in the process of being prepared into manuscripts for submittal to scientific journals for publication. Titles already published or submitted for publication are:

Swartzendruber, D. 1968. The applicability of Darcy's law. Soil Sci. Soc. Amer. Proc. 32:11-18.

Skaggs, R. W., L. F. Huggins, E. J. Monke, and G. R. Foster. Experimental evaluation of infiltration equations. Submitted for publication in the Trans. Amer. Soc. Agr. Engrs.